PERSISTENT AND TRANSIENT ANISOTROPIES

OF THE COSMIC RADIATION

By

JON GORDON ABLES

Bachelor of Arts
Knox College
Galesburg, Illinois
1959

Master of Science
Oklahoma State University
Stillwater, Oklahoma
1963

Submitted to the faculty of the Graduate College of
the Oklahoma State University
in partial fulfillment of the requirements
for the degree of
DOCTOR OF PHILOSOPHY
July, 1967

PERSISTENT AND TRANSIENT ANISOTROPIES

OF THE COSMIC RADIATION

Thesis Approved:

_____
Thesis Adviser

_____

_____

_____

_____
Dean of the Graduate College

658289

ii

PREFACE

One of the more remarkable characteristics of the cosmic radiation
is its high degree of uniformity; the flux changes very little with
time and is almost completely isotropic. Only in the past few decades
have measurements of the cosmic radiation been sufficiently precise to
detect temporal variations; and, the detection of anisotropies, with any
degree of certainty, became possible only with the improved instrumenta-
tion and world-wide monitoring facilities constructed as part of the
program for the International Geophysical Year. Although the observed
variations and anisotropies are small, it has become increasingly evident
that a great amount of information concerning the nature of the inter-
planetary medium, the solar corona, and even the sun itself, as well as
possible information about the origin of the cosmic radiation, is con-
tained in these small variations and anisotropies. The advent, in the
last decade, of artificial earth satellites and solar probes has greatly
increased the interest in cosmic rays and related phenomena. Not only
do these experimental vehicles provide a fresh viewpoint from which to
study cosmic rays, but also the cosmic-ray measurements provide valuable
cross-checks on other measurements made in space. An outstanding prob-
lem has been that of trying to relate measurements made by ground-based
monitors to those made in space.

When, in the summer of 1963, I joined the Cosmic Ray Group of the
Southwest Center for Advanced Studies (then the Graduate Research Center

of the Southwest) as a graduate research assistant, work already in progress included the design and construction of two large cosmic-ray neutron monitors, a cosmic-ray anisotropy detector for deep space probes, and a balloon-borne prototype of the anisotropy detector. One successful flight of the balloon-borne instrument had just been completed and my first task was to become familiar with this instrument, modify, and re-build it for a second flight, which took place in October of the same year. Professor K. G. McCracken, head of the Cosmic Ray Group and my adviser for this thesis, suggested that I should undertake a study of rapid variations in the cosmic radiation at high geomagnetic latitudes, utilizing a large-aperture, balloon-borne detector. I designed and constructed such an instrument, working in co-operation with the newly-formed Engineering Support Group, and two flights of the detector were made in the spring and summer of 1964. The second flight was made at Ft. Churchill, Manitoba, and we returned to Dallas with the intent of making a detailed analysis of the data accumulated from this flight.

The search for suitable analytic methods for the study of the balloon-detector data produced what was to become a major perturbation on my research program. Power-spectrum analysis as a technique for investigating the periodic structure of cosmic-ray variations was just beginning to appear in the literature, and a quest for the mathematical foundations of this powerful analytical tool led directly to the field of the statistical theory of communication, a subject which has enjoyed enormous growth in the past twenty years. This seemed to be an almost untouched subject, as far as the study of cosmic-ray variations was concerned, even though notable successes had been achieved in a number of diverse geophysical fields through the use of the concepts and

techniques of statistical communications theory and information
theory. Since the large neutron monitors were, by now, producing copious
amounts of data superior to any ever before available from such monitor-
ing facilities and since these data were thought to be better understood
than that from the balloon-monitor, the first attempts to use the
techniques gleaned from the information and communication theorists
and from experimenters in other fields, notably seismology, who were
already using these methods were made utilizing the neutron-monitor
data.

The almost immediate successes produced by the combination of the
growing, world-wide net of the new, large neutron monitors and the
modern signal-processing techniques pushed into the background the
balloon-borne detector work. A critical study of the long-debated
semi-diurnal variation of the cosmic-ray flux was followed by the
development of inverse convolution normalization for neutron monitors
and the revival of an older idea--time-direction contour mapping of
cosmic-ray anisotropies--which, with the aid of the new methods and
better data, has now become an extremely useful tool for the investiga-
tion of transient anisotropies. A brief period was taken from this work
to re-build and fly once more the balloon-borne detector at Ft. Churchill
in the summer of 1965--the only flight which is reported in this thesis.

In all phases of the research reported here Professor McCracken
has played a major role as teacher, adviser, and friend. Also, Dr. U. R.
Rao, his associate, has given important assistance in the neutron-
monitor work.

The excellent technical staff of the Center has provided unfailing
support without which the work reported here could not have been

TABLE OF CONTENTS

LIST OF TABLES

LIST OF FIGURES

CHAPTER I

COSMIC RAY PROPAGATION IN THE INTERPLANETARY MEDIUM

1.1 Introduction.

The cosmic radiation, first noted about 1900 because the ioniza-
tion it produces in the lower atmosphere results in the discharge of
even the best insulated electroscopes, is now known to consist princi-
pally of very energetic, charged particles incident upon the top of the
earth's atmosphere from all directions. About 87% of all the cosmic
radiation consists of protons, with alpha particles contributing about
12% and heavier nuclei about 1% (Biswas and Fichtel, 1964). Electrons
have also been detected in the cosmic radiation, but the total electron
flux is only about 10^{-6} of the proton flux (Meyer and Vogt, 1961). The
nucleonic flux is very energetic with the energy per nucleon integral
spectrum falling off only as $\approx E^{-1.5}$ above 10 GeV per nucleon. In the
range below 10 GeV the differential energy spectrum has a maximum at a
few hundred MeV--the shape and amplitude of the spectrum in this range
being dependent upon solar conditions (Palmeira and Pieper, 1965).
The total proton flux above 40 MeV has been estimated to vary from ≈ 0.2
particle/cm^2-sec-ster during sunspot maximum to ≈ 0.5 particle/cm^2-sec-
ster sunspot minimum (Dessler and O'Brien, 1965). In addition to this
11-year variation in anti-correlation with the solar sunspot activity,
evidence exists indicating that the propagation of cosmic rays is
influenced by the interplanetary medium. Although the correlation

1

between certain transient variations in the cosmic-ray flux and solar-surface phenomena was noted soon after relatively continuous monitoring of the cosmic-ray flux began (Forbush, 1938), it was not until a better understanding of the nature of the interplanetary medium and the influence of the sun upon this medium was obtained that satisfactory theoretical models for the experimentally observed variations could be formulated.

1.2 The solar corona.

At the apparent visual limb of the sun the continuous emission in the optical spectrum is observed to fall off by a factor of e with an increase of only about 100 km in radial distance from the sun's center, thus producing the sharp visual edge of the sun's disc. The region above this edge, the corona, is marked also by radical changes in the character of the optical spectrum. Whereas the emission from the visual surface of the sun, the photosphere, is continuous, broken only by sharp absorption lines, the spectrum of the corona is dominated by emission lines arising from forbidden transitions of highly ionized atoms. And while the first 10,000 km of the corona, the chromosphere, in which the emission spectra of singly ionized atoms predominates is, like the photosphere, quite stable with time, the outer corona is observed to undergo striking changes in response to such surface events as solar flares (Thomas and Athay, 1961; Parker, 1963).

The corona above 1.03 solar radii has been most thoroughly investigated through radio observations at wavelengths greater than 50 cm which indicate a temperature of about a million degrees--far greater than the $\approx 6000°$ temperature of the photosphere. Moreover, this temperature is found, without much variation, throughout the extent of the corona for which temperature measurements have been made. The density gradient

of the corona thus should assume the form given by the generalized
barometric formula for an isothermal gas

$$N_e = \text{const} \times e^{GMm/rRkT}$$

where N_e is the electron number density; G = gravitational constant;
M = sun's mass; m = mean molecular mass; r = heliocentric distance in
solar radii; R = sun's radius; k = Boltzmann's constant; T = temperature.
This relation is observed to be quite accurate for $r < 3$, beyond which
distance measured densities are uncertain. The corona itself is
observed to consist almost entirely of ionized hydrogen, there being
about 2×10^{18} electrons and as many protons above each square centimeter
of the sun's surface. A summary of coronal observations and measurements
is given by van de Hulst (1953).

1.3 The interplanetary medium--the solar wind.

The solar corona when visually observed during a total solar
eclipse or seen with the aid of the solar coronagraph is often strik-
ingly asymmetric, particularly at sunspot minimum, with long, tapered
'streamers' pointing outward which are strongly suggestive of an out-
ward flow of coronal material. Indeed, the extent of the solar corona
beyond a few solar radii was the subject of considerable conjecture
until the advent of direct measurements made possible by solar satellite
probes. The concept that the solar corona might, temporarily, extend as
far as the orbit of the earth was invoked by Chapman and Ferraro in the
early 1930's to explain the geomagnetic storm phenomena which were
apparently linked to solar surface events. Even earlier, Stormer had
postulated the existence of solar corpuscular radiation in connection
with his work on aurora (cf. Stormer, 1955), and in 1951 Biermann

suggested that the observed acceleration of ionized molecules in cometary tails could only be explained by a <u>continual</u> flux of solar plasma--a flux Parker was later to call the solar wind.

The consequences of Biermann's suggestion were mathematically explored by Parker (1958), who was able to demonstrate that a continual outflux of plasma from the sun is to be expected from the observed heating of the lower corona. This solar wind (so named because the mean free path of the ions is short compared with the earth-sun distance and hence the solar corpuscular radiation is gasdynamic in character) has now been experimentally confirmed (Neugebauer and Snyder, 1962). The density is ≈ 5 protons/cm^3 with a mean velocity ≈ 500 km/sec. Since this bulk velocity is roughly five times the mean thermal velocity of the ions, the flow is supersonic with a Mach number of ≈ 5. This flux is entirely sufficient to explain the acceleration of ions in cometary tails, and variations in the flux due to sudden increased heating of the coronal base by a solar flare could easily account for the observed geomagnetic storms which are often observed to follow flares. Excellent correlation has been observed between the solar wind velocity, as measured by instruments aboard the Mariner IV spacecraft, and the planetary geomagnetic activity index Kp (Snyder, et al., 1963).

If the kinetic energy density of the coronal plasma exceeds the energy density of embedded magnetic fields, then these fields are controlled by the plasma and may be transported away from the sun, since the coronal plasma may be treated as a perfectly conducting fluid for the time and space scales appropriate for the study of the solar wind propagation in interplanetary space (Parker, 1963). Because of the rotation of the sun, plasma emitted continuously from a single region on the

sun's surface will lie along an Archimedean spiral in space which, in the earth's frame of reference, co-rotates with the sun. Each elemental volume of plasma moves radially outward from the sun; it is merely the locus of successive elements which form the co-rotating spiral. However, if a magnetic field exists at the solar surface with a magnetic energy density less than the coronal plasma energy density, then this field is transported away from the sun by the continuously emitted plasma and, hence, will lie along the co-rotating spiral. The angle X made by such a field line at any point with the heliocentric radial direction will be related to the plasma velocity v_p and the sun's angular velocity ω_s by

$$\tan X = \frac{\omega_s r}{v_p}$$

where r is the heliocentric distance of the point of observation (Parker, 1963). The observed solar magnetic fields range from about 1 gauss to 1000 gauss, the more intense fields being confined to small regions with the result that the mean field is roughly 1 gauss (Babcock, 1953). As this field is transported outward by the solar wind, the expansion of the plasma results in the field intensity decreasing as $1/r^2$; the resulting field at the orbit of the earth should be $\approx 5\,\gamma$ $(1\gamma = 10^{-5}$ gauss). The prediction of a co-rotating, spiral, interplanetary magnetic field in the ecliptic plane has been verified by earth satellite and solar-probe experiments (Wilcox and Ness, 1965). However, an additional feature revealed by these experiments is that the interplanetary field is highly variable in direction and magnitude, presumably due to turbulence in the solar wind, with only the large scale mean field following the theoretical spiral.

The solar wind may continue its supersonic outward flow only as
long as its energy density exceeds the ambient interstellar energy
density comprised of the interstellar gas kinetic energy density, the
cosmic-ray gas kinetic energy density, and the interstellar magnetic field
energy density. Assuming an interstellar magnetic field of 1γ , Parker
concludes that the interstellar magnetic energy density is dominant and
predicts that the solar wind becomes sub-sonic in a standing shock some-
where between 45 and 90 astronomical units. Beyond this shock transition
the sub-sonic solar wind commingles with the interstellar gas, while
inside this boundary the interstellar medium is excluded, except for
the highly penetrating cosmic rays.

1.4 The interaction of cosmic rays with the interplanetary medium.

The motion of highly energetic cosmic-ray particles in the inter-
planetary medium presents a complex problem. The direct effect of the
solar wind plasma upon the cosmic radiation is very small; however, the
trajectories of the cosmic-ray particles, by virtue of their charge, are
strongly curved by the interplanetary magnetic field--and this field is
under the control of the highly conductive solar plasma. The cosmic ray
effects may be subdivided into four main categories:

(a) Long time scale, quasi-equilibrium, modulation of the extra-
solar cosmic-ray flux. The cosmic-ray flux observed at the earth under-
goes an 11-year variation in anti-correlation with sunspot activity.
Possible mechanisms for this modulation include convection of cosmic
rays by the solar wind and adiabatic deceleration in the expanding
interplanetary magnetic field (Parker, 1966). Electrostatic deceleration
theories have also been proposed, but these do not seem to be supported

by the experimentally observed energy and charge dependence of the modulation (Nagashima, et al., 1966).

(b) A persistent, whirlpool-like streaming of the cosmic-ray gas around the sun (counter-clockwise when viewed from the north ecliptic pole). This streaming is often called the 'diurnal' anisotropy of the cosmic-ray flux since it is responsible for the daily variation of about 1% peak-to-peak, seen in the records of earth-based monitors (McCracken and Rao, 1965). This effect has been explained as a combination of two different cosmic-ray fluxes; first, a simple rotational and outward radial motion due to drift perpendicular to the rotating, spiral interplanetary magnetic field (as first suggested by Ahluwalia and Dessler in 1962) and second, a diffusion of cosmic rays toward the sun along the direction of the magnetic field lines. The first motion produces a radial cosmic-ray density gradient while the second, diffusional motion, which is made possible only by the small-scale irregularities in the magnetic field (if not along the field then certainly at the solar cavity boundary), is proportional to this gradient and tends to reduce it. The net result is a balancing of the inward (toward the sun) and outward components of the two fluxes, leaving only the rotational component. The first unified theoretical treatment of this effect was given by Axford (1965) who was able to demonstrate that the cosmic-ray gas in the solar cavity should co-rotate with the sun. An earth-based cosmic-ray monitor will detect this rotation as an anisotropy due to the Compton-Getting effect (Compton and Getting, 1935). The theoretically predicted directional flux variation of about 1% with the maximum in the direction 90° east of the earth-sun line is in good agreement with the experimental findings.

(c) Sudden, transient decreases in the extra-solar cosmic-ray flux.
These so-called Forbush decreases are characterized by a rapid onset
(on the order of a few hours) followed by slow recovery (on the order
of days) and are correlated with visible solar flares. Each decrease
follows its associated flare by one or two days. Several explanations
of this effect have been advanced, but present interest centers on only
two theoretical models. The first, proposed by Gold (1959, 1962), supposes
that at the time of a solar flare a region of the chromosphere is super-
heated with the result that a great mass of plasma expands outward from
the sun into the normal quiet-day solar wind. This highly conducting
plasma has sufficient energy to transport the magnetic field of the
chromosphere into interplanetary space for considerable distances, often
several astronomical units. Since, however, the magnetic fields of the
chromosphere originate within the sun itself, the transported magnetic
field lines have their roots in the sun and thus form great arched loops
filling the volume of the enhanced plasma flow. The relatively strong
magnetic field of this structure, the so-called Gold 'bottle,' tends to
reflect the galactic cosmic-ray flux and, since the volume of the 'bottle'
is expanding, the average density of galactic cosmic rays is reduced in
its interior. As this region engulfs the earth, the earth's magnetic
field is perturbed by the increased solar wind pressure, and earth-based
cosmic-ray monitors register a sudden decrease in the cosmic-ray intensity.
The distinguishing feature of the Gold model for solar flare related
cosmic-ray decreases is the simply closed nature of the magnetic field
transported by an enhanced plasma flow from the sun. This configuration
could possibly trap radiation for a relatively long time and lead to the
appearance of strong, bi-directional cosmic-ray flux anisotropies in its
interior.

The second model, proposed by Parker (1961), supposes that a solar flare may sharply increase the heating of the solar corona causing an enhancement of the normal solar wind. The enhanced flow material overtakes the already present solar wind material at a rate exceeding the sonic velocity in the interplanetary medium with the result that a radially expanding shock wave, the so-called Parker 'blast wave,' is formed. The effect is to divide the interplanetary medium into three regions; the undisturbed medium ahead of the shock front, the shocked interplanetary plasma which lies between the shock front and the enhanced flow region, and the enhanced flow region itself. The interplanetary magnetic field assumes the spiral form appropriate to the plasma flow velocities in the undisturbed and enhanced flow regions. The required continuity of magnetic field lines produces sharp bends in the field lines at the inner and outer boundaries of the shocked material. The density of the shocked material is greater than the undisturbed plasma with the result that the magnetic field trapped in the shocked plasma is also greater than the ambient interplanetary field. The increased magnetic field and the sharp bends in the field lines at the shock front serve to reflect cosmic rays and to lower the galactic cosmic-ray density in the expanding volume behind the shock, as in the Gold model. In the Parker 'blast wave' model, however, the magnetic field lines are not simply closed and, in contrast with the Gold 'magnetic bottle,' are directly connected to the ambient magnetic field in the undisturbed region.

McCracken (1962) has made a careful analysis of the cosmic-ray flare effect with particular emphasis on those relatively rare events which produced energetic solar particles in sufficient quantity to be

easily observed by ground-based neutron monitors. By computing the effect of geomagnetic bending of the primary particle trajectories and thereby determining the mean directions of viewing for several neutron monitoring stations, he was able to relate the observed anisotropy of solar-produced cosmic rays to the interplanetary magnetic field. While confirming the general spiral configuration of the interplanetary field and providing some information on small scale irregularities, his observations were not incompatible with either the Gold 'bottle' or Parker 'blast wave' models.

CHAPTER II

ANALYTICAL METHODS FOR THE STUDY OF EXPERIMENTAL

COSMIC RAY DATA

2.1 Introduction.

The result of a cosmic ray experiment is often given simply as a
time-history function of one of the experimentally determined quantities.
Although direct examination of such a time-history may be sufficient
to establish the physical significance of the results, a number of
analytical techniques are commonly used to give less subjective measures
of important physical parameters. This is particularly true in studies
involving the search for hidden periodicities or quasi-periodic recurrent
structures, typical methods being harmonic analysis on a finite interval
and Chree's superposed epoch analysis.

Beginning with the work of Wiener (1949) new methods for the
analysis of time series have been developed which have enjoyed great
success in many widely differing fields. Known collectively as generalized
Fourier techniques, these methods have not, as yet, found as great an
application in the study of cosmic ray data as they deserve. One of
the objectives of the present study is to find ways of making use of
these powerful techniques for the study of cosmic ray anisotropies,
periodicities, and recurrence tendencies.

In the immediately following expository sections, it is assumed
that the data to be investigated are in the form of a continuous

time-history function defined on an infinite interval. The complications introduced by finite data sampling, that is, data available only as a finite, discrete time series, and by the addition of statistically random variation are deferred to the last sections of this chapter.

2.2 Spectral analysis.

If the time-history function f(t) is finite and is non-zero only on the interval t = 0 to t = T and has only a finite number of discontinuities, then it is resolved into its cisoidal components by Fourier transformation (F.T.) as

$$f(t) = \int_{-\infty}^{\infty} F(\omega) e^{i\omega t} \frac{d\omega}{2\pi} = F.T.^{-1}\left[F(\omega)\right]$$

where

$$F(\omega) = \int_{-\infty}^{\infty} f(t) e^{-i\omega t} dt = F.T.\left[f(t)\right]$$

Since f(t) is non-zero only on a finite interval, its Fourier transform may be computed even if it is a random noise function. The total energy carried by f(t) (as if it were a voltage applied to a resistance of one ohm) is

$$E_T = \int_{-\infty}^{\infty} f^2(t) dt = \int_{0}^{T} f^2(t) dt = \int_{-\infty}^{\infty} \frac{|F(\omega)|^2}{2\pi} d\omega$$

and the average power (in the same sense) is

$$S_T = \frac{E_T}{T} = \frac{1}{T} \int_{-\infty}^{\infty} \frac{|F(\omega)|^2}{2\pi} d\omega$$

From this the spectral power per unit radian frequency interval is identified as

$$S(\omega, T) = \frac{1}{2\pi T} |F(\omega)|^2$$

(Blackman and Tukey, 1958). For f(t) non-zero for all time, the spectral power density function may be written as

$$S(\omega) = \lim_{T \to \infty} \frac{1}{2\pi T} |F(\omega)|^2$$

if the limit converges. For many interesting examples, the limit does fail to converge (Davenport and Root, 1958). Even these cases may be included if the limiting process is more carefully specified as follows (Bennett, 1956)

$$S(\omega) = \lim_{\Delta\omega \to 0} \frac{1}{\Delta\omega} \left\{ \lim_{T \to \infty} \frac{1}{2\pi T} \int_{\omega - \Delta\omega/2}^{\omega + \Delta\omega/2} S(\omega, T)\, d\omega \right\}$$

That is, the spectral density over the finite time interval T is averaged over some small frequency interval, $\Delta\omega$, before the limit as $T \to \infty$ is taken. Then, $\Delta\omega$ is allowed to approach zero. $S(\omega)$ is commonly called simply the power spectrum of f(t).

Let the autocovariance function evaluated on the interval t = 0 to t = T be defined as

$$R(\tau, T) = \frac{1}{T} \int_0^T f(t) f(t+\tau)\, dt$$

Or, using the Fourier transform of f(t) and f(t+τ),

$$R(\tau, T) = \frac{1}{2\pi T} \int_0^T f(t)\, dt \int_{-\infty}^{\infty} F(\omega) e^{i\omega(t+\tau)}\, d\omega$$

$$= \frac{1}{2\pi T} \int_{-\infty}^{\infty} F(\omega) e^{i\omega\tau}\, d\omega \int_0^T f(t) e^{i\omega t}\, dt$$

$$= \frac{1}{2\pi T} \int_{-\infty}^{\infty} F(\omega) F(-\omega) e^{i\omega\tau}\, d\omega$$

$$= \int_{-\infty}^{\infty} S(\omega, T) e^{i\omega\tau}\, d\omega$$

In the limit as T→∞ (the same reservations made above in passing to the limit apply here also and the solution to the difficulty the same)

$$R(\tau) = \int_{-\infty}^{\infty} S(\omega) e^{i\omega\tau} d\omega$$

$$S(\omega) = \frac{1}{2\pi} \int_{-\infty}^{\infty} R(\tau) e^{-i\omega\tau} d\tau$$

so that $R(\tau)$ and $S(\omega)$ are a Fourier transform pair (Lee, 1960).

As the power spectrum of a time-history function is the Fourier transform of its autocovariance function, so the Fourier transform of the cross-covariance function of two different time-history functions defines their cross-spectral density function (cross-power spectrum). If x(t) and y(t) are the time-history functions, their cross-covariance and cross-spectrum are, respectively,

$$R_{xy}(\tau) = \int_{-\infty}^{\infty} x(t) y(t+\tau) dt$$

$$S_{xy}(\omega) = F.T.\left[R_{xy}(\tau)\right]$$

Since

$$R_{xy}(\tau) = R_{yx}(-\tau)$$

then

$$S_{xy}(\omega) = S_{yx}^{*}(\omega)$$

where ✳ denotes complex conjugation. In the same manner that the

power spectrum of a function f(t) may be interpreted as the power per

unit frequency interval which would be delivered to a one ohm resistor

by a voltage f(t), so may one interpret the cross-power spectrum of

two functions x(t) and y(t) as the power per unit frequency interval

delivered to an impedance for which an applied voltage of x(t) causes

a current y(t) to flow. In contrast to the power spectrum, which is

real and symmetric about ω =0 for f(t) any real function for which a

spectrum exists, the cross spectrum of two real functions is, in

general, complex and asymmetric. The magnitude of S_{xy} measures the

(magnitude of) coherent power per unit frequency interval in x(t) and

y(t) while the argument of S_{xy} measures, as a function of radian

frequency, the relative phase angle between the two functions. If the

functions have no cross-correlation (so that their cross-covariance is

zero for all τ) then $S_{xy} \equiv 0$ and the functions are said to be completely

incoherent (Lee, 1960).

2.3 Linear filtering.

Let f(t) be convolved with h(t) to form g(t). That is

$$g(t) = \int_{-\infty}^{\infty} f(\tau) h(t-\tau) d\tau$$

The Fourier transform of g(t) is, by the Fourier convolution theorem,

$$F.T. \left[g(t) \right] = F(\omega) H(\omega)$$

where

$$F(\omega) = F.T. \left[f(t) \right]$$

$$H(\omega) = F.T. \left[g(t) \right]$$

Hence, the power spectrum of g(t) is

$$S_g(\omega) = S_f(\omega) \, |H(\omega)|^2$$

Such an operation, modifying the original power spectrum of a function by a multiplicative function, is said to be a filtering operation and $|H(\omega)|^2$ is known as the gain-frequency characteristic of the filter function h(t). $H(\omega)$ is the complex transfer function of the operation (Blackman and Tukey, 1958). Several relationships are noted:

(a) If h(t) is normalized so that

$$\int_{-\infty}^{\infty} h(t)\,dt = 1$$

then

$$H(0) = 1$$
$$|H(0)|^2 = 1$$

(b) More generally, the value of the transfer function $H(\omega)$ at $\omega = 0$ is equal to the area under the h(t) weighting function curve.

(c) If h(t) is real and symmetric about t=0, then $H(\omega)$ is real and the filtering operation introduces no phase shifts other than simple phase reversals.

(d) The gain-bandwidth product of the filtering operation, defined most generally as

$$G.B.\,[\,h(t)\,] = \int_{-\infty}^{\infty} |H(\omega)|^2\,d\omega$$

is related to the value of h(t) at t=0 by

$$G.B.\,[\,h(t)\,] = 2\pi\,h(0)$$

(e) The time-bandwidth invariance property is given by

$$G.B.[h(kt)] = \frac{1}{k} G.B.[h(t)]$$

(f) The rise time of a filter, that is, the time required for

$$g(t) = \int_{-\infty}^{\infty} f(\tau) h(t-\tau) d\tau$$

to rise from zero to one when f(t) is the Heavyside unit step function, is given approximately by

$$Rise\ time \approx \frac{1}{G.B.}$$

for filters having normalized weighting functions.

As a special case, consider the filtering operation having a weighting function

$$h(t) = \frac{1}{T} \qquad -\frac{T}{2} \leq t \leq \frac{T}{2}$$

$$h(t) = 0 \qquad elsewhere$$

The output function

$$g(t) = \int_{-\infty}^{\infty} f(\tau) h(t-\tau) d\tau$$

$$= \int_{-\infty}^{\infty} h(\tau) f(t-\tau) d\tau$$

$$= \frac{1}{T} \int_{-T/2}^{T/2} f(t-\tau) d\tau$$

is recognized as the result of a centered moving average over the time

interval T. The transfer function is given by

$$H(\omega) = F.T.[h(t)]$$

$$= \int_{-\infty}^{\infty} h(t) e^{-i\omega t} dt$$

$$= \frac{1}{T} \int_{-\infty}^{\infty} e^{-i\omega t} dt$$

$$= \frac{\sin(\omega T/2)}{(\omega T/2)}$$

and the gain function by

$$|H(\omega)|^2 = \frac{\sin^2(\omega T/2)}{(\omega T/2)^2}$$

The transfer function is the well-known diffraction function having a value of unity at ω = 0 and zeros at

$$\omega = \frac{2n\pi}{T} \qquad n = 1, 2, 3, \cdots$$

Superposition analysis, a particular form of Chree's superposed epoch analysis, may readily be formulated as a convolution filter. The analysis is usually carried out by dividing the experimental time-history function into contiguous segments of uniform length and superposing by summing the segments. Clearly such a process will accentuate any long-lasting periodic components having periods related to the length of the segments, while suppressing random components and other periodic components. Convolution of the time-history function f(t) with a

weighting function h(t) defined as

$$h(t) = \sum_{n=-M/2+1/2}^{n=M/2-1/2} \delta(t-n\tau) \qquad M = \text{odd integer}$$

to form the filtered output function x(t), thus,

$$x(t) = \int_{-\infty}^{\infty} \sum_{n=-M/2}^{n=M/2} \delta(\sigma-n\tau) f(t-\sigma) \, d\sigma$$

where δ(t) is the Dirac impulse function, will achieve the superposi-
tion by summation of M segments of f(t) each of length τ. To find the
transfer function of the filter note that h(t) may be written as the
product of an infinite Dirac impulse comb with spacing τ and a rectangular
pulse function of duration T = Mτ, thus,

$$h(t) = k(t) \sum_{n=-\infty}^{\infty} \delta(t-n\tau)$$

$$k(t) = 1 \qquad -T/2 \le t \le T/2 \qquad T = M\tau$$

$$k(t) = 0 \qquad \text{elsewhere}$$

The Fourier transform of the infinite comb is evaluated as

$$D(\omega) = \int_{-\infty}^{\infty} \sum_{n=-\infty}^{\infty} \delta(t-n\tau) e^{-i\omega t} \, dt$$

$$= \sum_{n=-\infty}^{\infty} \delta(\omega - 2\pi n/\tau)$$

and of k(t) as

$$k(\omega) = \frac{\sin(\omega T/2)}{(\omega T/2)}$$

so that, the transform of a product of two functions being the
convolution of their individual transforms, one has for H(ω), the

filter transfer function,

$$H(\omega) = \int_{-\infty}^{\infty} D(\sigma) k(\omega - \sigma) d\sigma$$

$$= \sum_{n=-\infty}^{\infty} \frac{\sin\left[\frac{T}{2}(\omega - 2\pi n/\tau)\right]}{\left[\frac{T}{2}(\omega - 2\pi n/\tau)\right]}$$

If $T \gg \tau$ (that is $M \gg 1$) so that $(\frac{1}{\tau}) \gg (\frac{1}{T})$ then the individual terms in the above expression have negligible overlap and the transfer function is easily interpreted. Each of the terms represents a band-pass region with the basic $\frac{\sin X}{X}$ shape centered on $\omega = \frac{2\pi n}{\tau}$ and having a bandwidth $\Delta \omega \approx \frac{2\pi}{T}$ much smaller than their spacing, $\frac{2\pi}{\tau}$. The band-pass region centered on $\omega = 0$ (i.e., n=0) passes components of near zero frequency while the band-pass regions corresponding to n = $\pm 1, \pm 2, \ldots$ pass the fundamental wave having a period of τ and all of its harmonics. All other frequencies not lying in the near neighborhood of $\omega = \frac{2\pi n}{\tau}$, n=0, $\pm 1, \pm 2, \ldots$ are attenuated. The effect is to pass only those periodic waveforms which can be expressed as a Fourier sum of the form

$$X(t) = \sum_{n=-\infty}^{\infty} a_n e^{2\pi i \frac{nt}{\tau}}$$

2.4 Inverse filtering.

It is not uncommon that the time-history function which is available as the output of an experiment has already suffered one or more convolution filtering operations of the type described in the preceding section. The source of these pre-filterings may be within the physical phenomenon under study or within the instrument itself, since

all linear operations on a time-history function may be expressed as a convolution, or perhaps some preliminary data processing has been done, such as a moving average being taken. Often it is not possible to obtain unfiltered data because the instrumental filtering may be quite basic to the nature of the type of measurement being made and not subject to alteration. The question arises: Can a linear filter be constructed which will undo the work of the prefilters? In most situations this is not possible in the strictest sense; however, workable approximations are usually possible. For any such work it is, of course, necessary to know to some degree of approximation the time weighting function of the prefilter or its transfer function.

Taking h(t) as the weighting function of the prefilter and $H(\omega)$, the Fourier transform of h(t), as the transfer function, then if f(t) is the (unavailable) original time-history function one has

$$g(t) = \int_{-\infty}^{\infty} h(t-\tau) f(\tau) \, d\tau$$

$$G(\omega) = F.T. \left[g(t) \right] = F.T. \left[f(t) \right] H(\omega) = F(\omega) H(\omega)$$

so that

$$F(\omega) = H^{-1}(\omega) \, G(\omega)$$

$$f(t) = F.T.^{-1} \left[H^{-1}(\omega) \, G(\omega) \right]$$

$$f(t) = \int_{-\infty}^{\infty} k(t-\tau) \, g(\tau) \, d\tau$$

where

$$k(t) = F.T.^{-1} \left[H^{-1}(\omega) \right]$$

is the desired weighting function of the inverse filtering operation.
The difficulty with the above inversion is that $H(\omega)$ will almost
certainly have zeros and thus the inverse Fourier transform will not
exist.

The most satisfactory solution to this dilemma is to define a new
function $L(\omega)$ which is unity in the regions of interest and zero else-
where. If the frequency region of interest does not contain any of the
zeros of $H(\omega)$, then an inverse filter weighting function for these
frequencies alone is given by

$$k(t) = F.T.^{-1} \left[\frac{L(\omega)}{H(\omega)} \right]$$

where the quotient is taken as zero wherever $L(\omega)$ is zero. Given a
number of prefiltering operations with transfer functions H_1, H_2, H_3 . . .
H_N, then a single inverse weighting function for the total effect of all
prefilters is given by

$$k(t) = F.T.^{-1} \left[\frac{L(\omega)}{H_1(\omega) H_2(\omega) \cdots H_N(\omega)} \right]$$

or in terms of the weighting functions of the prefilters, $h_1(t)$, $h_2(t)$,
. . . $h_N(t)$,

$$k(t) = F.T.^{-1} \left[\frac{L(\omega)}{F.T.[h_1(t) * h_2(t) * \cdots h_N(t)]} \right]$$

where $*$ denotes convolution (Stokes, 1948; George, et al., 1962; Burch,
et al., 1964; Treitel and Robinson, 1964).

2.5 Heterodyning.

The Fourier transform of

$$g(t) = e^{i\omega_0 t} f(t)$$

is given by

$$G(\omega) = \int_{-\infty}^{\infty} e^{-i\omega t} e^{i\omega_0 t} f(t)\, dt$$

$$= \int_{-\infty}^{\infty} e^{-i(\omega - \omega_0)t} f(t)\, dt$$

$$= F(\omega - \omega_0)$$

where

$$F(\omega) = \int_{-\infty}^{\infty} e^{-i\omega t} f(t)\, dt$$

is the Fourier transform of $f(t)$. Hence, the power spectrum of $g(t)$ may be related to $S_f(\omega)$, the power spectrum of $f(t)$, by

$$S_g(\omega) = S_f(\omega - \omega_0)$$

showing that the net result of multiplication of a function by $e^{i\omega_0 t}$ is to shift its spectrum by an amount ω_0. Spectral components in the neighborhood of ω_0 in S_f lie in the neighborhood of zero frequency in S_g. It follows that the spectrum of

$$f(t) \cos \omega_0 t = \frac{1}{2}(e^{i\omega_0 t} + e^{-i\omega_0 t}) f(t)$$

is

$$\frac{1}{2}\left[S_f(\omega-\omega_o) + S_f(\omega+\omega_o) \right]$$

and the spectrum of

$$f(t) \sin \omega_o t = \frac{1}{2i}\left(e^{i\omega_o t} - e^{-i\omega_o t} \right)$$

is

$$\frac{1}{2i}\left[S_f(\omega-\omega_o) - S_f(\omega+\omega_o) \right]$$

(Blackman and Tukey, 1958).

2.6 Modulation and demodulation.

Given a time-history function of the form

$$f(t) = A(t) \cos\left(\omega_o t + \phi(t) \right)$$

$$= \frac{A(t)}{2}\left[e^{i\left(\omega_o t + \phi(t)\right)} + e^{-i\left(\omega_o t + \phi(t)\right)} \right]$$

that is, a cosinusoid amplitude modulated by A(t) and phase modulated by ϕ(t), let it be desired to recover A(t) and ϕ(t) from f(t). Suppose that A(t) and ϕ(t) are slowly varying functions compared with cos ω_ot so that the modulation products lie in a spectral region $\Delta\omega$ about ω_o much smaller than ω_o . Demodulation is effected most simply by heterodyning, to center the region $\Delta\omega$ about zero frequency, and subjecting the result to a low-pass convolution filtering operation. Thus, heterodyning by ω_o ,

$$g(t) = f(t) e^{i\omega_o t}$$

$$= \frac{A(t)}{2} e^{i\left(2\omega_o t + \phi(t)\right)} + \frac{A(t)}{2} e^{-i\phi(t)}$$

The heterodyned function g(t) is composed of two terms, the first being oscillatory with radian frequency $\approx 2\omega_0$, the second with radian frequency $\frac{d\phi}{dt} \ll 2\omega_0$. If now g(t) is convolved with a weighting function h(t) such that its Fourier transform $H(\omega)$ is unity in the neighborhood $\Delta\omega$ of $\omega = 0$ and zero elsewhere, the result

$$\bar{g}(t) = \int_{-\infty}^{\infty} h(\tau) g(t-\tau) d\tau$$

will effectively contain only the second term of g(t).

$$\bar{g}(t) = \frac{A(t)}{2} e^{-i\phi(t)}$$

The recovery of the modulating functions is now easily made.

$$A(t) = 2 |\bar{g}(t)|$$

$$\phi(t) = -\arg \bar{g}(t)$$

Simultaneous modulation in both amplitude and phase is often called complex modulation and the recovery process just described, complex demodulation (Bogert, et al., 1963).

The phase and amplitude of a spectral component may also be determined by harmonic analysis of a finite portion of the time-history function equal in length to the period of the component being examined. Separate, independent estimates of the phase and amplitude, may be made for each of many non-overlapping, contiguous segments of data, allowing changes in the amplitude and phase parameters to be traced out in time. For this one writes (for any one segment of data of length $T = \frac{2\pi}{\omega_0}$)

$$f(t) = \sum_{n=-\infty}^{\infty} C_n e^{-i\omega_n t} \qquad \omega_n = \frac{2\pi n}{T}$$

where

$$C_n = \frac{1}{T} \int_{-T/2}^{T/2} f(\tau) e^{i\omega_n \tau} d\tau$$

C_n is the complex amplitude of the Nth harmonic. The integrand of the above expression is simply f(t) heterodyned by ω_n while the integration is the same as convolution of the integrand with a weighting function D(t) of the form

$$D(t) = \frac{1}{T} \qquad -\frac{T}{2} \leqslant t \leqslant \frac{T}{2}$$

$$D(t) = 0 \qquad elsewhere$$

the result being evaluated at t=0. Hence, the commonly used method of moving harmonic analyses of a data function to measure phase and amplitude variations in a particular spectral component is equivalent to the heterodyning, filtering process described above as complex demodulation, with the filter weighting function being taken as a simple rectangular pulse of amplitude $\frac{1}{T}$ and duration T. The resulting transfer function is the familiar diffraction function discussed in Section 2.3 of this chapter.

2.7 Sampled data.

If in recording an experimental time-history function the continuous data function is sampled at instants, equal-spaced in time, and only these values noted, the resulting time series may be described by the product of the original time-history function, f(t), and a sampling function. Thus

$$f_s(t) = f(t) \sum_{n=-\infty}^{\infty} \delta_1(t - n\tau)$$

where

$$\delta_1(t) = 1 \qquad t = 0$$

$$\delta_1(t) = 0 \qquad \text{elsewhere}$$

and Υ is the sampling interval. The spectrum of the sampled function, f_s, may be related to the spectrum of the original time-history function, since multiplication in the time domain corresponds to convolution in the frequency domain. So, letting

$$F.T. [f(t)] = F(\omega)$$

$$F.T. [f_s(t)] = F_s(\omega)$$

and noting that

$$F.T. \left[\sum_{n=-\infty}^{\infty} \delta_1(t-n\Upsilon) \right] = \sum_{n=-\infty}^{\infty} \delta_1(\omega - n \frac{2\pi}{\Upsilon})$$

one finds

$$F_s(\omega) = \int_{-\infty}^{\infty} F(\sigma) \sum_{n=-\infty}^{\infty} \delta_1(\omega - \sigma + n \frac{2\pi}{\Upsilon}) \, d\sigma$$

or, exchanging the order of integration and summation,

$$F_s(\omega) = \sum_{n=-\infty}^{\infty} \int_{-\infty}^{\infty} F(\sigma) \delta_1(\omega - \sigma + n \frac{2\pi}{\Upsilon}) \, d\sigma$$

From the definition of δ_1, the convolution integral is easily evaluated giving

$$F_s(\omega) = \sum_{n=-\infty}^{\infty} F(\omega - n \frac{2\pi}{\Upsilon})$$

The term in this summation for n=0 gives simply $F(\omega)$, the original Fourier spectrum, while the other terms represent replicas of $F(\omega)$ shifted on the ω-axis by $n \frac{2\pi}{\Upsilon}$. By virtue of the relationship between the Fourier spectrum and the power spectrum, a similar expression gives

the power spectrum of the sampled function,

$$S_s(\omega) = \sum_{n=-\infty}^{\infty} S(\omega - n\frac{2\pi}{\tau})$$

where $S(\omega)$ is the original and $S_s(\omega)$ the sampled function power spectrum. If $S(\omega)$ is non-zero only in the region $-\frac{\pi}{\tau} \leqslant \omega \leqslant \frac{\pi}{\tau}$, the replica spectra which constitute $S_s(\omega)$ do not overlap and the application of a low-pass convolution filter having unity response in the region $-\frac{\pi}{\tau} \leqslant \omega \leqslant \frac{\pi}{\tau}$ and, zero response elsewhere, passes only the unshifted portion of $S_s(\omega)$ [simply $S(\omega)$] and thus recovers exactly the original time-history function. On the other hand, if the spectrum of $f(t)$ is wider than $\frac{2\pi}{\tau}$, overlapping between the original spectrum and the other, shifted, replica spectra occurs. Application of the ideal low-pass filter described above then fails to remove entirely the shifted spectra and $f(t)$ can not be exactly recovered from $f_s(t)$. The contamination of the spectrum due to overlap is known as ailiasing since spectral components with radian frequencies greater than $|\omega| = \frac{\pi}{\tau}$ (commonly called the Nyquist or folding frequency) will be reflected about the points $\omega = \pm\frac{\pi}{\tau}$ and appear as a components of lower frequency lying in the range $-\frac{\pi}{\tau} \leqslant \omega \leqslant \frac{\pi}{\tau}$, the principal spectrum region.

The common practice of averaging a time-history function over non-overlapping, contiguous time intervals of length τ and recording only these averages is best viewed as a two step process, a convolution filtering with a weighting function

$$h(t) = \frac{1}{\tau} \qquad -\frac{\tau}{2} \leqslant t \leqslant \frac{\tau}{2}$$

$$h(t) = 0 \qquad elsewhere$$

followed by sampling with spacing τ . If the original time-history

function contains spectral components with frequencies higher than

$\omega = \frac{\pi}{\tau}$, some ailiasing will occur even though the filtering operation

limits the high frequency content before sampling. This may be seen by

examining the gain function of the filter (see Section 2.3 of the

present chapter)

$$|H(\omega)|^2 = \frac{\sin^2(\omega \tau / 2)}{(\omega \tau / 2)^2}$$

from which

$$\left| H \left(\frac{\pi}{\tau} \right) \right|^2 = \frac{4}{\pi^2}$$

showing that the filter passes components near the Nyquist frequency

with only moderate attenuation in their power. If the original function

had strong spectral components with radian frequencies greater than and

near the Nyquist frequency, simple averaging and sampling will surely

result in data which is, at best, difficult to interpret. However, if

the original data has no strong components in the neighborhood of

$\omega = \frac{\pi}{\tau}$ the process may be adequate since the response of the filter falls

off as ω^{-2} beyond the Nyquist frequency. A much safer method is to

record moving averages of length τ with a sampling interval of $\frac{\tau}{2}$,

for which case the response of the filter is approximately zero in the

neighborhood of the folding frequency.

2.8 Signals and noise.

It is useful to consider an experimental time-history function as

a sum of two components, signal and noise. By "signal" one denotes some

information bearing part of the function which one desires to study and

regards the undesired remainder as "noise." As an example consider an

experiment which seeks to determine the magnitude of the cosmic-ray flux

by simply counting each cosmic-ray particle entering the instrument over some finite interval of time T. Let the true (unknown) rate be ν and take as an estimate of ν (t) the experimentally determined quantity $\frac{N(t)}{T}$ where N is the number of particles observed in time T, and a Poisson distribution of the particle arrivals is assumed for ν(t) = const. Here, the signal is ν(t) and the noise is the random variance in $\frac{N(t)}{T}$ due to the statistical nature of the arrival of particles and the finiteness of N(t) for any finite time interval.

The time-history function produced by the counting instrument is represented by a function consisting of Poisson distributed unit impulses with the probability of an impulse occurring in any interval $d\tau$ being given by $\nu(d\tau)$. The unit impulse function may be approximated by a rectangular pulse of amplitude A and duration $\Delta\tau$ and letting $A \to \infty$, $\Delta\tau \to 0$ in such a way that $A\Delta\tau = 1$ at all times. The autocovariance function of the counting function is evaluated as

$$
\begin{aligned}
R(0) &= \lim_{\substack{A \to \infty \\ A d\tau = 1}} A^2 P_{1 d\tau} \\
&= \lim_{A \to \infty} A^2 \nu \, d\tau \\
&= \lim_{A \to \infty} \nu A \\
&= \nu \, \delta(0)
\end{aligned}
$$

and, since each count is independent,

$$
\begin{aligned}
R(\tau) &= \lim_{\substack{A \to \infty \\ A \Delta\tau = 1}} A^2 P_{1 d\tau} P_{1 d\tau} \\
&= \lim_{\substack{A \to \infty \\ A \Delta\tau = 1}} A^2 \nu \, d\tau \, \nu \, d\tau \\
&= \nu^2 \qquad \tau \neq 0
\end{aligned}
$$

where $P_{1d\tau}$ is the probability of finding one impulse (count) in an interval $d\tau$. Hence,

$$R(\tau) = \nu\delta(\tau) + \nu^2$$

for $\nu(t) = $ const. The power spectrum is found by taking the Fourier transform of the autocovariance function.

$$S(\omega) = \frac{1}{2\pi} \int_{-\infty}^{\infty} (\nu\delta(\tau) + \nu^2) e^{-i\omega\tau} d\tau$$

$$S(\omega) = (\nu/2\pi) + \nu^2\delta(\omega)$$

The signal and noise are easily identified in the power spectrum. The signal, $\nu(t)$, is responsible for the impulse $\nu^2\delta(\omega)$ at $\omega = 0$ while the noise contributes the background power $\frac{\nu}{2\pi}$ constant at all frequencies. Evidently the way to extract the signal without any interference from the noise is to use a filter centered on zero frequency with vanishingly small bandwidth. In the thought experiment described, the filter employed is the unweighted moving average over time interval T which has, as pointed out before, a gain function

$$|H(\omega)|^2 = T^2 \frac{\sin^2(\omega T/2)}{(\omega T/2)^2}$$

Here the constant T appears because h(t) is unity over the interval T instead of being normalized to $\frac{1}{T}$ with the result that the filter output will be N, the number of counts in the interval, and not $\frac{N}{T}$ the experimental rate. The power spectrum of the filter output is

$$\overline{S}(\omega) = |H(\omega)|^2 S(\omega)$$

or, in terms of signal and noise components

$$\overline{S}_{sig}(\omega) = |H(\omega)|^2 \, \upsilon \, \delta(\omega)$$

$$\overline{S}_{noise}(\omega) = |H(\omega)|^2 \, \frac{\upsilon}{2\pi}$$

The signal is passed without attenuation since $|H(o)|^2 = 1$. The total variance due to noise is

$$\sigma_n^2 = \int_{-\infty}^{\infty} \overline{S}_{noise}(\omega) \, d\omega$$

$$= \frac{\upsilon}{2\pi} \int_{-\infty}^{\infty} T^2 \, \frac{\sin^2(\omega T/2)}{(\omega T/2)^2} \, d\omega$$

$$= \frac{\upsilon}{2\pi} T^2 \, \frac{2\pi}{T} = \upsilon T$$

But, $\upsilon T = \langle N \rangle$, the expected number of counts in time T, so

$$\sigma_n^2 = \langle N \rangle$$

$$\sigma_n = \sqrt{\langle N \rangle}$$

which is to say, the standard deviation of the estimate of the counts in the time interval T is the square root of the expected number of counts. This not unexpected result could have been found, perhaps more directly, through a purely probabilistic argument, but the above development indicates the flexibility of generalized Fourier methods.

When $\upsilon(t)$ is a constant, its spectral representation is, as shown above, an impulse at zero frequency. Thus one can make the filter band-width as narrow as possible (by increasing T) with the only effect being to reduce the noise contribution. If, however, $\upsilon(t)$ is not a constant

then the power spectrum of the counting function is

$$S(\omega) = V(\omega) + \frac{\nu}{2\pi}$$

V being the power spectrum of $\nu(t)$. If $V(\omega)$ is non-zero only in some region $\Delta\omega$ about zero frequency then, obviously, the bandwidth of the averaging filter may be reduced only to this limit without attenuating some spectral components of the signal. In such a case the noise contribution may be reduced to some minimum, but not eliminated entirely, the variance of the noise contribution being always

$$\sigma^2 = \frac{\nu}{2\pi} \int_{-\infty}^{\infty} |H(\omega)|^2 d\omega$$

2.9 Optimum filters.

The last example of the preceding section suggests the following question: If the spectra of the signal and noise components of an experimental time-history function overlap, so that no clear separation in the frequency domain is possible, what is the linear filtering operation that maximizes the signal to noise ratio? The methods which may be used to solve problems of this sort were first given by Kolmogoroff (1941) and Wiener (1949). The following treatment is essentially that of Lee (1960).

Let the time-history function f(t) be the sum of a signal h(t) and noise n(t). A linear filter with weighting function k(t) is sought such that its output x(t), resulting from the input of f(t), is optimum in the least mean square sense, that is, $\langle \epsilon^2 \rangle$ defined by

$$\langle \epsilon^2 \rangle = \langle [h(t) - x(t)]^2 \rangle$$

is a minimum or, in terms of the filtering operation,

$$\langle \epsilon^2 \rangle = \lim_{T \to \infty} \frac{1}{T} \int_{-T/2}^{T/2} \left[\int_{-\infty}^{\infty} k(\tau) f(t-\tau) d\tau - h(t) \right]^2 dt$$

which becomes, after expanding the squared expression and inverting the order of integration,

$$\langle \epsilon^2 \rangle = \int\int_{-\infty}^{\infty} k(\tau) k(\sigma) R_f(\tau-\sigma) d\tau d\sigma - 2 \int_{-\infty}^{\infty} k(\tau) R_{fh}(\tau) + R_h(0)$$

where R_f and R_h are the autocovariance functions of f and h respectively, and R_{fh} is the cross-covariance function of f and h. Now suppose $k(\tau)$ is the optimum filter function having mean square error E and let any other weighting function be given by $k(\tau) + \delta k(\tau)$ and have mean square error E'. Then

$$E' = \int\int_{-\infty}^{\infty} \left[k(\tau) + \delta k(\tau) \right] \left[k(\sigma) + \delta k(\sigma) \right] R_f(\tau-\sigma) d\tau d\sigma$$

$$- 2 \int_{-\infty}^{\infty} \left[k(\tau) + \delta k(\tau) \right] R_{fh}(\tau) d\tau + R_h(0)$$

which becomes, upon expanding and noting that R_f is an even function,

$$E' = E + 2 \int_{-\infty}^{\infty} \delta k(\tau) d\tau \left[\int_{-\infty}^{\infty} k(\sigma) R_f(\tau-\sigma) d\sigma - R_{fh}(\tau) \right]$$

$$+ \int\int_{-\infty}^{\infty} \delta k(\tau) \delta k(\sigma) R_f(\tau-\sigma) d\tau d\sigma$$

The last term may be written, by use of the definition of R_f, as

$$\lim_{T \to \infty} \int_{-T/2}^{T/2} \left[\int_{-\infty}^{\infty} \delta k(\tau) f(t-\tau) d\tau \right]^2 dt$$

which is $\geqslant 0$ for all k and f. Thus a necessary and sufficient condition that $E \leqslant E'$ (so that E is truly the least mean square error) is that the middle term in the above expression for E' vanish. That is,

$$\int_{-\infty}^{\infty} k(\sigma) R_f(\tau-\sigma) d\sigma = R_{fh}(\tau)$$

This equation (a Wiener-Hopf equation of the first type) may be solved for $k(\sigma)$ on the interval $-\infty \leqslant \sigma \leqslant \infty$ by Fourier transform techniques. Thus, taking the transform of the above equation,

$$\int_{-\infty}^{\infty} e^{-i\omega\tau} \int_{-\infty}^{\infty} k(\sigma) R_f(\tau-\sigma) d\sigma = \int_{-\infty}^{\infty} e^{-i\omega\tau} R_{fh} d\tau$$

or, letting $t = \tau - \sigma$ and rearranging,

$$\int_{-\infty}^{\infty} e^{-i\omega\sigma} k(\sigma) d\sigma \int_{-\infty}^{\infty} e^{-i\omega t} R_f(t) dt = \int_{-\infty}^{\infty} e^{-i\omega\tau} R_{fh} d\tau$$

or

$$K(\omega) P_f(\omega) = P_{fh}(\omega)$$

where $K(\omega)$ is the Fourier transform of $k(\tau)$, $P_f(\omega)$ is the power spectrum of $f(t)$ and $P_{fh}(\omega)$ is the cross-power spectrum of $f(t)$ and $h(t)$. It follows that

$$K(\omega) = \frac{P_{fh}(\omega)}{P_f(\omega)}$$

and

$$h(t) = \frac{1}{2\pi} \int_{-\infty}^{\infty} e^{i\omega t} K(\omega) d\omega$$

If, as is most often the case, the signal and noise are not correlated, then

$$P_{fh} = P_h$$

$$P_f = P_h + P_n$$

and

$$K(\omega) = \frac{P_h(\omega)}{P_h(\omega) + P_n(\omega)}$$

As an example consider a signal whose power spectrum is a constant, A, in the region $-B \leq \omega \leq B$ and zero elsewhere, immersed in noise of power N, constant at all frequencies. Then,

$$K_{opt.} = \frac{A}{A+N} \qquad -B \leq \omega \leq B$$

$$= 0 \qquad\qquad \text{elsewhere}$$

showing that the optimum filter is an ideal low-pass filter with an attenuation (in power) of $\left(\dfrac{A}{A+N}\right)^2$ in the pass region. The shape of the optimum filter's response is not surprising, but the fact that its power gain in the pass region should be less than unity for all $N > 0$ would have been more difficult to predict intuitively.

In the limiting case of small signal to noise ratio, the expression for the transfer function of the optimum filter may be simplified to

$$K(\omega) = \frac{P_h(\omega)}{P_n(\omega)} \qquad \left(\frac{P_h}{P_n}\right) \ll 1$$

or, for constant power noise as above,

$$K(\omega) = \left(\frac{1}{N}\right) P_h(\omega) \qquad \left(\frac{P_h}{P_n}\right) \ll 1$$

showing that the optimum transfer function has the same shape as the signal function itself. This sort of filter, called a matched filter, is often used when the expected signal to noise ratio is small; however, it should be noted that it is optimum only in the limit of this ratio being small and when used with strong signals will generate needless errors.

In most experimental situations, the power spectra of the signal and the noise are not well known so that it is futile to attempt an exact solution to the Wiener-Hopf equation, even though, with the advent of high speed electronic computing, excellent numerical solutions are available for any given signal and noise power distributions. The best use of the theory of optimum filters is then to serve as a guide, through the study of simple examples such as the one given above, for more intuitive approaches.

CHAPTER III

THE ANALYSIS OF NEUTRON MONITOR DATA FOR

PERSISTENT ANISOTROPIES

3.1 The neutron monitor.

Energetic cosmic-ray primary particles impinging upon the top

of the atmosphere interact with air nuclei to yield high energy mesons,

nucleons, fragmented nuclei, and photons. The nucleons and fragments

in turn collide with other nuclei producing more nucleons and fragments.

This nucleonic cascade continues until the daughter products possess

insufficient energy to continue the process. The neutron population so

produced in the upper atmosphere decreases exponentially with

atmospheric depth beyond that depth where production effectively

ceases (Simpson et al., 1953).

At near sea-level atmospheric depths the neutron component of the

cosmic-ray induced nucleonic cascade has suffered many elastic collisions

with air nuclei and therefore has a degraded energy distribution. A

suitable detector for this neutron flux is the $B^{10} F_3$ proportional counter

which utilizes the reaction

$$_5B^{10} + n \rightarrow \, _3Li^7 + \, _2He^4 + 2.5 \; MeV$$
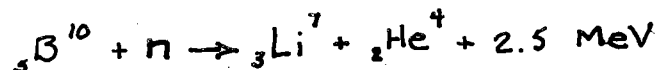
This reaction has a cross-section inversely proportional to the neutron

velocity and thus is well suited for the detection of thermal neutrons.

Instruments intended for cosmic-ray work usually are surrounded with layers of a moderator, such as paraffin or polyethylene, to complete the thermalization of the neutrons and to act as neutron reflectors, and lead to increase the counting rate by local secondary neutron production and to act as a shield against natural radioactivity to which the counters are sensitive (Simpson et al., 1953; Hatton and Carmichael, 1964). Additional discrimination against background radiation is often obtained by utilizing the proportional nature of the counters through pulse-amplitude discrimination to eliminate events with energies much less than 2.5 MeV.

The raw data from a neutron monitoring station is typically recorded as hourly count totals along with an accurate indication of barometric pressure. The totals must be corrected for the effect of the mass of the overlying atmosphere, as indicated by the barometric pressure. This correction is relatively large ($\approx 0.7\%$/mmHg) making very accurate pressure measurements necessary, but since this is the only meteorological correction which must be made (Simpson and Fagot, 1953), the neutron monitor is superior in its freedom from atmospheric variational effects when compared to the meson monitor which is dependent upon the atmospheric structure and not merely upon the total overlying mass. The neutron monitor is sensitive to primary particles with energies as low as 1 GeV making its lower energy response threshhold a strong function of geomagnetic latitude, since the vertical geomagnetic cut-off energy for primary protons varies from about 13 GeV at the geomagnetic equator to vanishingly small values near the magnetic poles. This feature is valuable in determining the primary energy dependence of

cosmic-ray events by comparing data recorded simultaneously at stations having differing geomagnetic latitudes.

A world net of cosmic-ray neutron monitoring stations has existed in some form since the mid-1950's with one or two pioneering stations existing before that time. The oldest monitors, usually known as IGY-type monitors, have counting rates of about 40,000/hr at mid-latitudes and sea-level. More recently much larger monitors (type NM-64) have been constructed following a design by Carmichael (Hatton and Carmichael, 1964). These new monitors yield counting rates in excess of 500,000/hr at sea-level, mid-latitude sites. The newer stations are usually equipped for automatic data recording and will operate for extended periods unattended, making it possible to place them in relatively remote locations. The data reduction is often accomplished by high-speed electronic data processors, resulting in a substantial reduction in the time between the occurrence of an event and the availability of corrected data. Two such stations are currently operated by the Cosmic Ray Group of the Southwest Center for Advanced Studies. These stations are located at Dallas, Texas, and Ft. Churchill, Manitoba, Canada. A typical cross-section of these detectors is shown in Figure 1. In addition to data from these two stations, a large library of neutron monitor data from many other co-operating institutions is maintained on IBM computer cards. Table I lists the names, locations, and other pertinent information of the stations used in this study.

3.2 Characteristics of persistent anisotropies.

The absorbing qualities of the earth and its atmosphere restrict the view of the neutron monitor to a more or less narrow cone centered on
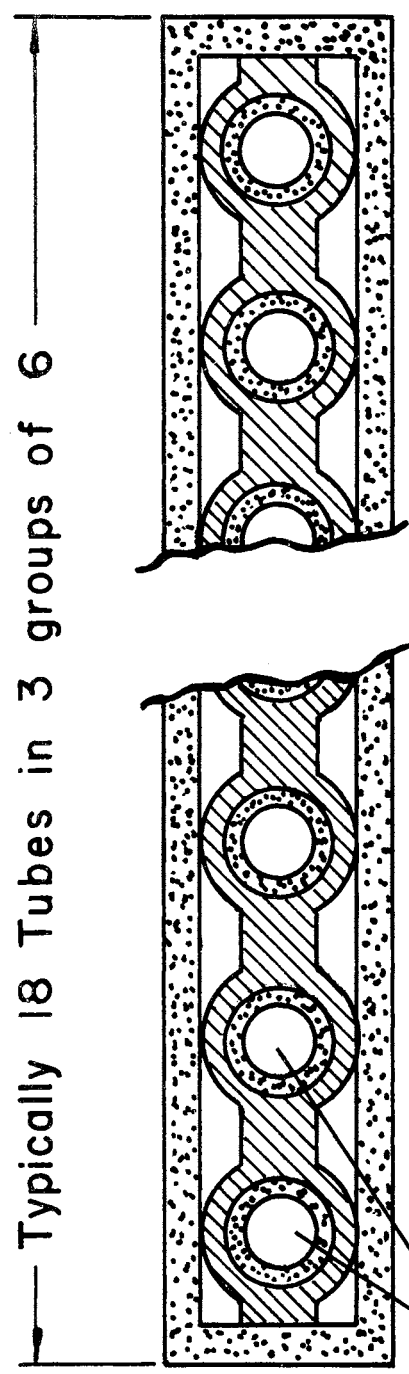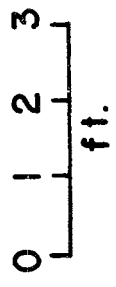
Typically 18 Tubes in 3 groups of 6

0 1 2 3
ft.

POLYTHELENE

LEAD

$B^{10}F_3$ proportional counter tubes :
stainless steel walls; ≈ 6 in. dia.;
≈ 6' long

Figure 1. Cross-Section of NM-64 Neutron Monitor.

TABLE I

NEUTRON-MONITOR STATIONS

Station	Type	Location	Geographic Latitude (N)	Geographic Longitude (E)	Elevation (M)	Cut-off Rigidity(GV)
Calgary	NM-64	Canada	51.08	-114.09	1140	1.09
Churchill	NM-64	Canada	58.75	- 94.09	39	0.21
Climax	IGY	USA	39.37	-106.18	3400	3.03
Dallas	NM-64	USA	32.78	- 96.80	130	4.35
Deep River	NM-64	Canada	46.10	- 77.50	145	1.02
Goose Bay	NM-64	Canada	53.33	- 60.42	SL	0.52
Inuvik	NM-64	Canada	68.35	-133.73	SL	0.18
Kerguelen	NM-64	South Indian Ocean	-49.35	70.22	SL	1.19
Leeds	NM-64	England	53.82	- 1.55	100	2.20
London	IGY	England	51.53	- 0.09	SL	2.73
Mawson	IGY	Antarctica	-67.60	62.88	15	0.22
Mt. Norikura	IGY	Japan	36.12	137.56	2770	11.39
Mt. Washington	IGY	USA	44.30	- 71.30	1917	1.24
Mt. Wellington	IGY	Tasmania	-42.92	147.24	725	1.89
Ottawa	IGY	Canada	45.40	- 75.60	101	1.08
Resolute	IGY	Canada	74.69	- 94.91	17	0.05
Sulphur Mt.	NM-64	Canada	51.20	-115.61	2283	1.14
Uppsula	IGY	Sweden	59.85	17.92	SL	1.43
Wilkes	IGY	Antarctica	-66.42	110.45	SL	0.05
Zugspitze	IGY	Germany	47.42	10.98	2960	4.24

SL = sea level

its zenith. As the trajectories prior to interaction with the atmosphere of the electrically charged cosmic rays are curved by the geomagnetic field, this cone of acceptance is deflected and distorted from its original direction and shape at the top of the atmosphere, so that its intersection with the celestial sphere may not be centered on the zenith direction of the monitor (see Appendix A). Moreover, the monitor turns with the earth in its diurnal rotation causing the viewing cone to scan a small circle on the celestial sphere.

A constant primary cosmic-ray anisotropy, fixed with respect to some extraterrestrial object, will be scanned repeatedly by the rotating cone of acceptance. The resulting variation in the monitor counting rate will be characteristic of that portion of the anisotropy scanned and, if the anisotropy is fixed and time-invarient, will repeat itself with each rotation of the earth. If the anisotropy is variable, but on a time scale large compared to one day, the observed periodic variation will undergo gradual modulation of its waveform. Such an anisotropy will be called a persistent anisotropy and its identifying characteristics may be summarized as follows:

(a) It produces a periodic, diurnal variation in the data time-history of an earth-based monitoring station.

(b) The period of the variation seen in earth-based stations is exactly equal to the rotation period of the earth as viewed by an observer fixed with respect to the anisotropy.

(c) The exact waveform of the periodic variation is related to the form of the anisotropy and if this form is variable in time then modulations in the data waveform reflect this variance.

3.3 <u>Evidence</u> <u>for</u> <u>a</u> <u>persistent</u> <u>anisotropy</u>.

In accord with the viewpoint expressed in the previous section, the examination of neutron monitor data for evidence of a persistent anisotropy may be reduced to the problem of detecting periodic variations which are coherent with the earth's rotation. Care must be exercised to exclude any periodic variations, coherent with the earth's rotation, which are not of primary cosmic-ray origin. The most important such effects for a neutron monitor are

(a) diurnal variations in the barometric pressure at the recording station due to solar heating of the atmosphere

(b) diurnal variations in the observed barometric pressure due to diurnal wind pattern variations which cause pressure variations in enclosures by the Bernoulli effect--an increase in wind velocity causing a decrease in pressure

(c) diurnal temperature variations in the building housing the monitor which cause variations in the data through the temperature sensitivity of the counters and, possibly, of the associated electronic equipment such as the high-voltage supplies and the pulse-amplitude discriminators

(d) diurnal variations in the electrical mains supply voltage which may affect the electronic equipment.

In modern stations the simple barometric effect is minimized by using automatic, servo-controlled, mercury column barometers capable of accuracies on the order of 0.1 mmHg and by recording data at short intervals, say every five minutes, and applying the pressure correction to each such reading <u>before</u> hourly totals are formed. The other effects named above are attacked at their source; by protecting the pressure measurement sampling location against wind streaming effects, by

maintaining the equipment in a temperature controlled environment, and by electronic regulation of all important electrical supplies.

Although even a cursory look at fully corrected neutron monitor data reveals a clear diurnal variation of about 1% peak-to-peak amplitude, and indeed this variation has long been noted, a much more objective approach is to examine the data time-history function in the frequency domain through power-spectrum analysis (Chapter II, Section 2.2). This method has the advantages that all frequencies within a broad band are searched without bias, the results are displayed in an easily interpreted way, and estimates of the statistical validity of the analysis are available to serve as guides in the attempt to determine the physical reality of any given feature.

Because it represented one of the largest and best maintained of the NM-64 monitors and because continuous data existed for a period longer than any other monitor of comparable size, the Deep River, Canada, station was chosen for a power-spectrum analysis study. Because of the discrete, finite nature of the data, numerical approximations were made to the continuous, infinite formulation of Chapter II following the procedures of Blackman and Tukey (1958) and Swinnerton-Dyer (1963). All computations were made with the IBM 360/50 electronic computer.

The data selected extended from day 60 of 1962 through day 80 of 1966 in hourly totals of the counting rate corrected for barometric variations. The data were examined for linear trend, obviously spurious data points, and missing data points. No significant trend was found and no trend correction was made. All unusual data points were found to be the result of key-punch errors and were corrected. Missing points

were filled with linear interpolations from neighboring values.

The 34,104 hourly values were reduced to 11,368 (N) contiguous 3-hour

sums $\{X_i\}$ from which the autocorrelation coefficients $\{C_r\}$ were

computed as

$$C_r = \left(\frac{N}{N-r}\right) \frac{\sum_{s=1}^{N-r} X_s X_{s+r}}{\sum_{s=1}^{N} X_s^2} \qquad r = 0, 1, \cdots r_{max}$$

The maximum lag index, r_{max}, was set at 648 giving a maximum lag-time

of 81 days. The finite cosine transform, $\{V_q\}$, of the autocorrelation

coefficients,

$$V_q = C_o + \sum_{r=1}^{m-1} 2C_r \cos \frac{qr\pi}{m} + C_m \cos q\pi \qquad q = 0, 1, \cdots m \leq r_{max}$$

was formed to give the raw spectral estimates. The raw estimates were

smoothed by convolution with the 3-point Hamming weights (Blackman and

Tukey, 1958) so that

$$U_o = 0.56 \ (V_o + V_1)$$

$$U_q = 0.23 \ V_{q-1} + 0.56 V_q + 0.23 V_{q+1}$$

$$U_m = 0.56 \ (V_{m-1} + V_m)$$

where U_q is the smoothed spectral estimate associated with the frequency

$(q/2m\tau)$, the unit lag-time τ being, in this case, three hours. The

spectral estimates behave, in slowly varying regions of the spectrum, as

chi-square variates with a number of degrees of freedom given by $k = \frac{n}{m}$

n being the total number of data points. The interval of spread centered

on the true value within which 60% of the estimates may be expected to

fall (60% confidence interval), measured in dB, is given by $10/\sqrt{k-1}$

(Blackman and Tukey, 1958).

A smoothed spectrum of the Deep River data computed with m=120, so
that k ≈ 94 and the 60% confidence interval ≈ 1 dB, is given in Figure 2.
The Nyquist frequency lies at $\frac{1}{2\tau}$ = 4 cycles per day (cpd). The important
features of this spectrum are

(a) a strong peak near zero frequency which may be attributed to
long time scale, aperiodic phenomena, e.g., Forbush decreases

(b) a general decrease with increasing frequency resulting, in
part, from the attenuation of higher frequencies by the use of 3-hour
totals in the computation

(c) an extremely strong peak at 1 cpd (≈ 15 dB above base-level)
which evidences the well-known diurnal variation and which has a width
less than the intrinsic resolution of the analysis$\left(\frac{1}{2m\tau}\right)$

(d) a generally elevated region (average ≈ 2 dB) in the neighborhood
of the 1 cpd peak (± 0.1 cpd)

(e) a well-defined peak of ≈ 5 dB above base-level with unresolved
width at 2 cpd

(f) an absence of any other peaks of statistical significance in
the frequency range covered, the lack of a peak at 3 cpd being particu-
larly notable.

The diurnal variation peak is the most prominent feature of this
spectrum and, since it represents a variation in the raw data of only
about 1% peak-to-peak, the considerable power of this method of analysis
is clearly indicated. This variation, and its implied primary anisotropy
have been intensively studied, definitive surveys being reported by
Rao, et al. (1963) and McCracken and Rao (1965). By means of harmonic
analysis of many years of data from many stations, they find the primary
anisotropy to have a peak-to-peak amplitude of 0.76%±0.04% with the
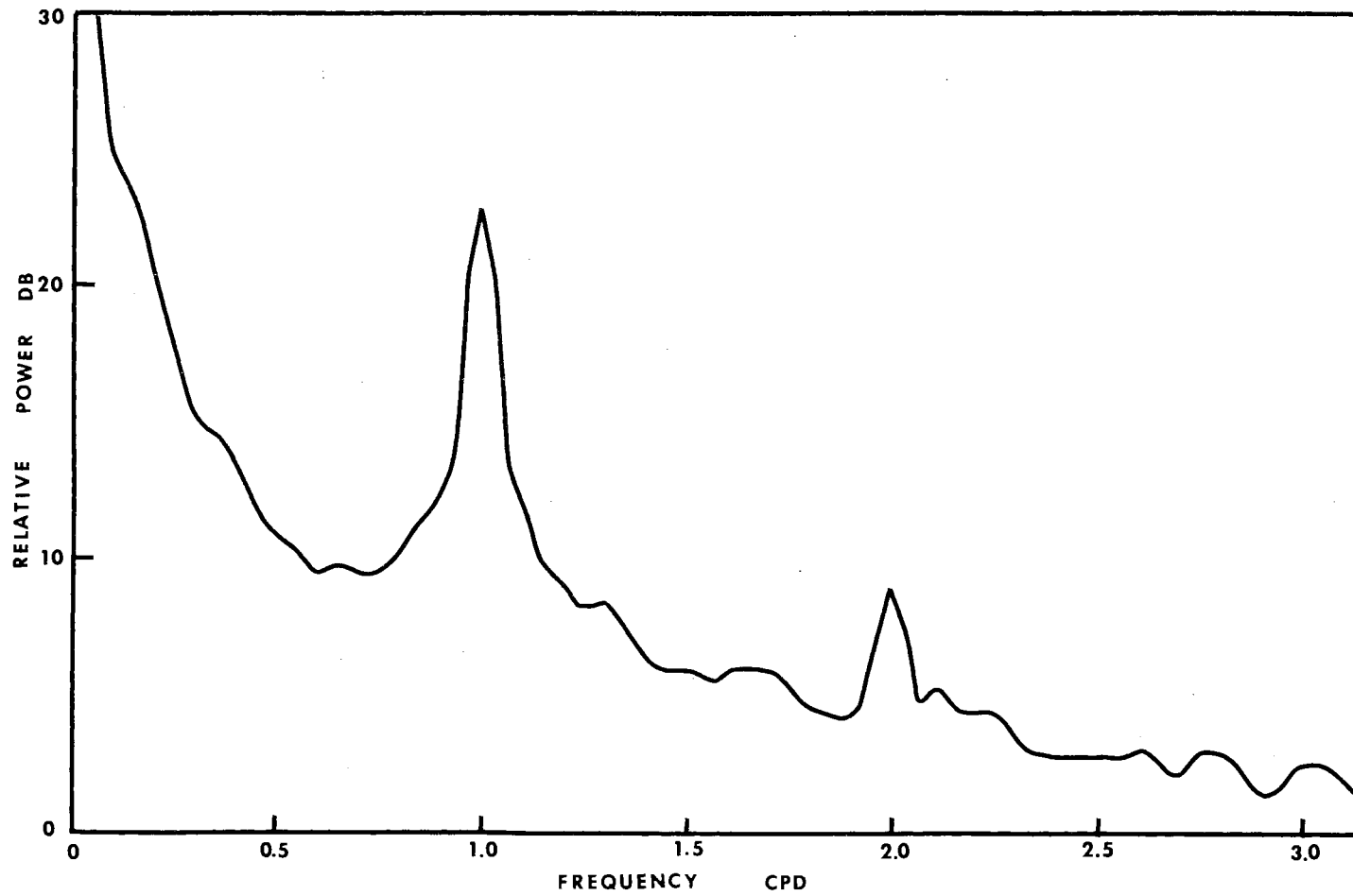
Figure 2. Power Spectrum of Deep River Data.

maximum in the plane of the ecliptic at $89.5° ± 1.6°$ east of the earth-sun line. This is in essential agreement with the theoretical predictions of the Axford-Parker model of the diurnal anisotropy (Axford, 1965; Parker, 1964). The power-spectrum analysis of the Deep River data, although unable to provide information about the orientation of the anisotropy, does support the conclusions of the previous work. Implications of the spectral analysis are

(a) that, to within the resolution of the analysis ($\frac{1}{30}$ cpd), the variation is coherent with the earth's rotation as shown by the unresolved spectral line at 1 cpd

(b) that, since the variance at 1 cpd is more than an order of magnitude greater than the variance at closely neighboring frequencies, the diurnal variation is distinct from the broad-band background variance, a fact not revealed by simple harmonic analysis

(c) that the diurnal anisotropy is not strictly time-invariant, as shown by the definitely greater variance at frequencies immediately adjacent to 1 cpd when compared to the general background variance in the same region. This variability has been evident in harmonic analysis studies, but the question of whether the variability was due to random variations superimposed upon an invariant anisotropy or to temporal variations of the anisotropy itself, or both, could not previously be answered. The presence of the enhanced spectral region in the neighborhood of the diurnal spectral peak is direct evidence for the modulation of the diurnal anisotropy.

The well-defined spectral peak with unresolved width at 2 cpd is of particular interest since it represents an often reported but equally frequently questioned feature of the cosmic-ray flux, the so-called

semi-diurnal variation. Katzman and Venkatesan (1960) have attributed

the semi-diurnal variation entirely to atmospheric effects and Rao,

et al., (1963) find the data obtained by a world net of neutron monitors

in 1957-58 inconsistent with a semi-diurnal anisotropy, but data from

crossed meson telescopes (Rao and Sarabhai, 1961, and Ahluwalia, 1962)

seem to provide clear evidence for such an anisotropy. In the hope of

resolving some of these conflicts a thorough study of the semi-diurnal

variation was undertaken using the improved data available from the new

large neutron monitors and the demodulation methods described in

Chapter II.

3.4 A world-wide survey of the semi-diurnal variation.

To ascertain the parameters of the primary anisotropy implied by

the semi-diurnal variation, complex demodulation techniques (Chapter II,

Section 2.6) were used to determine the amplitude and phase distributions

of the 2 cpd variational component of data from the world net of

neutron monitors for the years 1953-1965. The data on IBM cards were

checked for accuracy by using a checksum which had been independently

computed for each day of data. For those stations reporting only

bi-hourly data, linear interpolation was used to provide 24 values for

each day. Missing data points in the records were filled in using

linear interpolation for blank intervals of 6 hours or less. For blank

intervals of greater than 6 hours, an analytic model consisting

the sum of 1 cpd and 2 cpd sine waves of adjustable phase and amplitude

was fitted to the days of data just before and after the missing section,

and values taken from this model were used to fill the blank interval.

Finally all values from a given station were expressed as percentages

of the long-term mean counting rate of that station.

The 2 cpd component was heterodyned to zero frequency (Chapter II, Section 2.5) using both in-phase and quadrature reference waves. (The in-phase reference sine wave is defined here to have a zero-crossing and positive slope at 0 hr UT and the quadrature reference wave to have a maximum at 0 hr UT.) Thus from the data series $\{X_i\}$ of hourly values, two new series were formed

$$G_i = X_i \sin \frac{2\pi t_i}{12}$$

$$H_i = X_i \cos \frac{2\pi t_i}{12}$$

where t_i is the hour (UT) associated with X_i. The frequency components of $\{G_i\}$ and $\{H_i\}$ near zero-frequency were extracted by a linear convolution filter (Chapter II, Section 2.3) to form the smoothed series $\{\bar{G}_i\}$ and $\{\bar{H}_i\}$ thus

$$\bar{G}_i = \sum_{n=-N}^{N} W(n\tau) G_{i-n}$$

$$\bar{H}_i = \sum_{n=-N}^{N} W(n\tau) H_{i-n}$$

where $W(t)$ is a weighting function and the interval of convolution, $-N\tau \leqslant t \leqslant N\tau$ is chosen so that $W(t) \approx 0$ outside this interval.

The choice of a weighting function was dictated by the need for several, somewhat conflicting, characteristics:

(a) The frequency response function of the filter should have a single, flat-topped peak centered on zero-frequency.

(b) The filter should have unity gain at zero-frequency.

(c) The slopes of the response peak should be steep to define sharply the acceptance region in the frequency domain.

(d) The response of the filter to a sudden impulse or step function should be well behaved with little or no overshoot or ringing. The weighting function found to satisfy best these conditions has the form

$$W(t) = K \frac{\sin \alpha t}{\alpha t} e^{-\beta t^2}$$

The constant K is chosen so that

$$\int_{-\infty}^{\infty} W(t)dt = 1$$

thus assuring that the response at zero-frequency is unity.

In all, three such filter weighting functions were employed so that the effects of the variation of response bandwidth could be evaluated. The characteristics of these filters are given in Table II for t measured in days.

TABLE II

FILTER CONSTANTS

Filter No.	α	β	Bandwidth	Risetime	N
1	3.1416	0.25	1 cpd	1 day	32
2	0.62832	0.10	0.2 cpd	5 days	120
3	0.20944	0.00222	0.067 cpd	15 days	240

Since W(t) is the product of two functions, its Fourier transform is the convolution of the transforms of these two functions, hence the

response function, $V(\omega)$ may be given as

$$V(\omega) = \text{F.T.} \left[W(t) \right]$$
$$= K\, A(\omega) * B(\omega)$$

where $A(\omega)$ and $B(\omega)$ are given by

$$A(\omega) = \text{F.T.} \left[\frac{\sin \alpha t}{\alpha t} \right]$$
$$= \begin{cases} \pi/\alpha & |\omega| < \alpha \\ 0 & |\omega| > \alpha \end{cases}$$

$$B(\omega) = \text{F.T.} \left[e^{-\beta t^2} \right]$$
$$= \sqrt{\frac{\pi}{\beta}}\; e^{\omega^2/4\beta}$$

For the values of α and β chosen, $A(\omega)$ is a much more broadly peaked function than is $B(\omega)$ and so the convolution of the two functions most closely resembles the rectangular impulse function $A(\omega)$. This produces the desired single-peaked response, centered on zero frequency and having a relatively flat top and steep sides. On the other hand, the effect of the Gaussian exponential part of the weighting function is best viewed in the time-domain. The diffraction function, $\sin \alpha t / \alpha t$, decreases as $1/t$ in regions far removed from the origin making a rather long convolution interval $(-N\tau \leq t \leq N\tau)$ necessary. Also the response of this filter function to a unit step-function

$$R_{step}(t) = \int_{-\infty}^{t} \frac{\sin \alpha x}{\alpha x}\, dx$$

indicates a poor transient response with $\approx 30\%$ overshoot and many cycles of ringing. However, since, in the present case, the diffraction

function is multiplied by the Gaussian exponential function, the weighting function falls off as $e^{-\beta t^2}$ away from the origin, allowing the function to be truncated relatively near the origin and giving a desirably short convolution interval. Also, the overshoot and ringing of the diffraction function filter are strongly damped, improving the transient response. The bandwidth and risetime of the final, composite filter function are determined mainly by the constant α, the relationships being

$$\text{bandwidth} \approx \frac{\alpha}{\pi}$$

$$\text{risetime} \approx \frac{1}{\text{bandwidth}}$$

where the risetime is defined to be the time required for the output of the filter to rise from 0.1 to 0.9 in response to a unit step-function input. The step-function response of filter number 2, typical in overall shape of the response of all the filters used, is shown in Figure 3.

Since it has been demonstrated that harmonic analysis is a special case of complex demodulation (Chapter II, Section 2.6), and since moving averages of daily harmonic analyses of neutron monitor data have been extensively used in the study of periodic variations of the cosmic-ray flux, it is most instructive to compare the characteristics of the complex demodulation technique used here with the more common harmonic analysis. In Figure 4 the frequency response function of filter 1 is compared with the effective response function of daily harmonic analysis (fundamental component) and filters 2 and 3 are compared with the effective response function of a moving five-day average of daily harmonic analyses. The following contrasts are noted:

(a) Daily harmonic analysis and moving averages of daily harmonic

DAYS

0 1 2 3 4 5
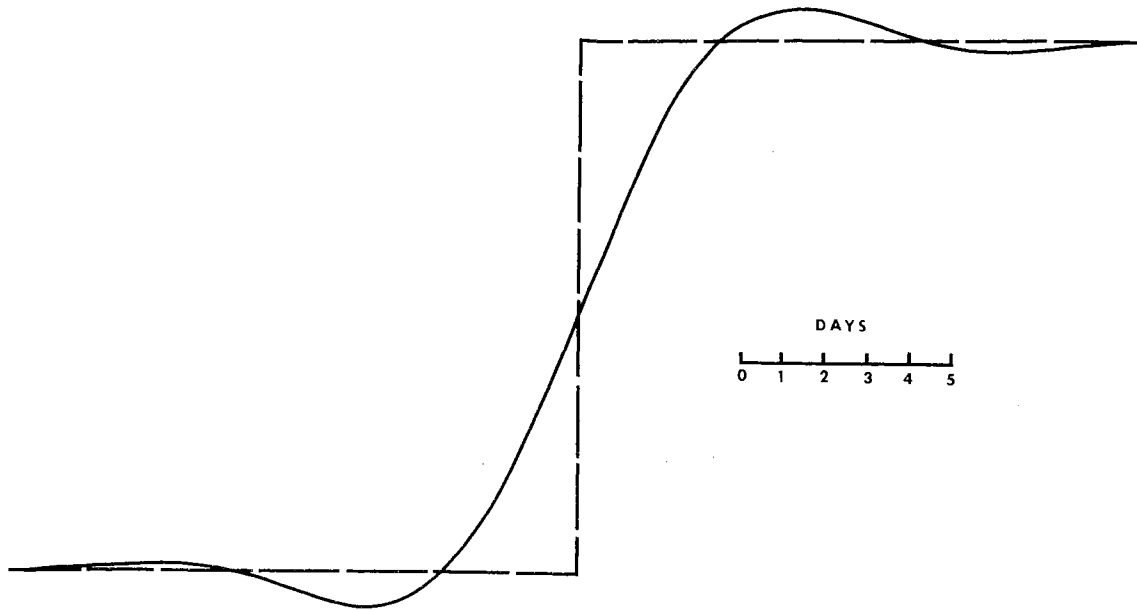
Figure 3. Filter Step-Function Response.

100

50

20

10

5

2

AMPLITUDE RESPONSE FUNCTIONS

DAILY HARMONIC ANALYSIS

FILTER NO. I
(ONE DAY RISE
TIME)

AMPLITUDE IN PERCENT

DEVIATION FROM CENTER FREQUENCY IN CYCLES PER DAY

-1.4 -1.3 -1.2 -1.1 -1.0 -0.9 -0.8 -0.7 -0.6 -0.5 -0.4 -0.3 -0.2 -0.1 0.1 0.2 0.3 0.4 0.5 0.6 0.7 0.8 0.9 1.0 1.1 1.2 1.3 1.4

AMPLITUDE RESPONSE FUNCTIONS

A—5 DAY MOVING AVERAGE OF DAILY HARMONIC ANALYSES

B—FILTER NO. 2 (5 DAY RISE TIME)

C — FILTER NO. 3 (15 DAY RISE TIME)

DEVIATION FROM CENTER FREQUENCY IN CYCLES PER DAY

Figure 4. Amplitude Response Functions.

analyses have responses far removed from the center frequency of interest in the form of many significant side lobes, whereas the filters 1, 2, and 3 have only a single response peak.

(b) The response peak of the filters used is more nearly constant (≈ 1) near the frequency of interest than the harmonic analysis functions.

(c) For roughly equivalent risetimes (the risetime of moving averages of daily harmonic analyses, using the previously given definition of risetime, is 0.8 times the averaging interval) the filters used have significantly narrower main lobes.

The advantages which one may expect from the use of these newer filter functions are

(a) a greatly decreased response to strong signal components lying outside the frequency region of interest (This is particularly useful in reducing the effects of trends in the data which are seen in power spectra as large peaks in the neighborhood of zero frequency.)

(b) less distortion of the frequency components of interest which lie in the neighborhood of the center frequency of the filter.

These advantages, it should be noted, are obtained without sacrificing a well-behaved transient response.

From the smoothed series, $\{\bar{G}_i\}$ and $\{\bar{H}_i\}$, phase and amplitude measures were obtained as

$$R_2(t_i) = \sqrt{\bar{G}_i^2 + \bar{H}_i^2}$$

$$\phi_2(t_i) = \frac{12}{2\pi} \arctan -\left(\frac{\bar{G}_i}{\bar{H}_i}\right) \quad \mathrm{mod}\ 12$$

where R_2 gives the peak amplitude, in per cent, of the semi-diurnal component associated with time t_i and ϕ_2 gives the phase as represented by the hour (UT) of the first maximum. For each year of data analyzed from each station, distribution histograms were prepared for both the amplitude and phase parameters. Figure 5 shows amplitude histograms for ten stations for the year 1964. A most probable amplitude (peak) of $\approx 0.07\%$ is indicated for all stations. The ratio of the diurnal to semi-diurnal variance is then given (in dB) as 20 log (0.76/0.14) = 14.7 dB, which agrees well with the value indicated by power-spectrum analysis of $\approx$ 15 dB, the difference, in dB, between the 1 cpd and 2 cpd spectral line amplitudes shown in Figure 2. This value is also representative of the amplitude observed in the entire period 1953-1965.

Phase distribution histograms for the same stations and year are shown in Figure 6, plotted in both UT and <u>asymptotic time</u>. Asymptotic time is defined as the mean local time of the asymptotic cone of acceptance. The use of asymptotic time corrects for the geomagnetic deflection of the cosmic-ray primaries and allows the true direction of the anisotropy responsible for the variation to be determined. The correction from UT to asymptotic time is dependent upon the frequency of the periodicity as well as its assumed energy spectrum and the location of the observatory in question. Correction values used in this study were taken from McCracken, et al. (1965). The important features of these histograms are:

(a) All stations show strong peaks in their phase distribution histograms. This implies that the phase of the semi-diurnal variation is not random, but tends to be coherent with the diurnal rotation of the earth.

HISTOGRAM OF R₂ USING 15 DAY RISE TIME FILTER FOR 1964

HISTOGRAM OF φ₂ USING 15 DAY RISE TIME FILTER FOR 1964
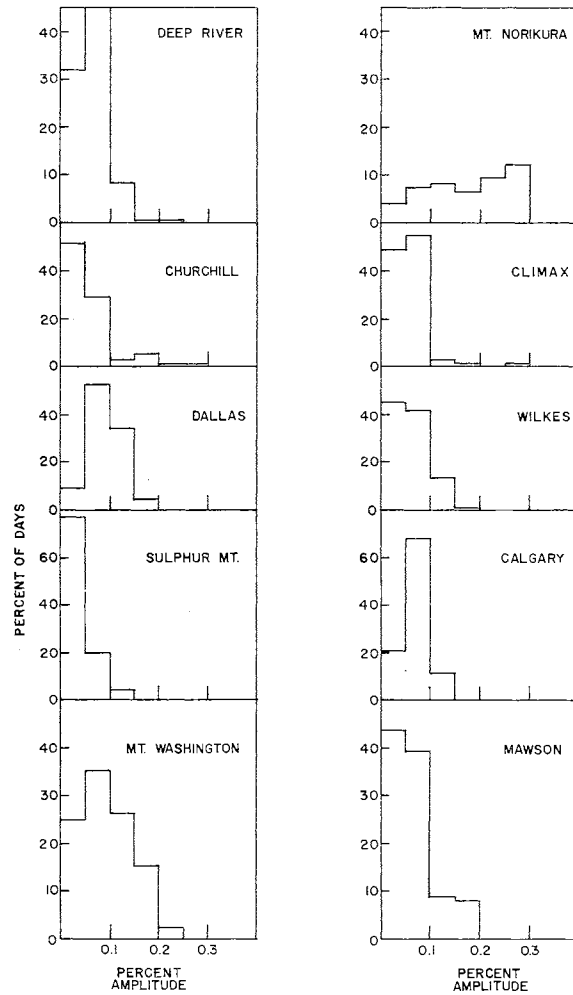
Figure 5. Semi-Diurnal Amplitude Distributions.
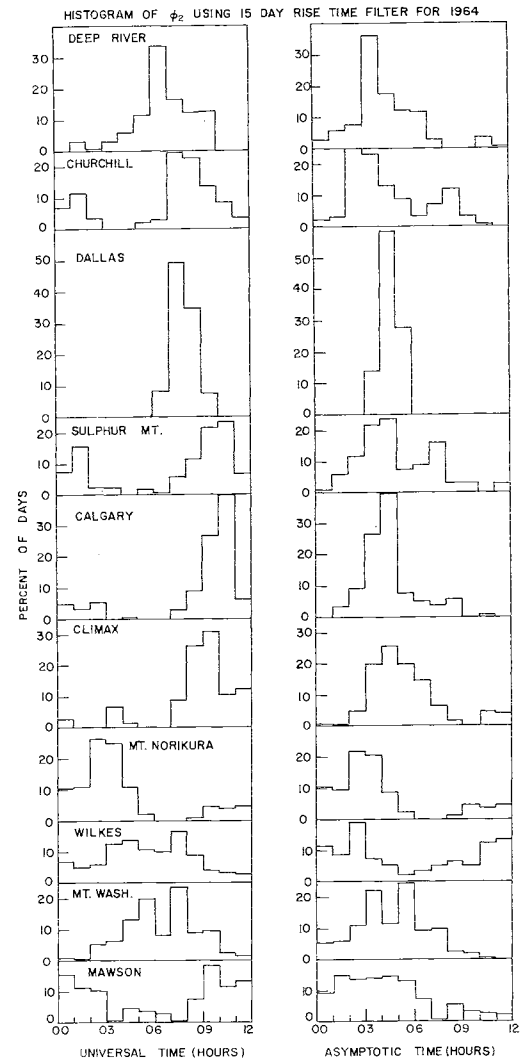
Figure 6. Semi-Diurnal Phase Distributions.

58

(b) Inter-station agreement for the most probable phase of the variation is obtained only when the distributions are given in asymptotic time. This is a clear indication that the semi-diurnal variation is consistent with a bidirectional spatial cosmic-ray anisotropy fixed with respect to the earth-sun line.

Katzman and Venkatesan (1960) have attempted to explain the semi-diurnal variation as a simple barometric effect resulting from incorrect correction coefficients. Since the phase of the semi-diurnal barometric wave tends to be constant when expressed in local time for mid-latitude stations (Katzman and Venkatesan, 1960) phase distributions of the cosmic-ray semi-diurnal variation were examined in local time. The inter-station agreement was found to be substantially inferior to the agreement in asymptotic time, thus indicating the probable failure of a purely barometric explanation for the semi-diurnal variation. The difficulty of other investigators in finding a consistent semi-diurnal anisotropy, e.g., Rao, et al. (1963), can probably be traced to the lack of truly well-corrected data from large stations such as the NM-64 type, and the use in their analyses of simple harmonic analysis techniques which are not selective enough to exclude all interfering effects.

A summary of the results of the survey covering the years 1953-1965 is given in Figures 7 and 8. The time of maximum of Figure 7 refers to asymptotic time while the arrows of Figure 8 indicate the direction of the maxima of the inferred anisotropy. The semi-diurnal phase is remarkably constant for the solar cycle 1954-1965. When expressed in asymptotic time, excellent inter-station agreement is found for the years 1962-1965, the standard error being as small as 8° for 1963 and only slightly larger for other years. For the period 1957-1961 the
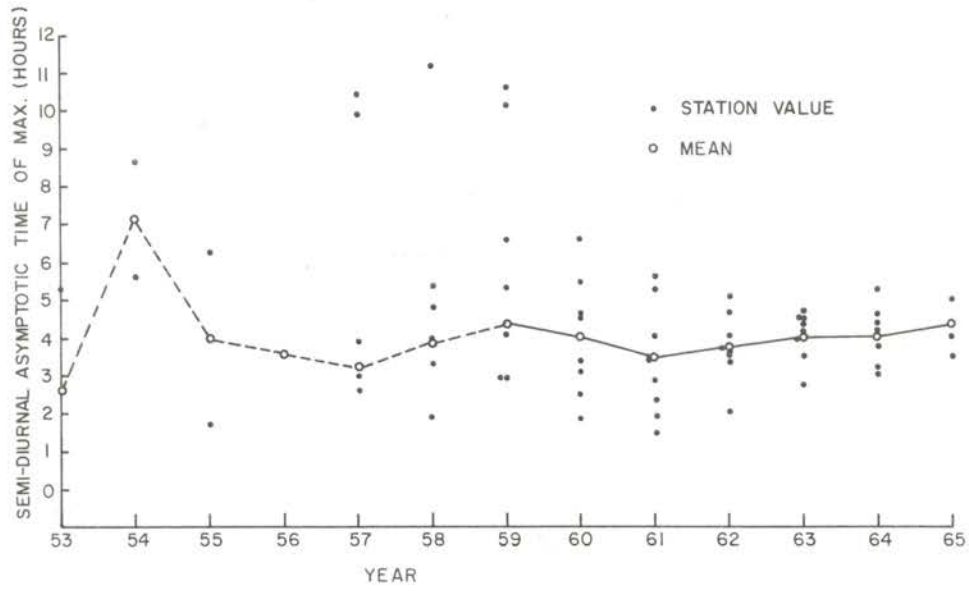
Figure 7. Semi-Diurnal Phase 1953-1965.
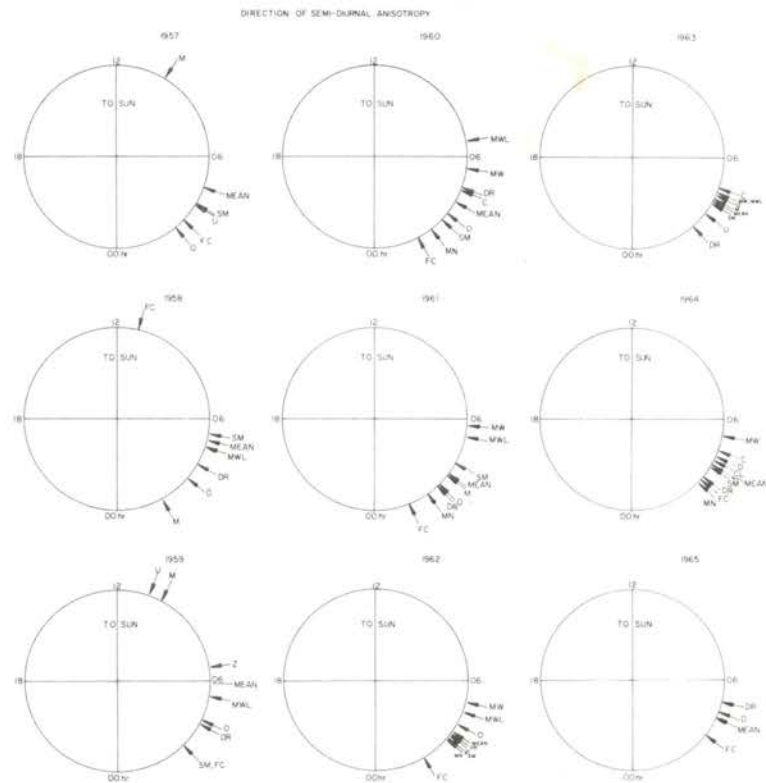
Figure 8. Semi-Diurnal 24-Hour Dials.

dispersion increases, but reasonable agreement is retained with only one or two stations being exceptional cases. Prior to 1957 the number of reporting stations is too small to produce definite results. The steadily decreasing scatter among individual stations for later years is more reasonably attributed to the constant improvement of monitoring facilities than to a basic change in the cosmic-ray variation.

The results of this survey indicate a primary bidirectional anisotropy having maximum flux along a line $\approx 60°$ east of the earth-sun line, a direction which is essentially perpendicular to the mean interplanetary magnetic field reported by Ness and Wilcox (1964). This indicates that the pitch-angle distribution (the pitch-angle is the angle between the particle trajectory and the magnetic field) of cosmic-ray particles, when reckoned in the frame of reference co-rotating with the sun, has a tendency to be more dense for pitch-angles near 90° and relatively less dense for small pitch-angles.

At the time of writing, there is no satisfactory theory for the semi-diurnal anisotropy due, in part, to the lack of firm experimental verification of the existence of this effect. With the results herein reported, not only is the presence of the effect no longer in question, but also good measurements of the parameters of the anisotropy are now available. Hopefully these results will encourage further theoretical work on the source of this phenomenon.

3.5 The sidereal variation problem.

When viewed from the position of distant stars, the earth is seen to make 366 revolutions on its axis for each revolution about the sun and thus, a cosmic-ray anisotropy fixed with respect to the distant

stars would induce a periodic variation in the data of a ground-based monitor having a frequency of 366/365 cpd. This so-called sidereal variation is much sought after since it holds the promise of giving information about the source of the cosmic radiation. While, in the case of the primary particles responsible for the major part of the counting rate of a neutron monitor, there are serious questions to be answered concerning the effect of diffusion in the turbulent solar magnetic field, this study shall be concerned only with the problems arising from the attempt to separate the sidereal variation from other variations. The important interfering variations are

(a) the diurnal variation. This strong periodic variation is separated from the sidereal variation by only 0.00274 cpd in the frequency-domain.

(b) modulation sidebands of the diurnal variation. When a periodic wave, e.g., $\cos\omega_0 t$, is amplitude modulated by another wave, e.g., multiplied by $(1+M\cos\omega_m t)$, then one result is the production of spectral components with frequencies $\omega_0 \pm \omega_m$ since

$$(1 + M\cos\omega_m t)\cos\omega_0 t =$$
$$\cos\omega_0 t + \frac{M}{2}\cos(\omega_0+\omega_m)t + \frac{M}{2}\cos(\omega_0-\omega_m)t$$

Of great concern here is the possibility of an annual modulation of the diurnal variation since the upper sideband for such modulation would be identical in frequency to the sidereal variation. A thorough survey of modulation effects including phase modulation as well as amplitude modulation is given by Jackyln (1962).

(c) random variations. These may come from two sources. First, due to the finite counting rate of any monitor and the probabilistic

nature of the arrival of particles at the counter, there is always a random variation in monitor data with a standard deviation $\geqslant \sqrt{N}$ where N is the expected number of counts in the counting interval. Second, there is, almost certainly, a random fluctuation in the primary flux itself due to scattering in the turbulent solar magnetic field.

These interfering variations result in severe restrictions for any analysis seeking to discover a sidereal variation in cosmic-ray data:

(a) The analysis process must be sufficiently frequency-selective to be able to differentiate between the diurnal and sidereal variations. From the time-bandwidth invariance property of linear filters it may be inferred that at least one year of data is necessary to achieve the necessary selectivity. In actual practice several times this much data would be needed since, in order to eliminate spurious response lobes lying outside the major lobe of a frequency-selective linear filter, it is necessary to use data time intervals longer than the absolute minimum required by time-bandwidth invariance.

(b) In order to distinguish a periodic variation from random, frequency-independent variations an analysis must produce a spectral density estimate whose variance, expressed as a confidence interval in dB, is less than the expected ratio of the periodic variation power (variance) to the power of the random variations in the same frequency neighborhood. The random variation power in the neighborhood of 1 cpd is not small, as may be seen in the power-spectrum analysis of the Deep River data, and for a measure of this power to have a variance such that the 60% confidence interval is, say, 1 dB requires $10/\sqrt{k-10} = 1$ so that $k \approx 100$ (Section 3.3 of the present chapter). This implies a time-span of data ≈ 100 times the reciprocal bandwidth of the analysis

(Blackman and Tukey, 1958). As noted above, the bandwidth requirement is severe due to the closeness of the strong diurnal variation-- leading to a necessary selectivity of ≈ 0.003 cpd, i.e., ≈ 1 cycle per year--so that a total time-span of data of ≈ 100 years is required. Even if, as has been suggested (Conforto and Simpson, 1957), the diurnal variation should disappear for some small part (one year) of the 11-year solar cycle, letting the bandwidth requirement be relaxed some- what , it is doubtful that the above figure could be successfully reduced the necessary two orders of magnitude.

(c) The possibility of a sideband of the diurnal variation coincident in frequency with the sidereal variation is a most serious problem. It has been suggested (Farley and Storey, 1964) that one may compare the relative strengths of the upper and lower annual sidebands of the diurnal variation and attribute any difference to a true sidereal variation. One may note that this requires both high frequency-resolution, to separate the sidebands, and, simultaneously, high amplitude-resolution--perhaps even better than the 1 dB relative to the random variation background used in the example above. The above comments apply, with the conclu- sion that perhaps even more than 100 years of data would be necessary for a meaningful analysis unless the sidereal variation amplitude is as large as the diurnal variation, which is contrary to the observations.

3.6 The 27-day variation.

One of the first periodicities noted in cosmic-ray data was the 27-day recurrence tendency of Forbush decreases. This effect is traceable to the rotation of the sun which has a period of about 25 days at its equator and about 30 days near its poles. The synodic period of rotation (the rotation period as observed from the moving earth) is

about 27 days for a rather broad band about the equator of the sun. Given the improved data of the newer neutron monitors and the insight provided by modern correlation and spectral analysis techniques, it is still informative to examine this phenomenon.

A plot of the autocorrelation function of the Deep River data (Section 3.3 of the present chapter) is shown in Figure 9. Significant peaks are noted not only at 27 days lag, but also at 54 days lag. No significant peak is seen, however, at 81 days lag. This would seem to indicate that the active centers on the sun responsible for the 27-day modulation of the cosmic-ray flux have lifetimes of about two solar rotations. This finding contrasts with the report of McCracken, et al., (1966) who find evidence for the existence of very long lived (≈ 2 years) 27-day recurrent decreases in the data from the Pioneer 6 solar probe. It would appear that the solar wind structures responsible for the recurrent decreases seen in the Pioneer instrument (mean energy of response ≈ 13 MeV) have little effect upon the flux seen by an earth-based neutron monitor (mean energy of response ≈ 10 GeV).

From this autocorrelation function a high resolution power-spectrum was computed. This spectrum (Figure 10) has a frequency resolution of 0.012 cpd and a 60% confidence interval of ≈ 3 dB. The spectral peak at $\frac{1}{27}$ cpd is not pronounced, but harmonics are noted at $\frac{2}{27}$, $\frac{3}{27}$, $\frac{4}{27}$, $\frac{5}{27}$, and $\frac{6}{27}$ cpd. This unusually rich harmonic structure is indicative of a periodic waveform which is sharply impulsive, that is, the period of recurrence is 27 days, but the individual recurring events have a much shorter time scale. This, of course, is characteristic of the Forbush decrease effect.
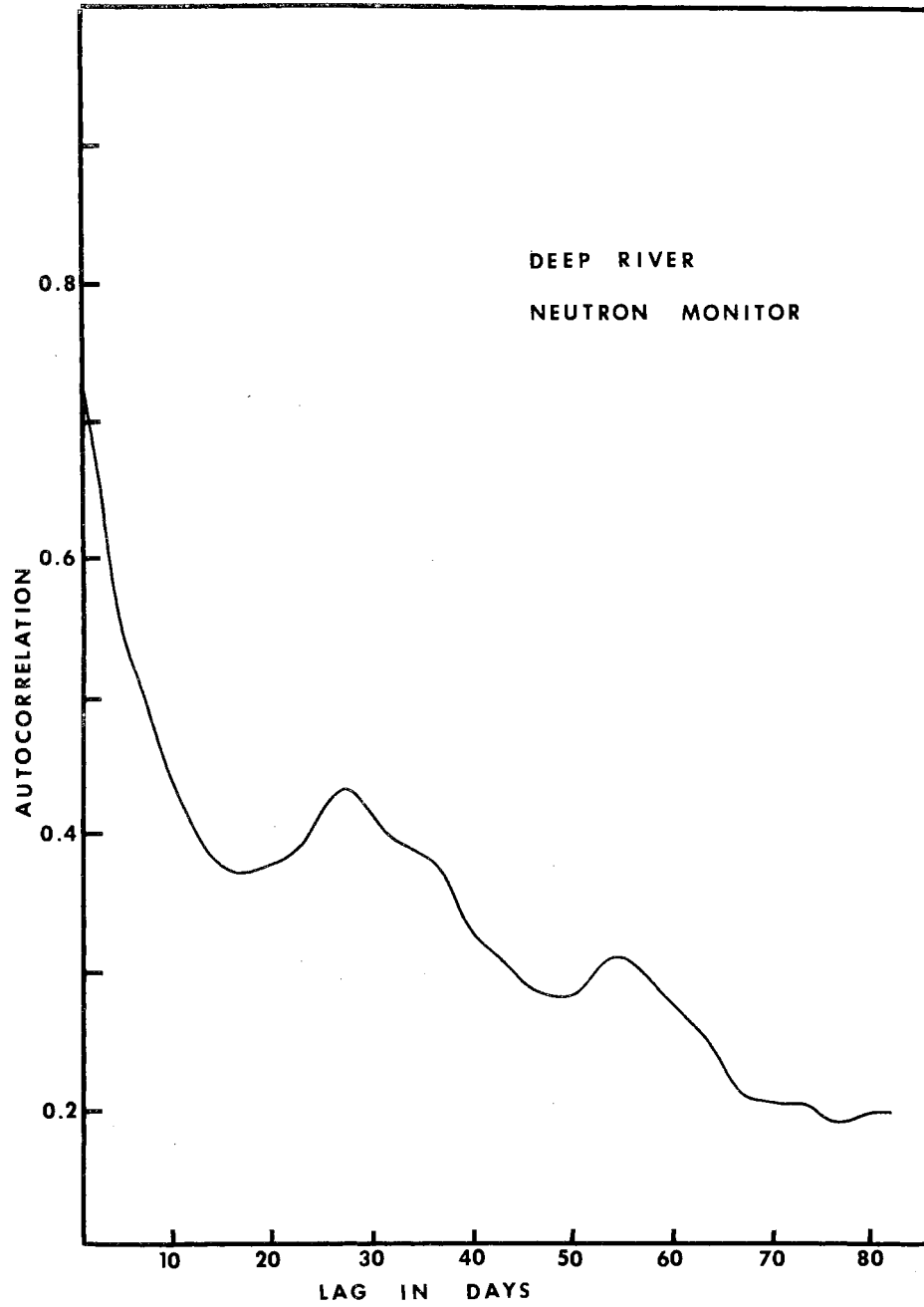
Figure 9. Autocorrelation Function of Deep River Data.
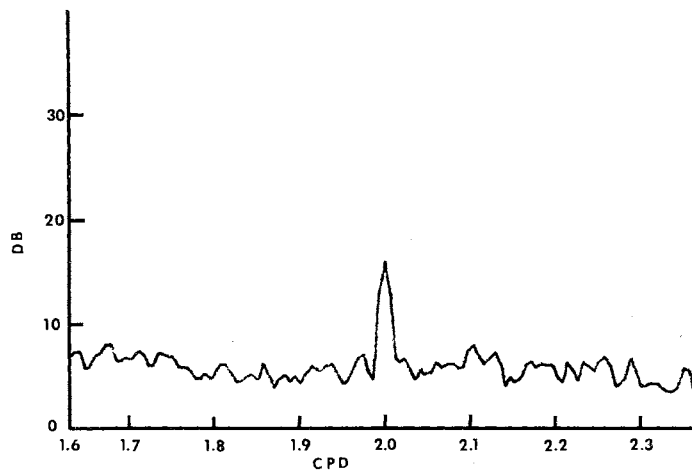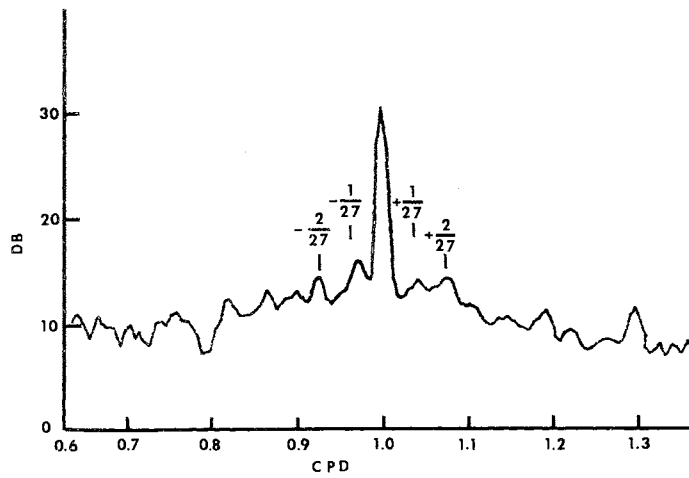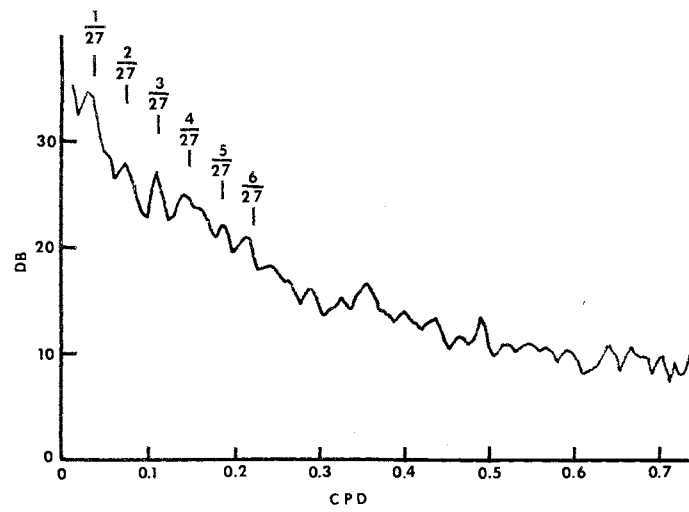
Figure 10. High-Resolution Spectrum of Deep River Data.

A particularly interesting feature of this spectrum is the appearance of modulation sidebands about the diurnal peak at $1 \pm \frac{1}{27}$ cpd and $1 \pm \frac{2}{27}$ cpd. This is direct evidence for the modulation of the diurnal anisotropy by 27-day recurrent structures in the solar wind. It should be carefully noted that the mere existence of both a 1 cpd and a $\frac{1}{27}$ cpd periodicity in the data is not sufficient to produce such sidebands. Rather, the modulation sidebands indicate an interdependence between the effects.

3.7 Long period variations.

The lack of cosmic-ray data covering periods longer than a decade or two discourages the attempt to study long period variations by means of power-spectrum analysis. On the other hand, geomagnetic activity data is available dating from the third quarter of the nineteenth century, that is, the so-called magnetic character figure C_i which has been tabulated for the period 1884-1964 as monthly averages (Handbook of Geophysics, Chapter 11). In view of the established strong correlation between the planetary magnetic activity index K_p, which is similar to C_i, and the solar wind velocity (Snyder, et al., 1963) a power-spectrum analysis of this data is not without interest to the student of cosmic-ray variations. Accordingly, the 80 years of data available were subjected to analysis, with the result shown in Figure 11. Strong peaks are noted at $\frac{1}{11}$ cycle per year (cpy) and at 2 cpy. The lack of any significant peak at 1 cpy is somewhat surprising since the 23° dihedral angle between the earth's equitorial plane and the ecliptic plane will cause an annual variation in the earth-sun geometry. Any possibility for cancellation of the annual effect through equal and opposite variations in the data from the northern and southern hemispheres is reduced by the fact that, for the
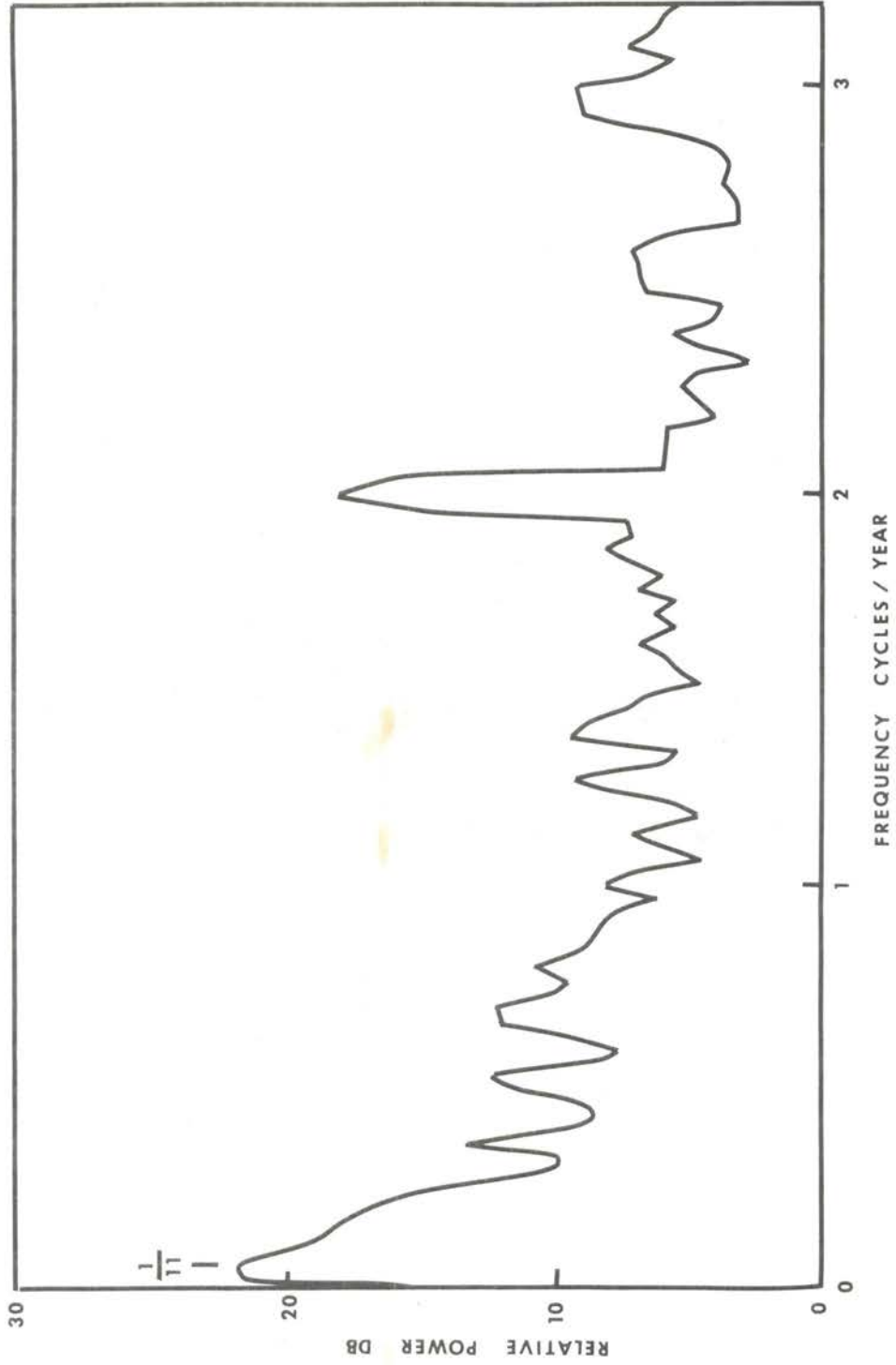
Figure 11. Power Spectrum of C_i Data.

entire period for which data is available, the majority of the reporting

stations lie in the northern hemisphere and, furthermore, that no

correction is made in the computation of C_i for this uneven distribu-

tion. Also it has been noted that the daily magnetic variations do

show a very pronounced annual modulation (Chapman and Bartels, 1951).

The simplest conclusion one could make from these observations is that

the semi-annual variation of geomagnetic activity is related to the

relative orientation of the earth's magnetic moment and the earth-sun

line, these directions being perpendicular twice yearly, and that the

modulation effect is global in extent while, on the other hand, the

modulation of the daily magnetic variations is more probably associated

with the angle made between the zenith direction of the recording sta-

tion, at local noon, and the direction of the earth-sun line, since this

angle undergoes a strictly annual variation for a station whose latitude

has a magnitude greater than 23°.

The peak at $\frac{1}{11}$ cpy which is strong but not well resolved in

frequency in this analysis evidences the well known 11-year variation in

solar activity. The frequency resolution of this spectrum is not

sufficient to detect a 27-day variation. Indeed, the appearance of

such a variation would need be regarded with suspicion since the

original data consisted of monthly averages.

CHAPTER IV

THE SEPARATION OF SPATIAL AND TEMPORAL

VARIATIONS IN THE COSMIC RAY FLUX

4.1 Introduction.

One of the outstanding problems associated with the study of

cosmic-ray variations is the separation of spatial and temporal effects

as viewed by a non-stationary monitoring station, e.g., an earth-based

station whose cone of acceptance scans the celestial sphere with the

diurnal rotation of the earth. In the case of the diurnal and semi-

diurnal variations discussed in the preceding chapter, the identification

of a time-invariant spatial anisotropy was possible only because these

anisotropies are long-lived compared with one day. The delineation of

sharp, short-lived anisotropies requires making comparisons between the

data from independent monitoring stations whose viewing directions

differ significantly.

A systematic approach to making such comparisons has been suggested

and utilized in the study of Forbush pre-decrease anisotropies (McCracken,

1958; Fenton, et al., 1959). The central concept of this method is to

display the cosmic-ray flux intensity as a function of time and space by

constructing equal-intensity contours on a plane whose rectilinear axes

are time and direction in the ecliptic plane relative to the earth-sun

line. In this plane the mean direction of viewing of a station is a

point which moves 15° eastward for each hour advance in time, tracing

71

out a <u>station</u> <u>track</u>. At hourly intervals along this station track, hourly count totals may be placed to indicate a measure of the cosmic-ray intensity at that time and direction and, given enough stations with sufficiently differing tracks, one may construct equal-intensity contours which portray accurately the time-space variations of the cosmic-ray flux (Figure 12).

The practical implementation of this scheme presents several problems:

(a) The sensitivities (absolute counting rates) of monitoring stations are not all equal, necessitating some form of normalization of each station's data, and since the sensitivity of a station may vary due to changes in its environment and deterioration of its detectors, the normalization must constantly be re-evaluated for all stations.

(b) The intersection of the asymptotic cone of acceptance with the celestial sphere does not have the same variation of transmission with direction for all stations. This implies that each station will respond differently to complex cosmic-ray anisotropies, and necessi-tates a variational frequency dependent correction of the raw data from each station.

(c) The mean asymptotic directions of differing stations will, in general, scan different small circles on the celestial sphere; hence, a correction must be applied to the data to minimize the dependence on latitude.

(d) Since the spacing, in longitude, between stations will not be uniform, some method of interpolation on a plane must be used which is not dependent upon regularly spaced data.
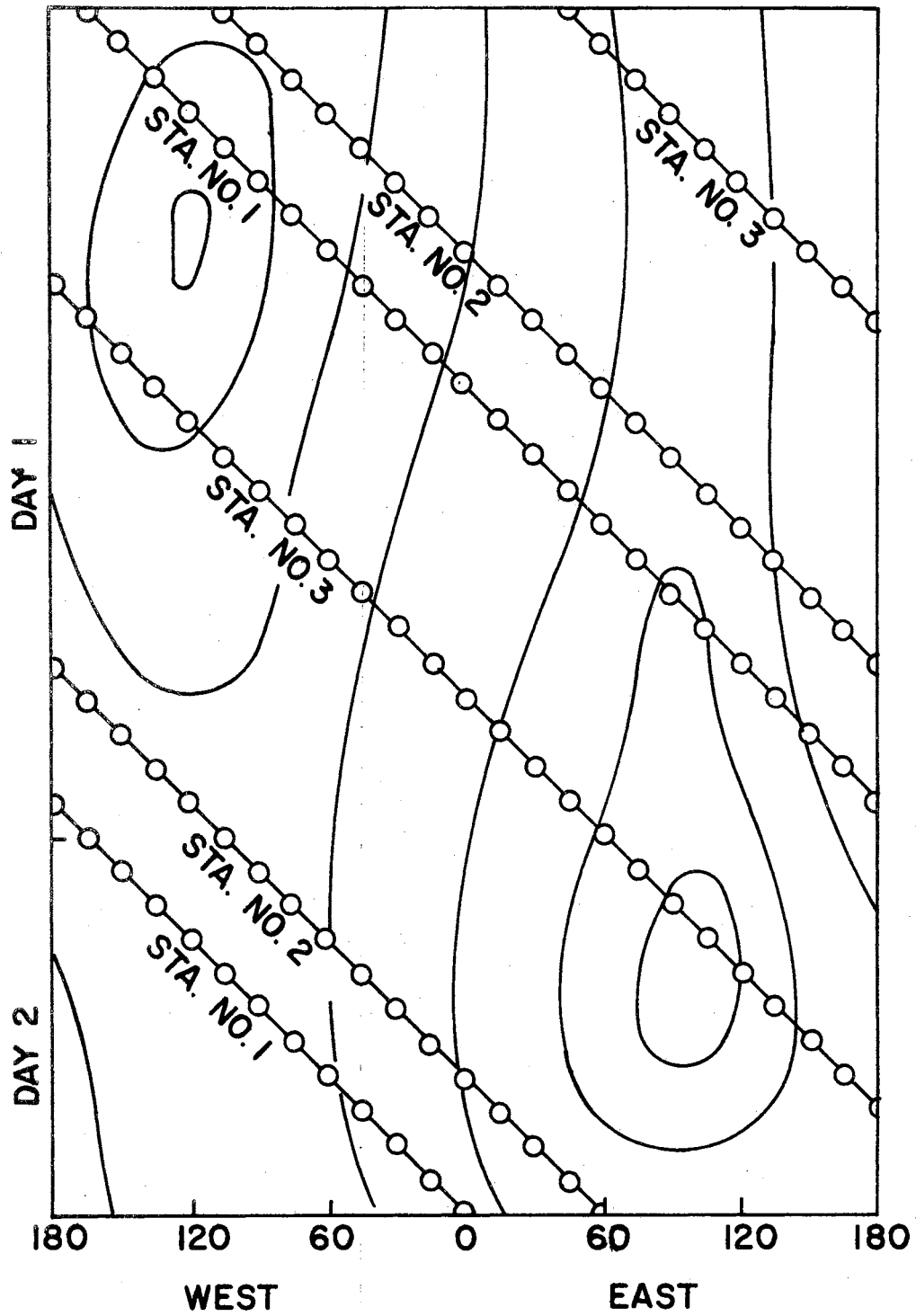
Figure 12. Hypothetical Cosmic Ray Contour Map.

(e) All station records contain random fluctuations which are not related to the cosmic-ray primary flux. These arise from the statistical nature of the measurements, and from uncompensated instrumental and environmental changes. It is desirable that the interpolation routine used be able to discriminate between uncorrelated fluctuations and those variations which are supported by neighboring values in the time-direction plane (i.e., hour-to-hour, or station-to-station conservation).

The method developed herein is superior to that employed in the earlier work principally in the solution of these problems, since only points (a) and (d) were effectively solved previously. In addition, the early works were only partly quantitative with much reliance being placed on the subjective interpretation of the observer. In contrast, the present method has been reduced to a computational algorithm suitable for use with electronic data processors and which requires almost no subjective decisions to be made by the investigator.

4.2 Variational normalization by inverse filtering.

If the primary cosmic-ray flux is described as the sum of an isotropic flux $J_0(R)$ and an anisotropic flux ΔJ, a function of latitude (Λ), longitude (Ψ), and rigidity (R) such that

$$\frac{\Delta J}{J_0} = A(\Lambda, \Psi) R^\beta$$

then one may define, for any detector type and location in the earth's magnetic field, a directional sensitivity function $V(\Lambda, \Psi, \beta)$ such that the fractional change in the detector counting rate $\frac{\Delta N}{N}$ due to flux ΔJ is given as an integral over all solid angles ω as

$$\frac{\Delta N}{N} = \int_{\Omega = sphere} V(\Lambda, \Psi, \beta) A(\Lambda, \Psi) d\omega$$

(Rao, et al., 1962). The function V is known as the variational coefficient function for the detector and succinctly describes its directional characteristics. Thus, the solid angle $\Delta\Omega$ over which V is significantly different from zero defines the monitor's asymptotic cone of acceptance. Here it is convenient to consider V as a function of longitude alone, defined by

$$V(\Psi) = \int_{-\pi/2}^{\pi/2} V(\Lambda, \Psi, \beta=0)\, d\Lambda$$

a simplification which is particularly applicable for stations whose cones of acceptance are confined to low latitudes. This includes all stations with geomagnetic latitudes less than $\approx 60°$. The condition that $\beta = 0$ is not unduly restrictive since V is only a weak function of β in the range $-1 \leq \beta \leq +1$. Values of $V(\Psi)$ appropriate for neutron monitors have been computed for many station locations and tabulated for values of β in the range -1.5 to $+0.6$ (McCracken, et al., 1965).

As the diurnal rotation of the earth causes the cone of acceptance of the ground-based neutron monitor to scan the anisotropy $A(\Lambda, \Psi)$, the fractional change in the monitor's counting rate is a function of time given by a convolution integral (considering only the longitudinal dependence)

$$\frac{\Delta N(t)}{N} = \int_{\Psi_1}^{\Psi_2} V(\Psi) A(\dot{\Psi}_e t - \Psi)\, d\Psi$$

where $\dot{\Psi}_e$ is the angular velocity of the earth's rotation, relative to the earth-sun line, and $A(\Psi)$ is related to $A(\Lambda, \Psi)$ by

$$A(\Psi) = \int_{-\pi/2}^{\pi/2} A(\Lambda, \Psi)\, d\Lambda$$

The limits of the convolution integral (Ψ_1 , Ψ_2) are taken as the effective longitudinal extent of the cone of acceptance, and it has been assumed that $|\Psi_1 - \Psi_2| < 2\pi$. This convolution of the anisotropy function with the variational coefficient function of the monitor may be viewed as a linear filtering operation (Chapter II, Section 2.3). Since the data record of a monitor is usually thought of as a time-history function, it is convenient to measure angle in hours or days using the relation $\Psi = \dot{\Psi}_e t$, taking Ψ as east longitude, $\dot{\Psi}_e$ the earth's rotational velocity, and t in universal time, the result being that one speaks of the variational <u>frequency</u> and <u>phase</u> response of the monitor and plots the variational coefficient function versus <u>time</u>. Thus for a variational coefficient function V ($\dot{\Psi}_e t$) one has a complex amplitude response characteristic, H, a function of frequency f,

$$H(f) = F.T. \; V(\dot{\Psi}_e t) = \int_{\Psi_1}^{\Psi_2} V(\dot{\Psi}_e t) \, e^{-2\pi i f \dot{\Psi}_e t} \, d\dot{\Psi}_e t$$

which specifies the variational gain-phase response of the monitor. It is important that, in using this nomenclature, one carefully distinguishes between true time variations in the primary flux and time variations in the data record caused by the scanning of a fixed, time invariant anisotropy. The above discussion is predicated upon the assumption that the anisotropies being scanned are time invariant, a condition which is effectively met if the time scale of any temporal change is greater than $(\Psi_2 - \Psi_1)/\dot{\Psi}_e$, i.e., the time required for the asymptotic cone to scan its own width.

With this viewpoint of the effect of the cone of acceptance of a station acting as a linear filter distorting the original waveform of an anisotropy and with each station having a different filter

characteristic, the problem of attempting a detailed comparison of records from different stations becomes clear. A possible solution is also indicated. That is, it should be possible to devise, for each station, a numerical convolution filter, inversely related to the effective filter of the acceptance cone, which would undo the effects of this prefiltering, at least to the extent of reducing the combined filter response to a common characteristic for all stations.

One seeks, then, a weighting function k(t), different for each station, which when convolved with the data from its own station will produce a combined filter characteristic L(f), the same for all stations. L(f) should have the following features:

(a) It should have a low-pass characteristic, i.e., frequency components below a certain cut-off frequency should be passed with little or no attenuation while those above this frequency should not be passed. All frequencies are of interest; however, in the practical case an upper limit exists to the meaningful components because of the effects of recording data as total counts over some finite interval, usually one hour, and because the attenuation of high frequency components by the finite width of the acceptance cone may result in their recorded amplitude being less than the ever-present statistical fluctuation.

(b) L(f) should be real, i.e., the combined filter characteristic should produce no phase shift at any frequency. This is equivalent to saying that the mean direction of viewing of the station should not be frequency dependent after the inverse filtering operation.

(c) The shape of L(f) should be chosen so that the transient response is well-behaved, i.e., the impulse response should be well localized and exhibit a minimum of ringing. These conditions may be

met by a number of functions; the one used in the present study is

$$L(f) = (1 - (\alpha f)^2)^2 \qquad |f| \leq \frac{1}{\alpha}$$

$$L(f) = 0 \qquad |f| > \frac{1}{\alpha}$$

where α is the absolute cut-off frequency (point at which the response becomes zero).

The weighting function of the inverse filter is found by inverse Fourier transformation (Chapter II, Section 2.4).

$$k_s(t) = F.T^{-1}\left[\frac{L(f)}{H(f)}\right]$$

$$= \int_{-\infty}^{\infty} \frac{L(f)}{H_s(f)} e^{2\pi i f t} df$$

The subscript s has been used to indicate that the weighting function k is unique for each station and is determined by the station variational response function, H, which in turn was derived from the station variational coefficient function. The variational coefficient functions which have been computed are not given as continuous functions, but are tabulated on 5° (20 minute) intervals. Since $k_s(t)$ is to be convolved with discrete count sums, totaled over some finite interval (usually one hour), it is sufficient to know k_s only at hourly (15°) intervals. Accordingly the Fourier integrals may be replaced by appropriate approximating sums. Thus, the real and

imaginary parts of H(f) are computed as

$$H_r(f) = \frac{1}{2n} \sum_{j=-n}^{n} V(\Psi_j) \cos \frac{2\pi(\Psi_j - \Psi_0)mf}{n}$$

$$H_i(f) = \frac{1}{2n} \sum_{j=-n}^{n} V(\Psi_j) \sin \frac{2\pi(\Psi - \Psi_0)mf}{n}$$

$$f = 0, \frac{1}{m}, \frac{2}{m}, \cdots \frac{n}{m} \; ; \; m = \frac{n\Delta\Psi}{2\pi}$$

In the present study $\Delta\Psi = \Psi_j - \Psi_{j-1}$ was taken as 15° and $V(\Psi_j)$ as 15°

sums centered on Ψ_j. Ψ_0 was taken as the direction of maximum

sensitivity (the angle associated with the largest tabulated value of

the variational coefficient function). This angle becomes, after

convolution, the frequency independent mean direction of viewing of the

station. The value of n should be at least large enough that n $\Delta\Psi$ is

greater than the width of the acceptance cone, in order to assure that

the sums are good approximations to the original integrals. In this

work the very conservative value n = 36 has been used. The units of f

are cycles per revolution (day). The real and imaginary parts of $\frac{L(f)}{H(f)}$

are then given by

$$\left(\frac{L}{H}\right)_r = \frac{L_r H_r + L_i H_i}{H_r^2 + H_i^2}$$

$$\left(\frac{L}{H}\right)_i = \frac{L_i H_r - L_r H_i}{H_r^2 + H_i^2}$$

And, finally, k(t) is computed as

$$k(t) = N \sum_{f=0}^{\left(\frac{n}{m}\right)-1} \left(\frac{L}{H}\right)_r \cos \frac{2\pi f}{2n} \left(\frac{t}{24}\right)$$

$$+ N \sum_{f=0}^{\left(\frac{n}{m}\right)-1} \left(\frac{L}{H}\right)_i \sin \frac{2\pi f}{2n} \left(\frac{t}{24}\right)$$

$$t = 0, \pm 1, \pm 2, \cdots \pm n$$

$$f = 0, \frac{1}{m}, \frac{2}{m}, \cdots \frac{n}{m}$$

where N is a normalization factor chosen so that

$$\sum_{t=-N}^{n} k(t) = 1$$

The units of t are hours.

Variational coefficient functions for three moderately high latitude neutron monitoring stations are shown in Figure 13 and the corresponding variational amplitude and phase responses are shown in Figures 14, 15, and 16. Even for these stations, whose cones of acceptance are as narrow as any station with geomagnetic latitude less than 60°, the response functions have, for the work here contemplated, undesirable characteristics:

(a) Variational frequency components higher than $\approx$ 2 cpd are severely attenuated.

(b) The phase response of each station is strongly frequency dependent.

(c) Although the amplitude response characteristics of these stations are rather similar, strong differences appear in their phase responses.
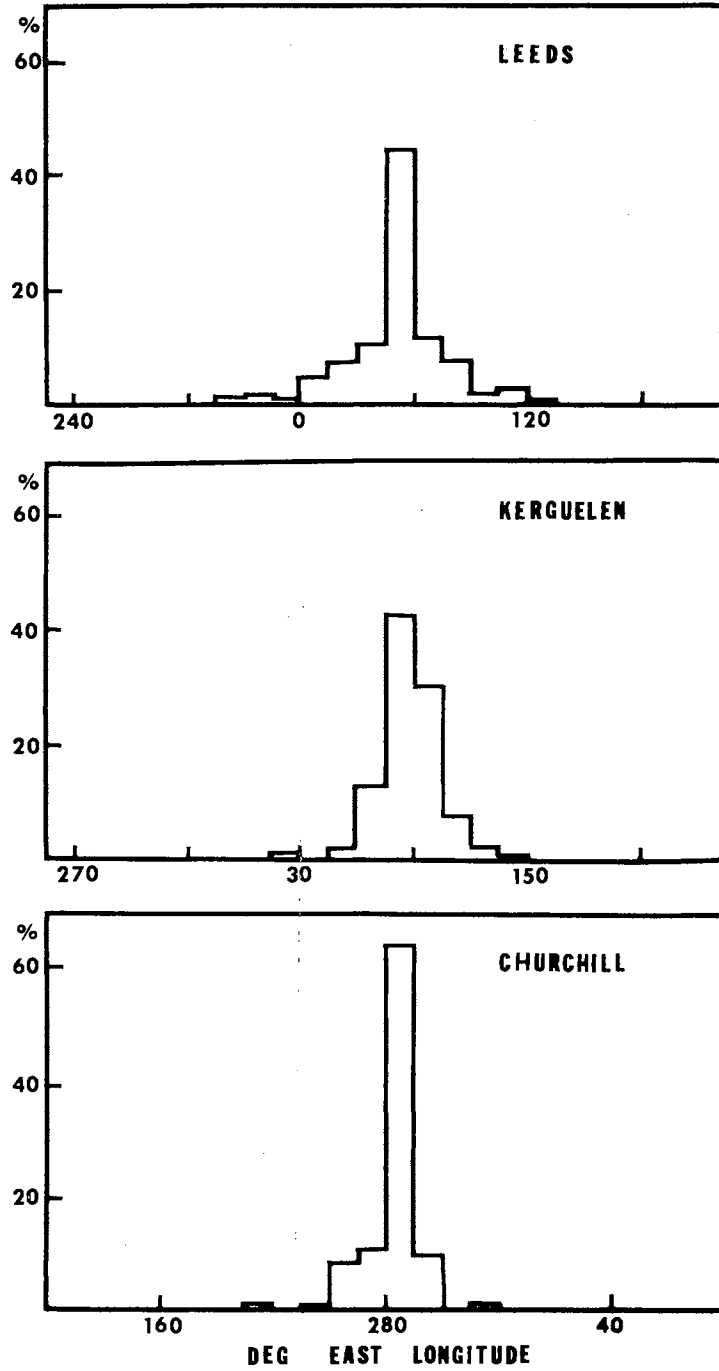
Figure 13. Variational Coefficient Functions.
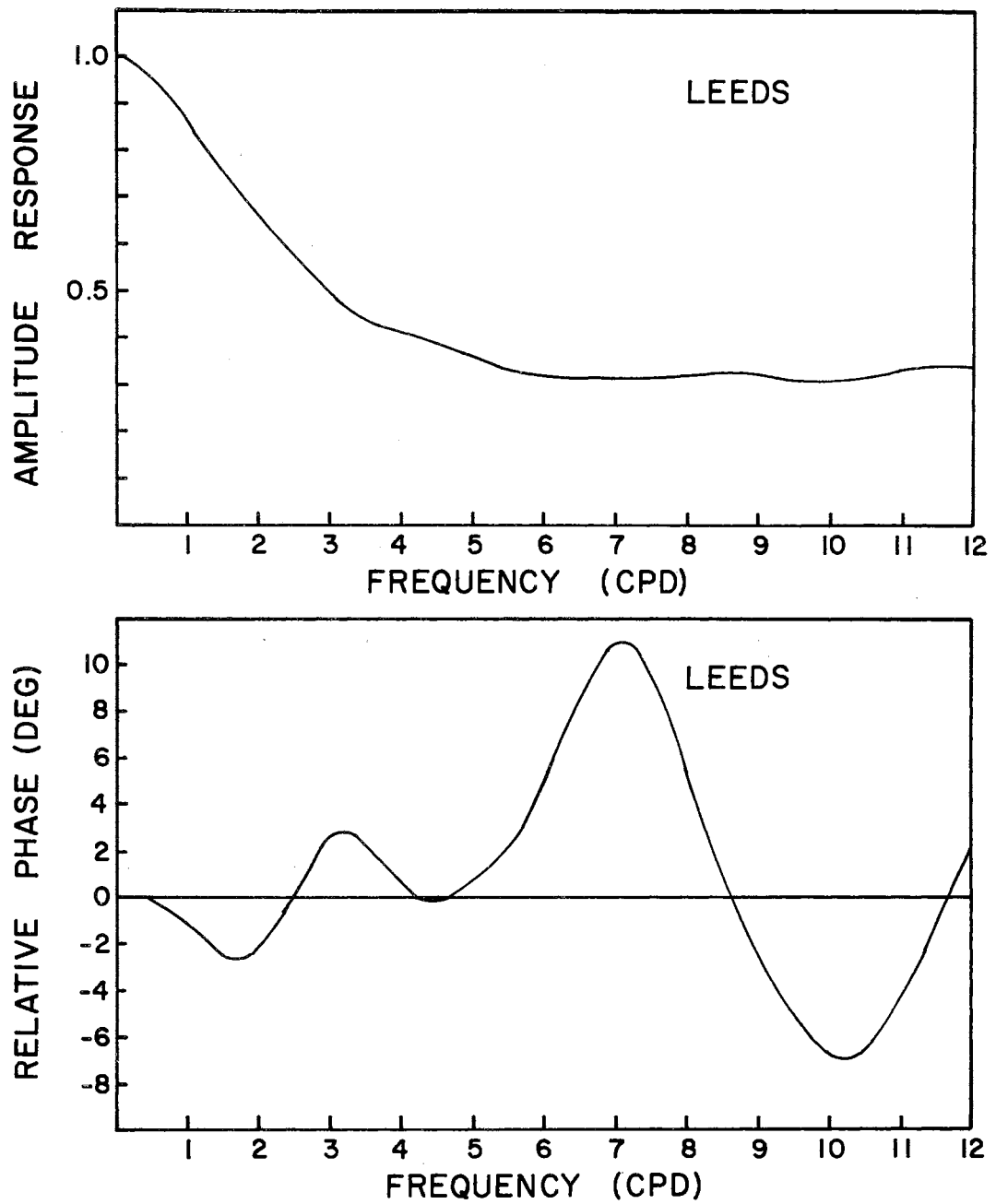
Figure 14. Variational Response (Leeds).
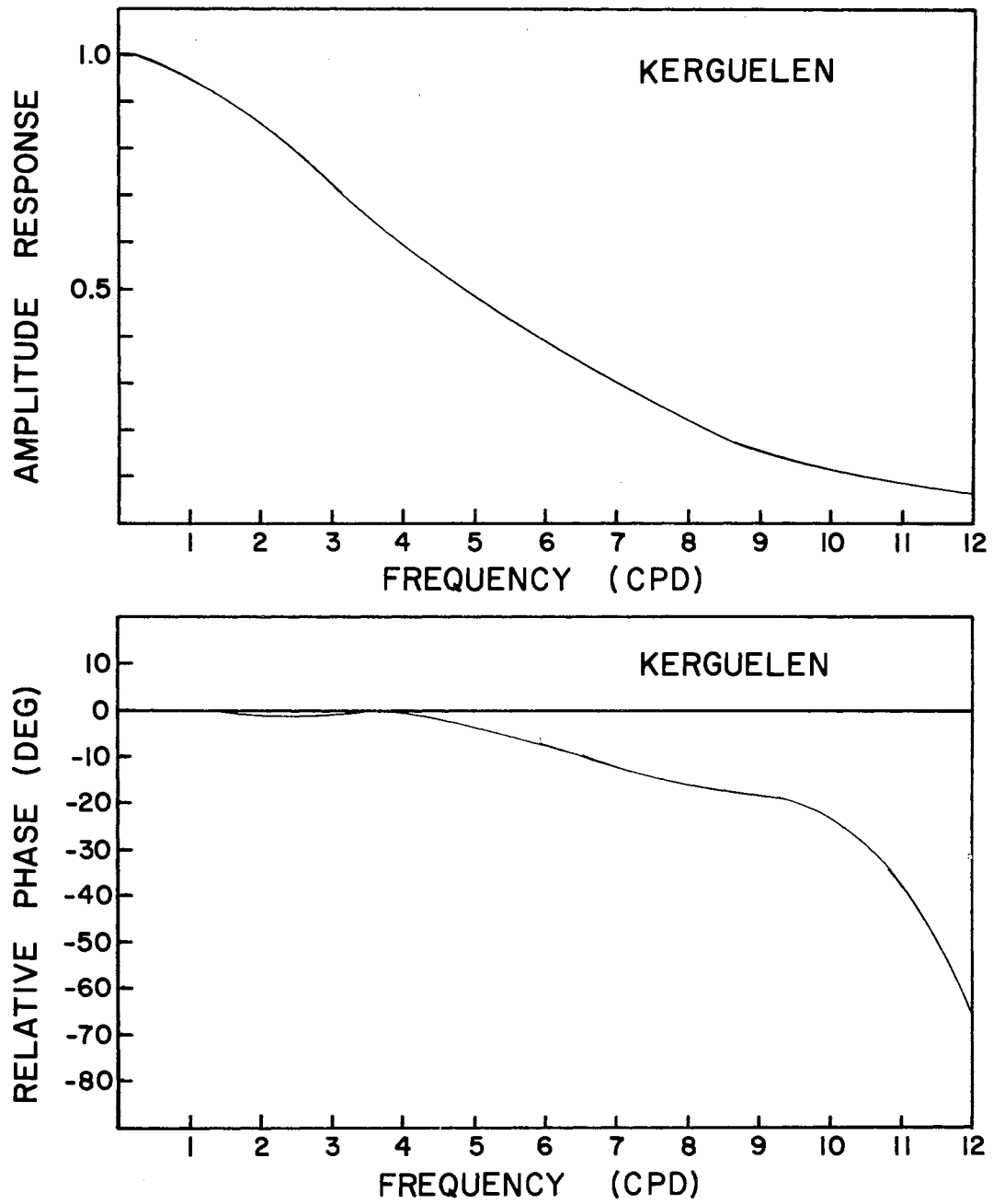
Figure 15. Variational Response (Kerguelen).
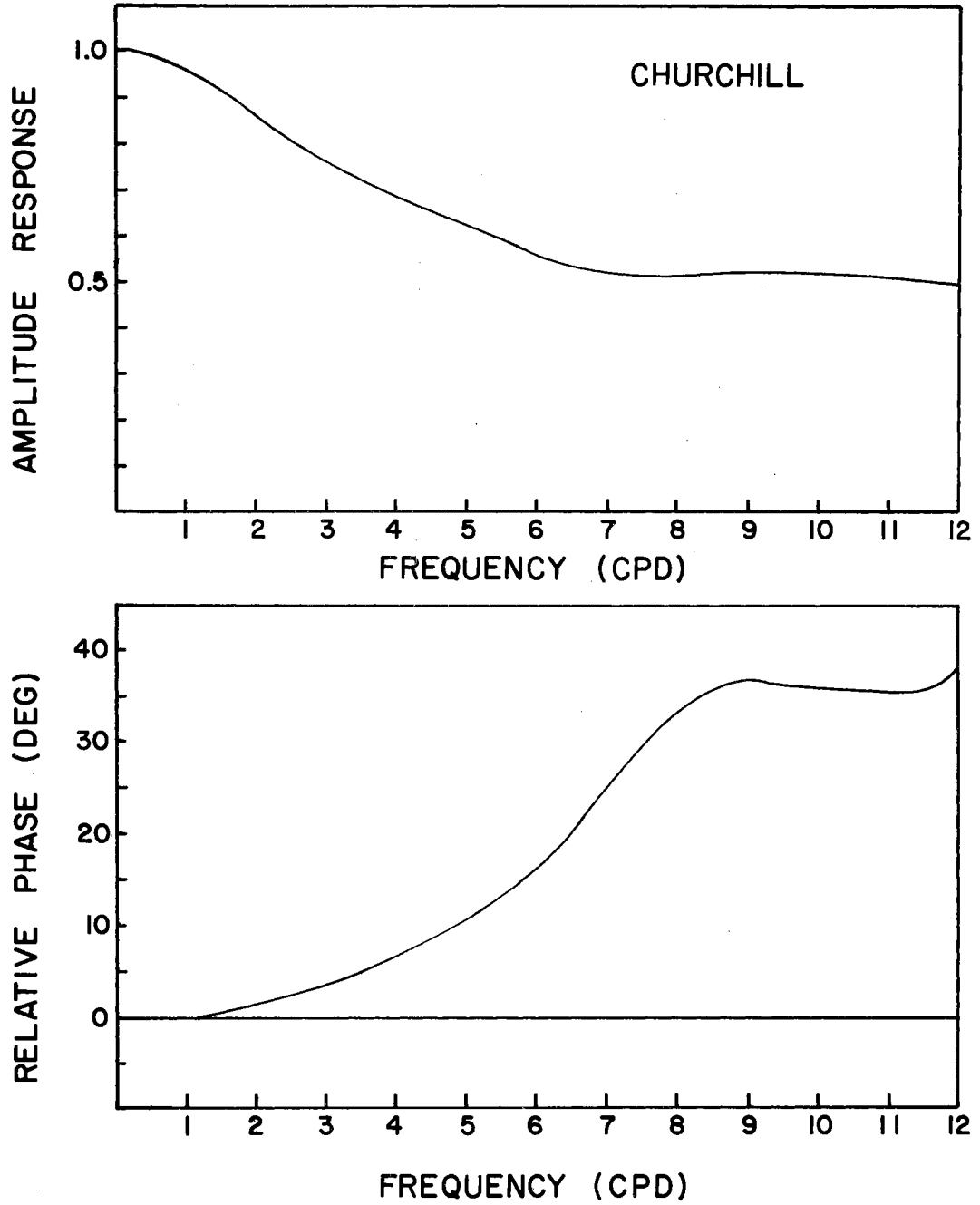
Figure 16. Variational Response (Churchill).

For lower latitude stations, e.g., Dallas, which have broader cones of acceptance (Figure 17), these defects become even more serious.

As a check on the inverse filtering process and the computational algorithms developed above, hourly weights were computed for the inverse filter appropriate for the variational coefficient function of the Dallas neutron monitor using

$$L(f) = \left[1 - \left(\frac{f}{8}\right)^2 \right]^2$$

which gives an 8 cpd absolute cut-off frequency. These weights were convolved with a data time series which represented the computed response of the Dallas monitor to a unit unidirectional flux with a superposed unit omnidirectional flux. Thus

$$\underline{d}(t) = \sum_{\tau=t-n}^{\tau=t+n} d(\tau)k(t-\tau)$$

where d(t) is the raw data value for hour t and $\underline{d}(t)$ the corresponding value after inverse filtering and where t is allowed to have only integral values, as in the case of any station which reports only hourly counting totals. The result is displayed in Figures 18 and 19. The following important points are noted:

(a) The response of the monitor to a unit unidirectional flux traces out the latitude independent variational coefficient function of the monitor; hence, this response is generally broad and asymetrical. After inverse filtering, however, the response is significantly narrowed and symmetrical about the position of the unidirectional flux.

(b) The effective transient response is improved in that, for a unidirectional flux only one significant response peak is seen after inverse filtering whereas spurious responses are noted in the raw data.
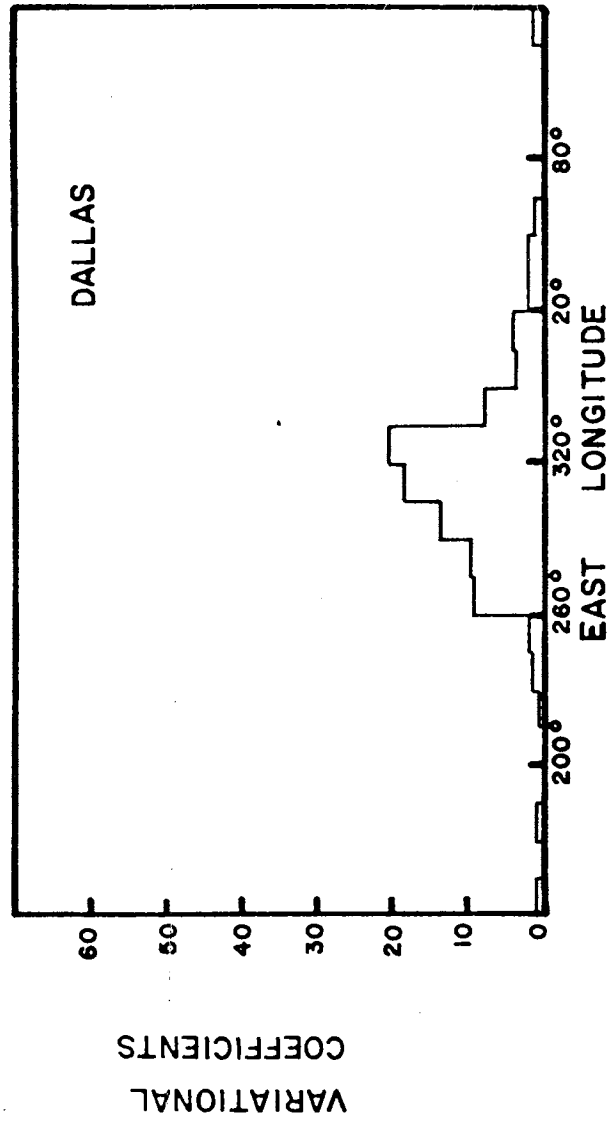
Figure 17. Variational Coefficient Function (Dallas).
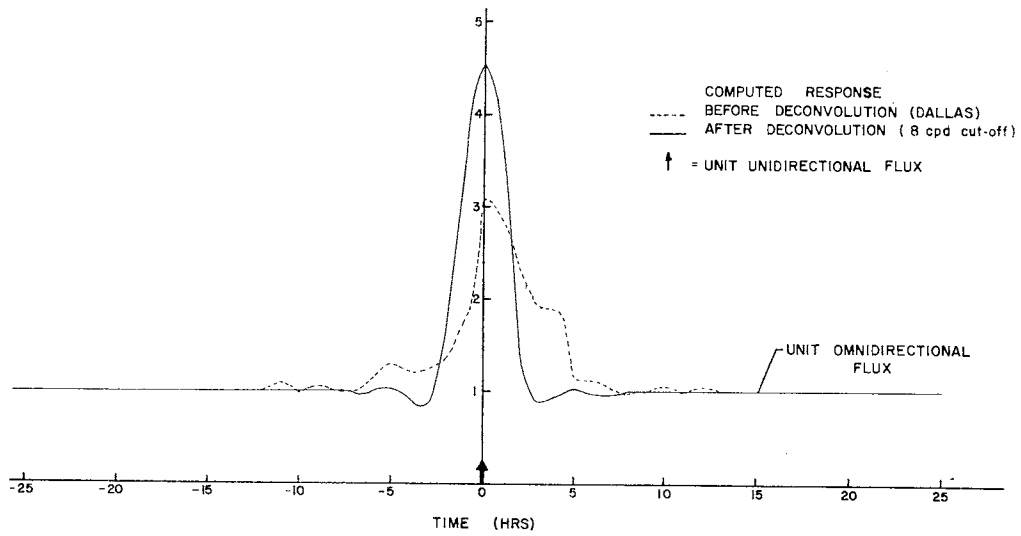
Figure 18. Deconvolution Example (One Flux).
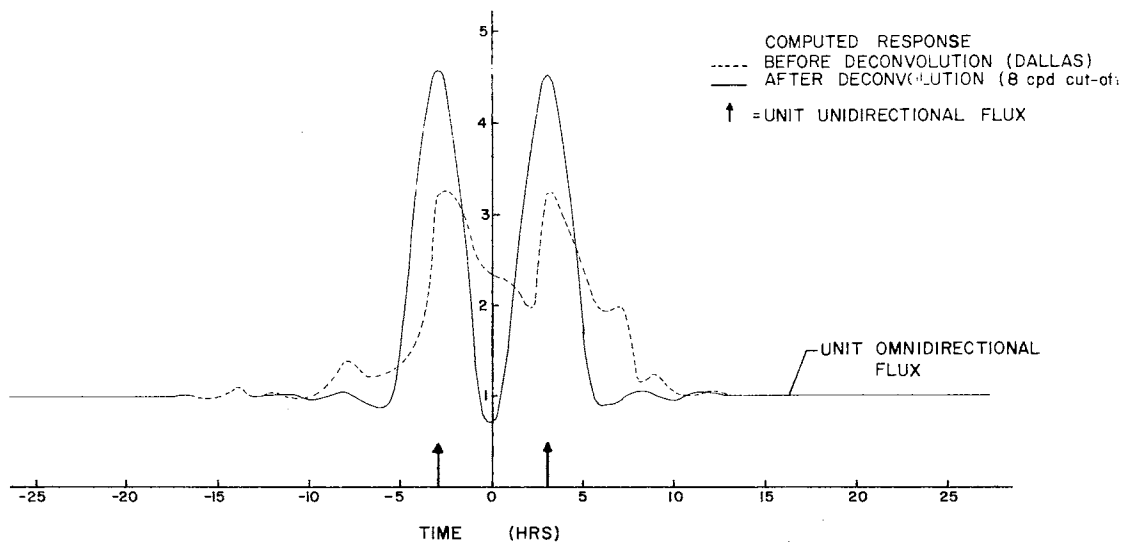
Figure 19. Deconvolution Example (Two Fluxes).

(c) When two unidirectional fluxes are closer together than the effective width of the station cone of acceptance, the response to each is, in the raw data, smeared into the other. After inverse filtering the separate identities of the two fluxes are restored (Figure 19).

(d) The effect of inverse filtering may be viewed as replacing the original cone of acceptance of a station, as represented by the variational coefficient function, by a new cone represented by the Fourier transform of L(f). Since the same function, L(f), may be used for all stations, inverse filtering can effectively reduce the acceptance cones of all stations to a standard form, thus allowing meaningful inter-comparisons to be made.

4.3 Construction of the time-direction intensity contour map.

Actual construction of a time-direction intensity map was begun with the selection of nine monitoring stations for inclusion in this study (Table III). The choice of these stations was dictated by several factors including the availability of data, the desirability of high counting rates, the need for mid-latitude station locations to produce acceptance cones which are neither too broad, due to too low a latitude, or make too large an angle with the equatorial plane, due to too high a latitude, and the requirement that, so far as possible, the mean directions of viewing be distributed uniformly in longitude. All stations chosen employ the large NM-64 type monitor developed for the International Quiet Sun Year with the exception of Mt. Wellington, which was the only mid-latitude station available in the Asiatic-Pacific region.

TABLE III

SELECTED NEUTRON-MONITOR STATIONS

Station	Type	Location	Geographic Latitude (N)	Geographic Longitude (E)	Elevation (M)	Cut-off Rigidity(GV)
Calgary	NM-64	Canada	51.08	-114.09	1140	1.09
Churchill	NM-64	Canada	58.75	- 94.09	39	0.21
Deep River	NM-64	Canada	46.10	- 77.50	145	1.02
Goose Bay	NM-64	Canada	53.33	- 60.42	SL	0.52
Inuvik	NM-64	Canada	68.35	-133.73	SL	0.18
Kerguelen	NM-64	South Indian Ocean	-49.35	70.22	SL	1.19
Leeds	NM-64	England	53.82	- 1.55	100	2.20
Mt. Wellington	IGY	Tasmania	-42.92	147.24	725	1.89
Sulphur Mt.	NM-64	Canada	51.20	-115.61	2283	1.14

SL = sea level

For each station inverse filter weights relative to the function

$$L(f) = \left[1 - \left(\frac{f}{6}\right)^2 \right]^2$$

were computed and the raw data, after being scrutinized for spurious values and patched by linear interpolation to fill minor gaps, was convolved with these weights to produce variationally normalized data time-history functions. An example of the data before and after inverse filtering is shown in Figures 20 and 21. The absolute cut-off of the combined response function is 6 cpd.

Two separate methods were used to effect a sensitivity correction to account for the differing counting rates of the various stations. The first method used consisted of expressing the output of each station as a deviation in per cent from its mean rate for the current month, the analysis being carried forward on a month-to-month basis. In the second method used, only a single station record was expressed as a deviation percentage. The other stations were normalized to this, selected, station's variance by multiplying each of the other records by a constant selected so that the variances of all stations were made equal, i.e.,

$$\sum (d_i - d_{mean})^2 = const$$

Both methods suppress true variations with time scales of one month or more as well as suppressing the long-term drift of the detection efficiency. This situation can be improved only when a suitable sensitivity calibration technique is available for determining the absolute sensitivity of a monitor. An advantage of the second method given above is that differences in the detector characteristics, such
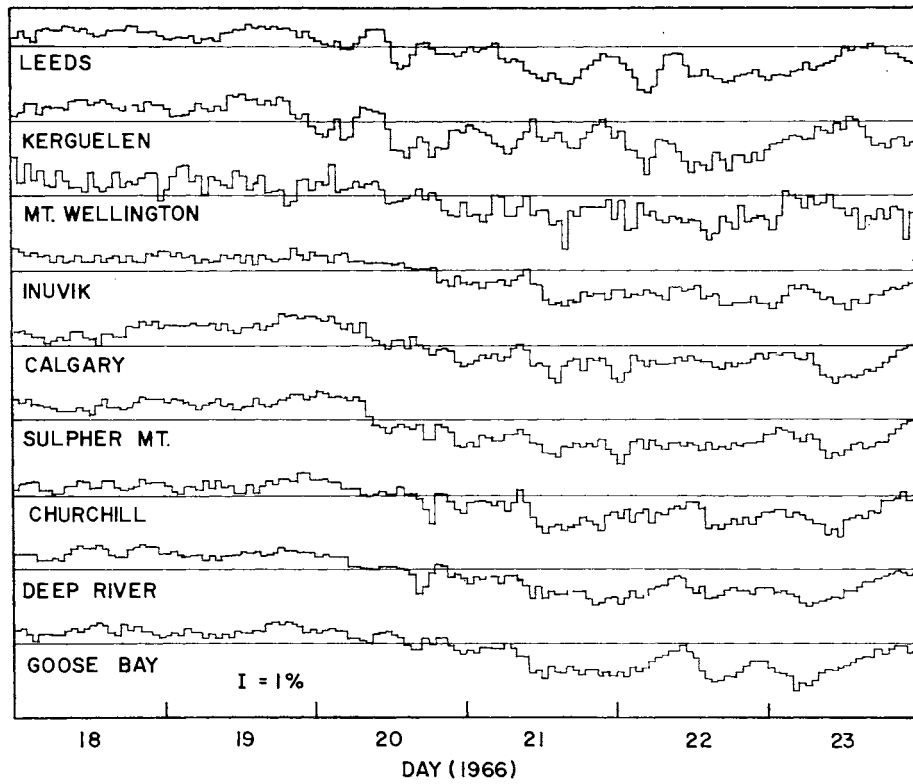
Figure 20. Raw Neutron-Monitor Data.
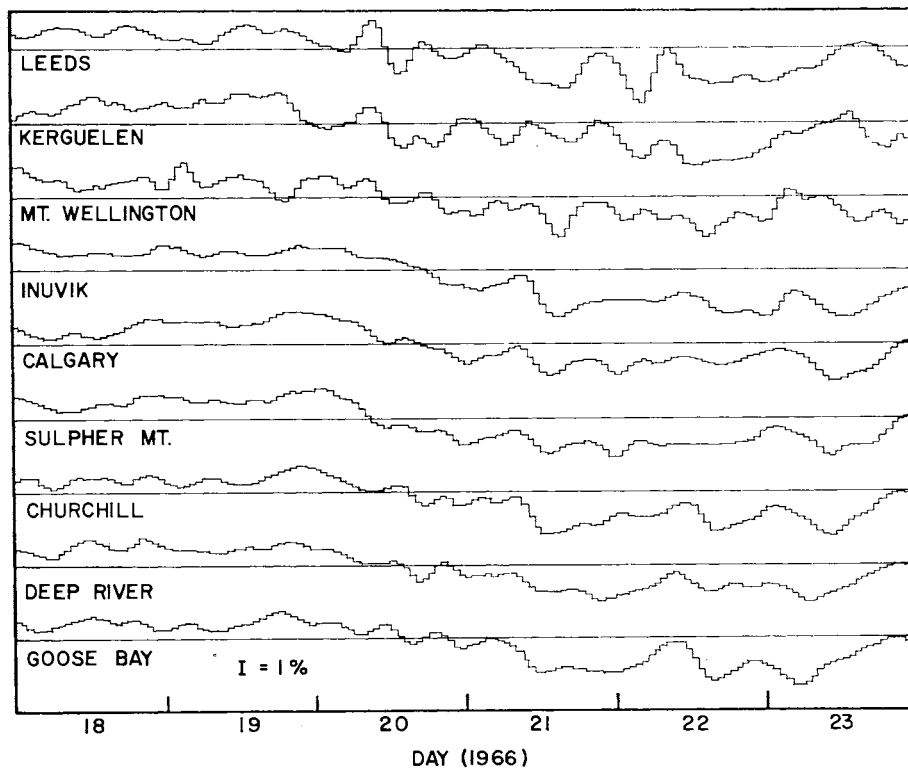
Figure 21. Deconvolved Neutron-Monitor Data.

as variation in elevation, which can produce differences in the variance of records from otherwise identical stations, are suppressed. In practice this method seemed to produce the better results. The station chosen to normalize all others was Deep River since this station has a long history of good stability and freedom from meteorological effects.

Close examination of the diurnal anisotropy (McCracken and Rao, 1965) has shown that the amplitude of this anisotropy varies as the cosine of the asymptotic latitude. Also, in this study the standard deviation of the variation of most neutron monitors, after correction for the finite width of their asymptotic cones, is observed to be roughly proportional to the cosine of the mean asymptotic latitude. This suggests that perhaps most anisotropies are strongest in the ecliptic plane, falling off as the cosine of the angle made with the ecliptic. Following this assumption one can make a tilt correction by multiplying each data value by the reciprocal of the cosine of the instantaneous angle made by the mean direction of viewing of the station with the ecliptic plane. Denoting this angle by θ, then

$$\sin \theta = \cos(\alpha + \beta) + (1 + \cos \gamma) \sin \alpha \sin \beta$$

where α is the angle between the axis of the earth and the normal to the ecliptic plane ($23° \, 27'$) and β is the colatitude of the station's mean direction of viewing. The angle γ is the instantaneous right ascension of the mean direction of viewing, which is, measured in hours of arc, equal to the local mean sidereal time of the viewing meridian. γ may be computed (in radians) from

$$\gamma = (\psi_s^h \cdot 0.2617994) + 1.744093 + (0.2625162 \, \Delta t_{UT}^h)$$

where ψ_s^h is the east longitude of the mean direction of viewing, measured in hours of arc, and Δt_{uT}^h is the number of hours (UT) which have elapsed since 0^h UT, January 1.

The normalized, latitude corrected, inverse filtered, hourly data from all stations form a matrix $\underline{d}_{ij}$, i = 1, 2, ..., N = number of stations used, j= 1, 2, ..., M = number of hours in the time interval under consideration. Associated with each $\underline{d}_{ij}$ are a time t_j and angle θ_{ij} giving the location of the datum in the time-direction plane. An estimate of the value of the intensity function at an arbitrary point (t_o, θ_o) is given by

$$
\underline{d}(t_o, \theta_o) = \frac{\sum_{ij} g(\theta_{ij} - \theta_o) h(t_j - t_o) \underline{d}_{ij} W_i}{\sum_{ij} g(\theta_{ij} - \theta_o) h(t_j - t_o) W_i}
$$

This represents a two-dimensional convolution over the observed data by the weighting functions $g(\theta)$ and $h(t)$, the ith column of the data matrix, representing the data from the ith station, being weighted by W_i. The convolution product is most easily investigated in the frequency domain, the Fourier transforms of g and h giving, respectively, the reciprocal angle response (hereafter called the wave-number response) and the reciprocal time (frequency) response of the two-dimensional filtering process which the convolution implies. The weights $\{W_i\}$ are chosen to be a measure of the reciprocal station density, (stations per unit angle)$^{-1}$, to compensate for the uneven spacing of monitoring stations around the world. A rough, but sufficient, estimate of this quantity is given by the angular separation between the ith station's nearest eastward and nearest westward

neighbors. For the present work, g and h were taken as simple triangular functions,

$$g(\theta) = \Theta - |\theta| \qquad |\theta| \leqslant \Theta$$

$$g(\theta) = 0 \qquad |\theta| > \Theta$$

$$h(t) = T - |t| \qquad |t| \leqslant T$$

$$h(t) = 0 \qquad |t| > T$$

giving a two-dimensional low-pass filter where the constants Θ and T determine the cut-offs of the filter in wave-number and frequency respectively.

An alternate approach to the estimation of the intensity function at an arbitrary point, one which is commonly used to construct baro-metric pressure contour maps and the like, is to pass a polynomial surface through a limited number of points in the neighborhood of the point at which the mapped parameter is to be estimated and to accept the value of the polynomial at this point. The disadvantage of this technique for neutron-monitor data analysis lies in the implied assumption that, to within the working accuracy of the analysis, the available data is correct. The neutron-monitor data is known to contain random fluctuation components, not related to the primary cosmic-ray flux, which can mask true variations of interest. In an attempt to overcome the effects of statistically poor data some workers have used the least squares criterion to fit an overdetermined polynomial surface to the data. The advantages of the filter approach employed in this study are:

(a) No specific model, such as a polynomial surface, need be assumed.

(b) A direct physical interpretation of the effect of the interpolation process is available through the variational response characteristics of the filter.

(c) Viewed as a weighted average over data values in the vicinity of (t_b, Θ_b) the process is clearly one which reduces incoherent random fluctuation while tending to preserve coherent variations.

(d) If g and h are even functions, their Fourier transforms will be real, indicating that phase relationships in the original data are not distorted.

The choice of values for Θ and T is determined by the experimental data. On the one hand, it is desirable that Θ and T be large so that, the resulting averaging interval being large, the random statistical fluctuations inherent in the data are greatly reduced. On the other hand, too large values for Θ and T may result in attenuation of meaningful rapid variations. One way to determine reasonable limits to the size of Θ and T is to find the maximum variational frequency for which high correlation is preserved for two mid-latitude stations whose cones of acceptance scan almost the same regions at the same time, but which are so geographically located that their local environmental conditions are not strongly related. For such a pair of stations it is reasonably certain that correlation in their counting variations is due to variations in the primary cosmic-ray flux.

A frequency dependent measure of correlation is the coherence, R, given by

$$R(f) = \frac{P_{12}(f)}{\sqrt{P_1^2(f) + P_2^2(f)}}$$

where P_1 and P_2 are the power spectra, respectively, of stations 1 and 2, and P_{12} is the cross-power spectrum of the same stations (Chapter II, Section 2.2). Accordingly the power spectra, cross-power spectrum, and coherence of data from the Leeds, England, and Kerguelen Island stations were computed using algorithms analogous to the ones given previously for power-spectrum analysis (Chapter III, Section 3.3). The results, shown in Figure 22, indicate that

(a) A high degree of coherence exists for the entire interval, zero frequency to 1 cpd.

(b) In the frequency region higher than one cpd the coherence drops off sharply.

(c) An isolated region of relatively high coherence exists in the neighborhood of 2 cpd.

It should be noted that, although these stations lie in different hemispheres of the earth, their mean directions of viewing differ by only 30° in longitude.

The values of $\odot$ and T used in this study were 5 hours of arc and 15 hours respectively yielding effective cut-offs of approximately 1.6 cycles per radian and 3.2 cycles per day. In view of the lack of coherence demonstrated by the Leeds-Kerguelen data in the frequency region above 2 cpd, these values for $\odot$ and T would appear to be too small. However, it was desired that the resolution be high enough to reveal most of the detail of events such as Forbush decreases and relativistic particle producing solar flares. Since the time scale of such phenomena may, in some cases, be measured in minutes, and since these occurrences are rare enough that the strong, high-frequency variational components produced by them are not persistent enough to make their presence known
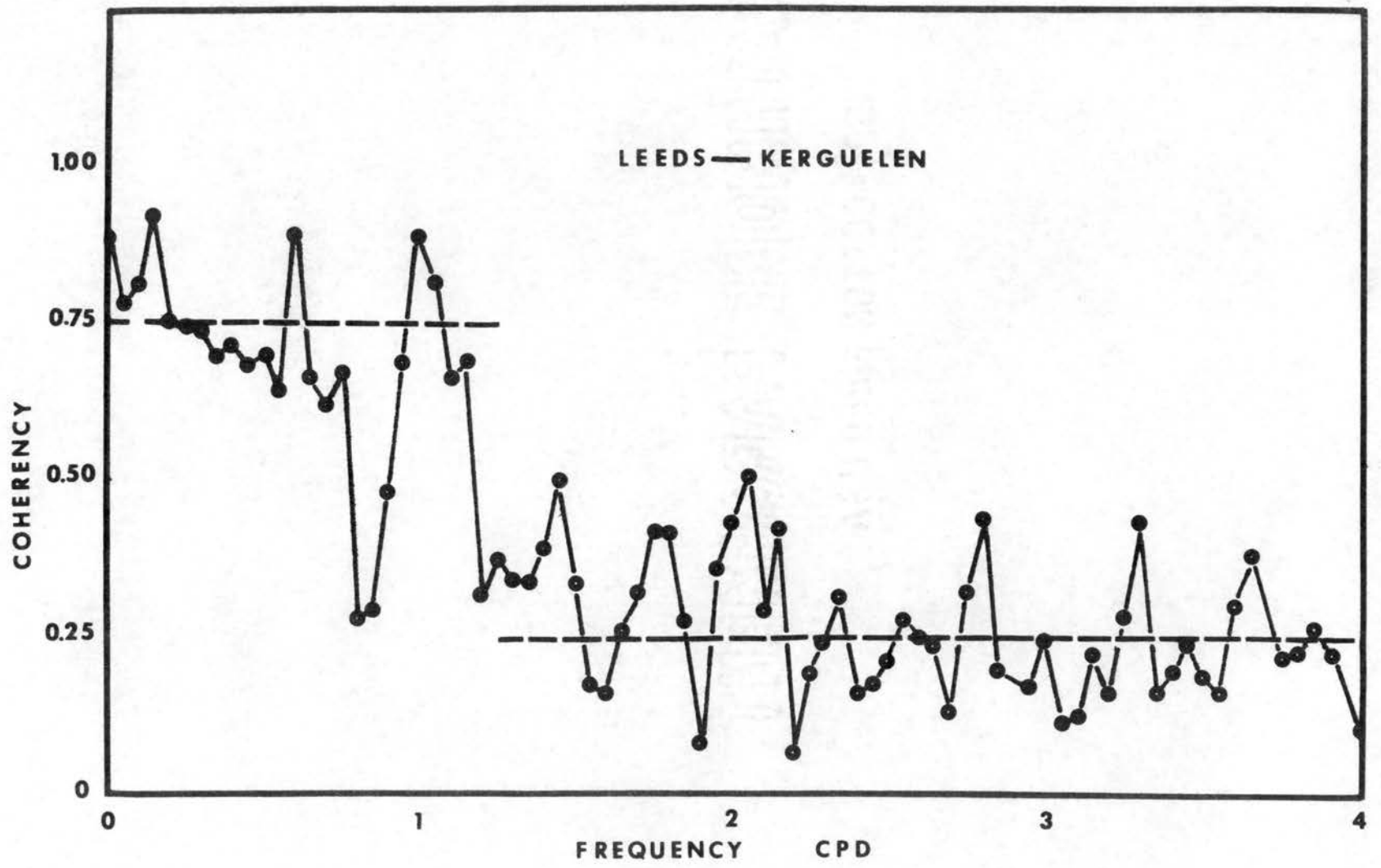
Figure 22. Coherency (Leeds-Kerguelen).

in a long-time-scale power-spectrum analysis, these values for ☉ and T
represent a compromise between larger values, which would give maximum
reduction of random variations without distorting meaningful variations
during undisturbed periods, and smaller values consistent with the
time scale of certain rare, but important, events.

Using the methods described in this section, cosmic-ray intensity
contour maps were constructed for the months of January, February, and
March of the year 1966. All computations necessary to produce
intensity estimates at the intersection points of a rectangular grid
with cells one hour by 15°, in the time-direction plane, were made on
the IBM 360/50 computer, and the intensity contours were drawn by hand
on large printed arrays of these values. The final contour maps were
produced from photographic reductions of these large-scale drawings.
Although the entire three-month period was examined in the large-scale
arrays, only selected, important events were reduced to actual contour
maps. These maps include

(a) the period January 3-7, 1966, during which the recovery from
a decrease late in December 1965 is observed

(b) the Forbush decrease of 20 January 1966

(c) a small decrease beginning 19 February 1966

(d) a small decrease beginning 13 March 1966

(e) the large Forbush decrease of 23 March 1966.

The 20 January 1966 Forbush decrease event represents a particularly well
defined example of such decreases. Also, this decrease was the first
to be observed in this study and, consequently, has been the one most
thoroughly analyzed of all the events listed above.

4.4 The Forbush decrease of 20 January 1966.

Figure 23 shows the cosmic-ray intensity contour map for the period

of time 19-23 January 1966 which includes a Forbush decrease of about 4%

of the pre-decrease intensity. The map indicates well the salient

features of this event:

(a) The event appears first at 2000 UT on January 19 as a decreased

cosmic-ray intensity from a limited set of directions centered on the

direction 65° west of the earth-sun line (Figure 24 shows a cross-section

of this decrease). This anisotropy persists until about 0900 UT on

January 20.

(b) About 1000 UT on January 20, a general decrease of about 1%

takes place in all directions except in the region between 65° and 90°

west of the earth-sun line. The decrease is sudden, with a time scale

of less than 3 hours (the resolving time of the intensity map).

(c) Following the general isotropic decrease and for the next 16

hours an anisotropic flux of particles is seen. The anisotropy is well

defined in direction, an intensity cross-section (Figure 25) indicating

the direction of maximum flux to be $84° \pm 3°$ west of the earth-sun line.

The flux maximum is roughly 0.8% greater than the mean intensity for

other directions. A small ($\approx 0.2\%$) decrease is seen during this time

at 95° east of the earth-sun line.

(d) About 1000 UT on January 21, a second isotropic decrease of

about 1% having a time scale of about 5 hours is seen.

(e) A short-lived, extremely anisotropic depression of about 1%

centered on $51° \pm 1°$ west of the earth-sun line and lasting for only

a few hours is clearly indicated at about 0400 UT on January 22.
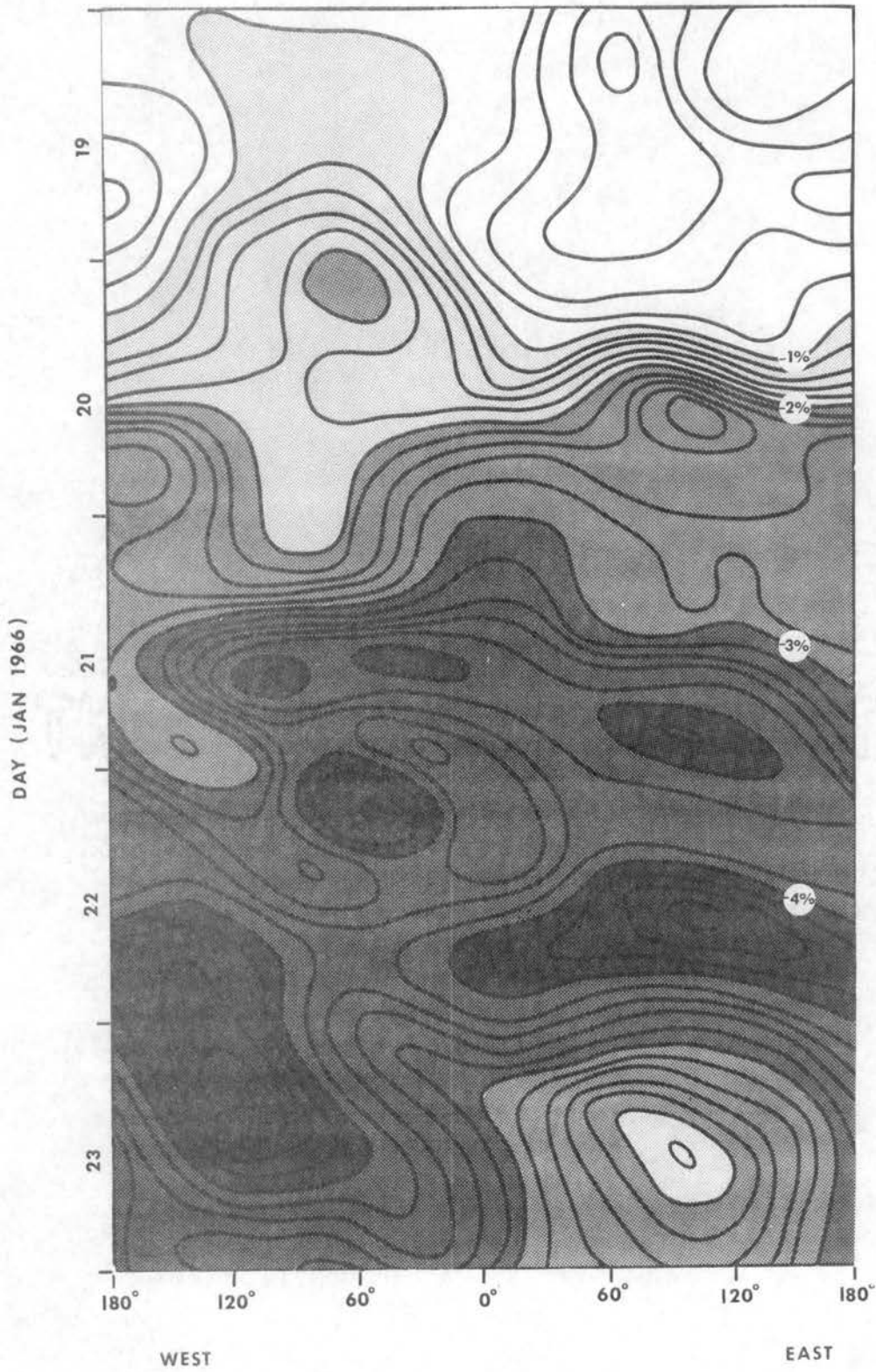
Figure 23. Intensity Contour Map for 19-23 January 1966.
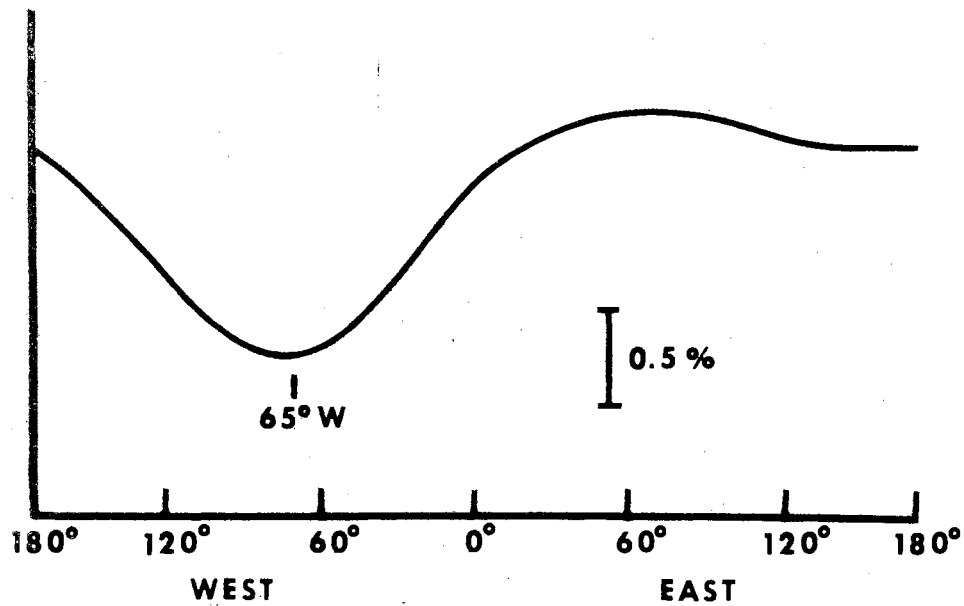
Figure 24. Pre-Decrease Cross-Section.
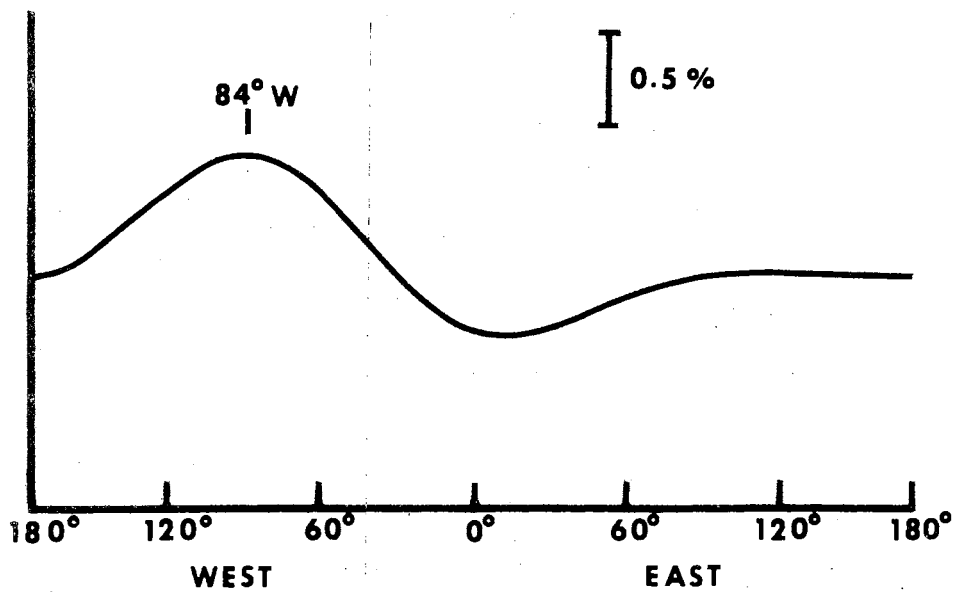
Figure 25. Anisotropic Excess Flux Cross-Section.

(f) The strongly anisotropic recovery phase of the Forbush decrease begins in the early hours of January 23, the cosmic-ray intensity from directions between 80° and 100° east of the earth-sun line being a maximum.

Parker (1963) has suggested that the Forbush decrease may be explained on the basis of an interaction between the cosmic rays and a magnetogasdynamic shock wave in the interplanetary medium resulting from the expansion of the enhanced chromosphere and corona at the time of a solar flare, and has obtained a similarity solution for such a shock. The result pictures a strong shock moving radially outward from the sun at a super-sonic velocity on the order of 1000 km/sec. The shocked material extends radially inward from the shock front to a contact surface with the enhanced flow region behind which the material velocities are sub-sonic. The plasma density behind the shock front is four times the density of the unshocked material ahead of the front. The normal spiral interplanetary magnetic field is sharply kinked at the shock front, and again at the contact surface; the field behind the contact surface is again the normal spiral field related to the radial plasma flow velocity by

$$\tan X = \frac{r \omega_s}{v_p}$$

where X is the angle between the radial direction and the magnetic field, ω_s is the angular rotation velocity of the sun, and v_p is the radial plasma flow velocity. In the shocked region, the magnetic field is compressed with the plasma and since

$$\frac{|B_1|}{|B_0|} = \frac{\cos X_0}{\cos X_1}$$

where the subscripts 0 and 1 represent the regions just before and just after the shock, respectively. The direction of the magnetic field just behind the shock is given by

$$\cos X_1 = \frac{1}{4} \cos X_0$$

The resulting magnetic field configuration is shown in Figure 26. To test this so-called blast-wave model against the precise experimental picture provided by the cosmic-ray intensity contour map, requires first that a usable correlation be found between the cosmic-ray intensity contours and one or more of the parameters of the Parker theory, and second that the results of the theory be restated as functions of these parameters related to the observable features of the intensity map.

McCracken and Ness (1966) have recently demonstrated in a convincing manner the close correlation between the direction of the interplanetary magnetic field and sharply defined short-lived (a few hours to a few days) cosmic-ray anisotropies. Through a comparison of the simultaneous magnetic and cosmic-ray anisotropy data from independent instruments carried by the Pioneer VI solar probe, they find that the magnetic field direction and the characteristic direction of transient cosmic-ray anisotropies are almost always the same. Thus it would seem that the cosmic-ray intensity contour map, which displays clearly the anisotropic nature of the cosmic-ray flux during a Forbush decrease, could provide information concerning the direction of the mean magnetic field over volumes of space corresponding to the scale size of a 10 GeV proton gyroradius (≈ 0.04 AU in a 5 γ field). In addition, if the decrease event can be reasonably associated with a particular solar flare, and if particular features of the intensity map can be associated
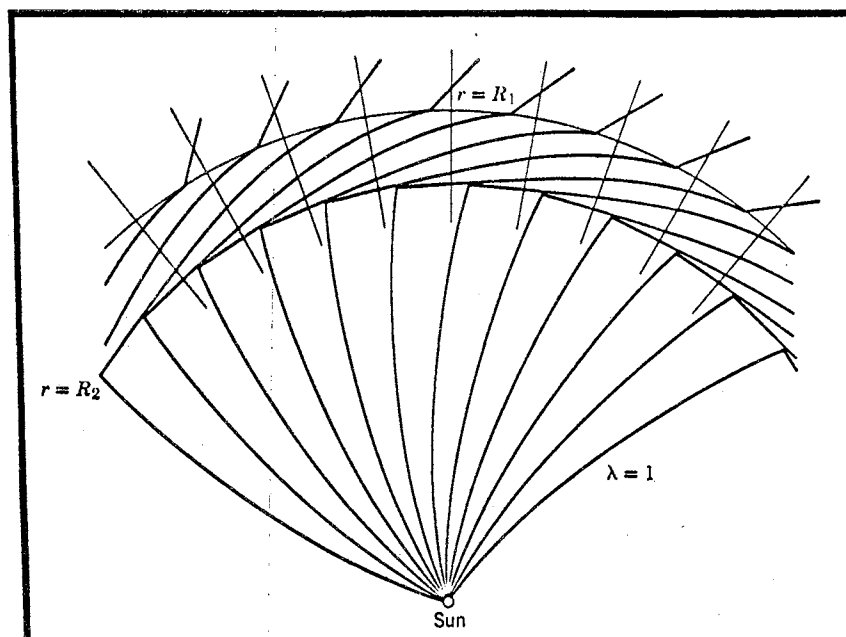
Figure 26. Magnetic Field for Parker Blast Wave.

with the passage of the shock front and the contact surface of the enhanced coronal flow, then the sun-earth transit times for these features can be determined. Parker has shown that the sharp bending of the interplanetary magnetic field at the shock front and at the contact surface could partially exclude cosmic rays from the expanding volume behind the shock, producing a two-step decrease in cosmic-ray intensity with the passage of these two magnetic constrictions. The two-step nature of the decrease of 20 January 1966 has already been noted. Also, examination of solar flare observation records (CRPL-FB-261) reveals that a flare of importance 3B was seen close to the center of the solar disc (19°N 27°E) at about 1100 UT on January 17. Activity in the same region continued to be high for the following 36 hours with another, smaller, flare (importance 2B) at about 2300 UT on January 18. One is thus lead to view the Forbush decrease event of January 20, in terms of the Parker blast-wave model, in the following manner:

(a) At 1100 UT on January 17, 1966, a solar flare increased the local heating of the solar corona to an extent sufficient to produce a shock wave in the interplanetary medium, the radial coronal flow being enhanced for some time afterward by continued activity on the sun, forming a driving, contact surface behind the shock front.

(b) The approaching shock resulted in an anisotropic decrease in cosmic-ray intensity, prior to the arrival of the shock at the earth, in the direction 65° west of the earth-sun line, indicating a value of 65° for X_o, the direction of the undisturbed interplanetary field. Such precursor-decreases have been previously discussed by McCracken (1962).

(c) The passage of the shock front at the earth was marked by a sudden isotropic decrease in the cosmic-ray intensity at 1000 UT

on January 20. Thus the sun-earth transit time of the shock was
2.5×10^5 sec.

(d) A well-defined maximum in the cosmic-ray flux during the
interval 1000 UT January 20 to 1000 UT January 21 is indicative of a
magnetic field in the shocked region in the direction $X_1 = 84°$ west of
the earth-sun line. During the time 0600-1200 UT on January 20, the
Pioneer VI spacecraft, situated 5.0×10^6 km from the earth at an
angle of 60° east of the earth-sun line, observed a strongly anisotropic
flux of energetic storm particles (Bryant, et al., 1962) in the energy
range 7.5 - 45 MeV with maximum flux 74° west of the earth-sun line
(McCracken, private communication). The correspondence in time and the
similar anisotropy directions suggest that the excess flux seen by the
neutron monitors was the high energy tail of the particle distribution
seen by Pioneer.

(e) The passage of the contact surface at the earth was marked by
the second isotropic decrease at 1000 UT on January 21 yielding a sun-
earth transit time for this feature of 3.5×10^5 sec.

(f) The sharp, short-lived anisotropy centered on 51° west of the
earth-sun line at about 0400 UT on January 22 is indicative of an
angle $X = 51°$ for the spiral interplanetary magnetic field in the enhanced
flow region behind the contact surface.

The principal results of the Parker blast wave theory are readily
expressed in terms of the transit times and magnetic field directions,
making possible a test of the consistency of the above description with
the theory. The similarity solution of the equations for the shock
introduces the similarity parameter

$$\eta = t\, r^{-\lambda}$$

a function of time t and radius r. The exponent λ is taken as a constant for any particular shock and is a function of the ratio $(\frac{\eta_1}{\eta_2})$ where η_1 and η_2 are the constant values of η associated with the shock front and the contact surface respectively. Parker has computed $(\frac{\eta_1}{\eta_2})$ for several values of λ in the range $1 \leqslant \lambda \leqslant \frac{3}{2}$. Figure 27 is a graph of these values versus λ with a smooth curve connecting them for aid in interpolation. The ratio $(\frac{\eta_1}{\eta_2})$ is related to the transit times since, by the definition of η,

$$\frac{\eta_1}{\eta_2} = \frac{T_1 Re^{-\lambda}}{T_2 Re^{-\lambda}} = \frac{T_1}{T_2}$$

where R_e is the sun-earth distance. For the January 20 event then,

$$\left(\frac{\eta_1}{\eta_2}\right) = \frac{2.6 \times 10^5 \, sec}{3.5 \times 10^5 \, sec} = 1.35$$

and reference to Figure 27 yields

$$\lambda = 1.2$$

The velocities of the shock front and the contact surface are found by noting that

$$v = \frac{dr}{dt} = \frac{d}{dt}\left(t^{1/\lambda} \eta^{-1/\lambda}\right) = \frac{t^{1/\lambda - 1}}{\lambda \eta^{1/\lambda}} = \frac{r}{\lambda t}$$

and hence,

$$v_1 = \frac{Re}{T_1 \lambda} = \frac{1.5 \times 10^5 \, km}{2.6 \times 10^5 \, sec \times 1.2} = 480 \quad km/sec$$

$$v_2 = \frac{Re}{T_2 \lambda} = \frac{1.5 \times 10^5 \, km}{3.5 \times 10^5 \, sec \times 1.2} = 360 \quad km/sec$$
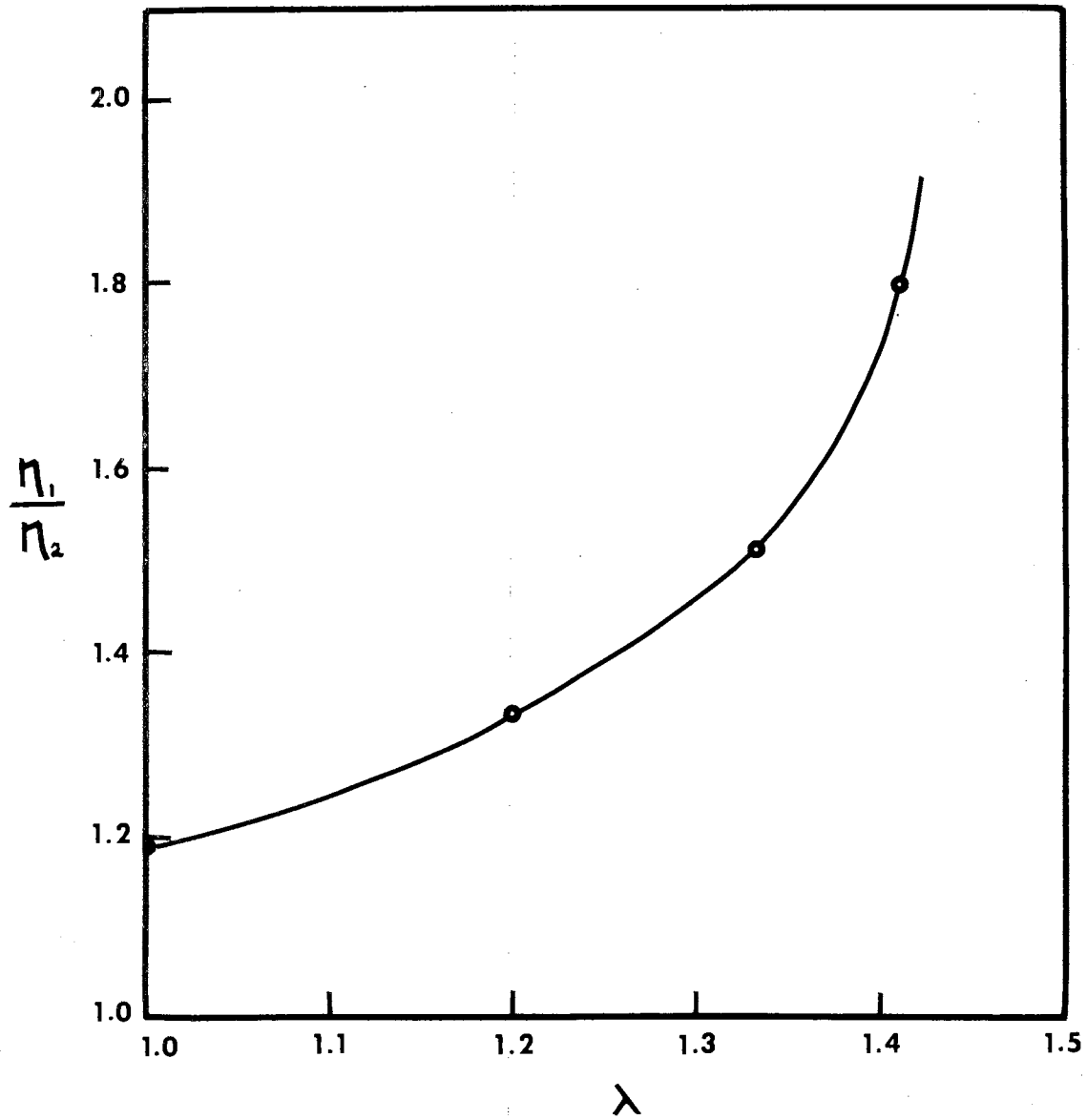
Figure 27. (η_1/η_2) Versus λ According to Parker.

where v_1 and v_2 are the shock front and contact surface velocities, respectively, at the orbit of the earth. The following points of agreement between the theoretical model and the experimental description are noted:

(a) The parameter λ is related to the total energy of the shock, a value of $\frac{3}{2}$ indicating a shock whose energy is constant, a value of 1 indicating that the energy increases linearly with time, and, in the present case, a value of 1.2 corresponding to a shock whose total energy increases as $t^{1/2}$. Hence, in this case, the rate at which work is done on the shock by the superheated coronal gases decreases with time, as might well be expected for such an impulsive ($\approx$ 2 hour duration) phenomena as a solar flare.

(b) If the undisturbed magnetic field angle is, as indicated, $65°_W$, then the field angle just behind the shock is

$$X_1 = \text{arc cos} \left(\tfrac{1}{4} \cos 65° \right) = 84° \, W$$

in complete agreement with the value inferred from the cosmic-ray anisotropy.

(c) The velocity of the contact surface indicates the velocity of the enhanced flow region just behind the shocked region, and thus the angle X_2 of the spiral magnetic field in the enhanced flow is

$$X_2 = \text{arc tan} \, \frac{R_e \omega_s}{v_2}$$

$$= \text{arc tan} \, (440 \, \text{km/sec})/(360 \, \text{km/sec})$$

$$= 51° \, W$$

which agrees exactly with the value inferred from the anisotropy

observed on January 22.

(d) Finally, one should note the qualitative agreement between the

two-step decrease predicted by the model for shocks having $\lambda < \frac{3}{2}$ and the

two-step decrease observed in the intensity contour map.

This striking agreement between the theoretical model and the

experimental measurements is strong support for the blast-wave theory of

Forbush decreases as well as the underlying assumptions concerning the

relationship between the interplanetary magnetic field and transient

cosmic-ray anisotropies. Although the detail with which the rather small

January 20 event is revealed in the intensity contour map is exemplary,

the results of the analysis of this event should be confirmed through

analyses of other, perhaps larger and even more detailed, events of the

same kind. In the present study the only other decrease which was

observed and with which a definite solar flare can be identified, is

the large Forbush decrease of 23 March 1966. Unfortunately this event

is marked not by a single large flare, but several flares ranging in

importance from 2B on March 20 and 21 to 3B on March 24 with many smaller

flares in the intervening times. As a result, this event is too complex

to attempt an analysis in terms of a simple blast-wave model. Two

features, however, were noted; first, the decrease was very sudden and

essentially isotropic, suggesting, as in the January 20 event, the

passage of a sharp discontinuity in the interplanetary medium and,

second, the main decrease was not preceded by a precursor-decrease in

the direction of the interplanetary magnetic field, indicating that

such predecreases are not a consistent feature of the Forbush decrease.

4.5 <u>Forbush</u> <u>decreases</u> <u>associated</u> <u>with</u> <u>M-region</u> <u>magnetic</u> <u>storms</u>.

McCracken, et al., (1966) have reported the observation of cosmic-ray decreases observed by the Pioneer VI spacecraft which are not preceded by solar flares. These decreases are observed to recur every 27 days and it is concluded that they are associated with semi-permanent shocks in the interplanetary medium initiated by a continuous emission of fast plasma from a restricted area of the sun. Strong correlation is noted between the recurrent decreases and recurrent M-region magnetic storms. Examination of the times of occurrence for these events in the Pioneer data reveals that the small decreases noted in the neutron monitor data on February 19 and March 13 belong to these recurring sequences.

The event of March 13 was so small that only gross features can be discerned, but the event of February 19, Figure 28, is fairly well resolved. An anisotropic predecrease is seen centered on the direction 45° west of the earth-sun line. The main, isotropic decrease of approximately 1% is followed, about 24 hours later, by a second isotropic decrease of 0.5%. During the time between these two decreases, a strong maximum in the cosmic-ray flux is noted in the direction 100° west of the earth-sun line. This resembles closely the January 20 event with the exception that the anisotropic flux seen after the first decrease is reversed in direction. If, as before, this flux is assumed to be along the magnetic field, and similarly the predecrease to indicate the field direction before the decrease, then the ratio of the cosines of the field angles before and after the decrease is

$$\frac{\cos X_0}{\cos X_1} = \frac{|B_1|}{|B_0|} = \frac{\cos 45°}{\cos(180° - 100°)} = 4$$
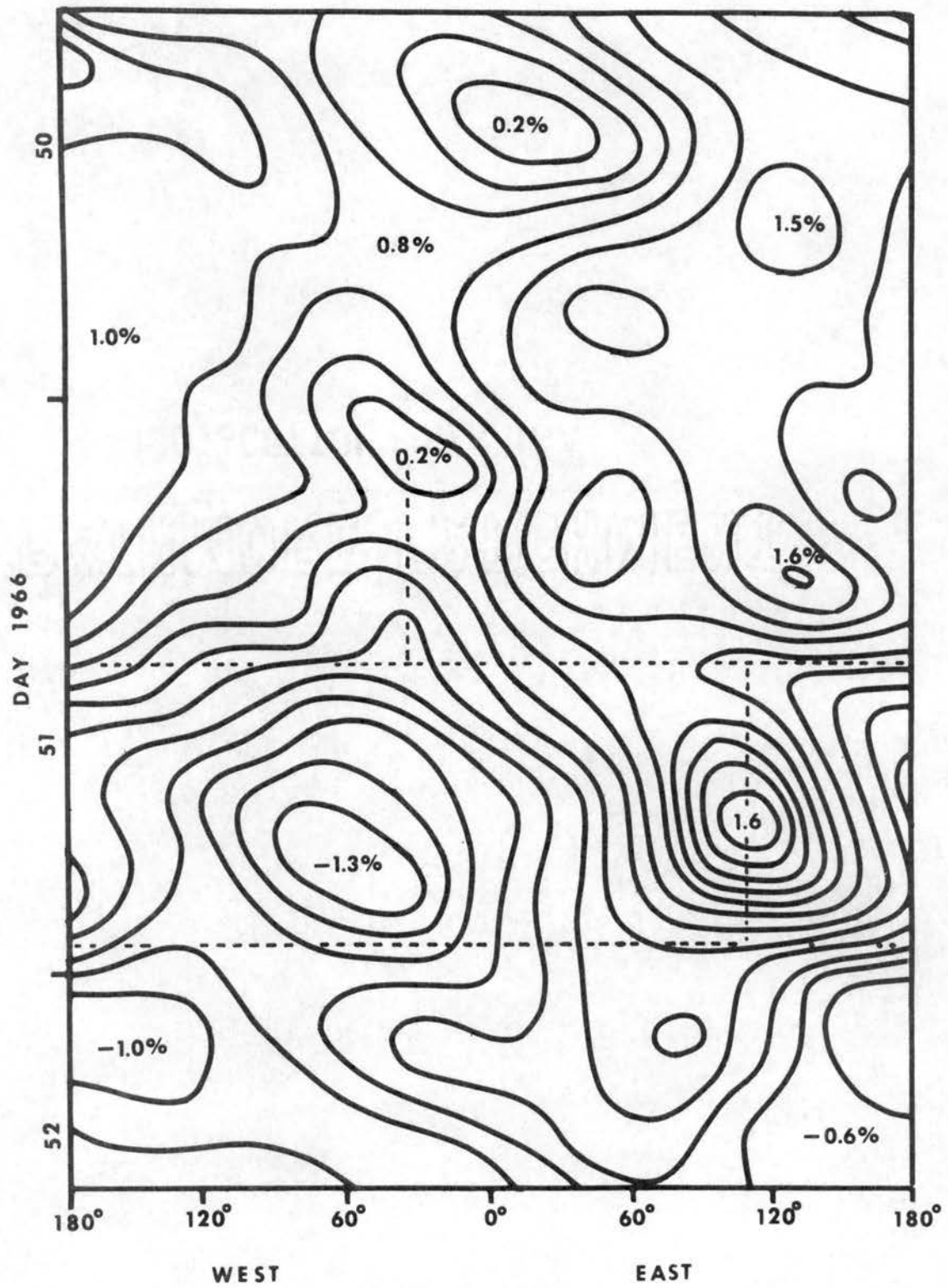
Figure 28. Intensity Contour Map 19 February 1966.

the value expected due to the compression of the interplanetary plasma by a shock. Since no solar flares of importance greater than one were observed in the week preceding the decrease (CRPL-FB-259), considerable support is given to the standing shock theory for these recurring decreases. On the other hand, the fact that some of these decreases are very weak in the neutron-monitor data, e.g., the March 13 event, while others are not seen at all could indicate that the distance from the sun at which the leading edge of the enhanced flow sector of the expanding solar wind steepens into a shock often, if not most of the time, exceeds one astronomical unit.

CHAPTER V

ENERGETIC PARTICLE RADIATION IN THE MAGNETIC

FIELD OF THE EARTH

5.1 Interaction of the earth's magnetic field with the solar wind.

The solar wind consisting of about 10 protons/cm^3, and as many

electrons, flowing radially outward from the sun at velocities of

several hundred kilometers per second forms a highly conducting fluid

which carries with it the ambient interplanetary magnetic field

(Chapter I). When this fluid reaches the orbit of the earth, the

earth's field is pushed back, being compressed on the sunward side of

the earth while, at the same time, the earth's magnetic field excludes

the flowing plasma from a large, teardrop-shaped region about the earth.

The tail of the teardrop, which results from the plasma being forced to

flow around the earth's field rather than through it, extends away from

the earth in the anti-sun direction for a large distance. The magnetic

field of the earth is completely confined to this teardrop region, the

magnetosphere. The boundary between the earth's field and the inter-

planetary medium, the magnetopause, has been observed experimentally by

several satellite instruments including those carried by Explorers 10,

12, and 14, and IMP's 1 and 2 (Heppner, et al., 1963; Ness, et al., 1964;

Ness, 1965). Since the streaming velocity of the plasma is much higher

than the Alfven velocity in the plasma (see Section 5.3 of the present

chapter), it has been predicted that a detached bow-shock is formed

114

upstream from the magnetopause, a supposition which is also supported by the satellite data. The volume between the bow-shock and the magneto-pause is usually referred to as the transition region and contains compressed solar-wind plasma and interplanetary magnetic field. Outside the shock surface the interplanetary medium is undisturbed (Figure 29). The distance from the earth to the magnetopause on the sunward side is typically about 10 earth radii with the shock located several earth radii beyond the magnetopause toward the sun. The extent of the tail is an unsettled question at this time, theoretical predictions ranging from a few tens of earth radii (Johnson, 1960) to many astronomical units (Dessler, 1964). The thickness of the magnetopause appears to be quite small, on the order of the gyroradius of a 1 keV proton in a 70 γ field (Beard, 1964). While a computation of the expected shape of the entire magnetosphere is very lengthy, a good estimate of the radius of the magnetosphere in the direction of the sun is given by equating the magnetic and particle pressures, which yields

$$r = R_e \left[\frac{B_o^2}{2\pi n m_p v^2} \right]^{1/6}$$

where R_e is the radius of the earth, n the proton number density of the solar wind, m_p the proton mass, v the plasma velocity, and B_o the magnetic field at the earth's equator (the earth is here assumed to have a dipole field). This indicates that the dependence of this distance on the solar wind velocity is not strong, going as $v^{-1/3}$, and hence is not appreciably changed by the normal fluctuations of the solar wind. However, shock waves in the interplanetary medium, such as perhaps result from solar flares, may be followed by short-lived enhanced flows with velocities several times the normal values. In such an event, the

shock front

magnetosphere

magnetopause
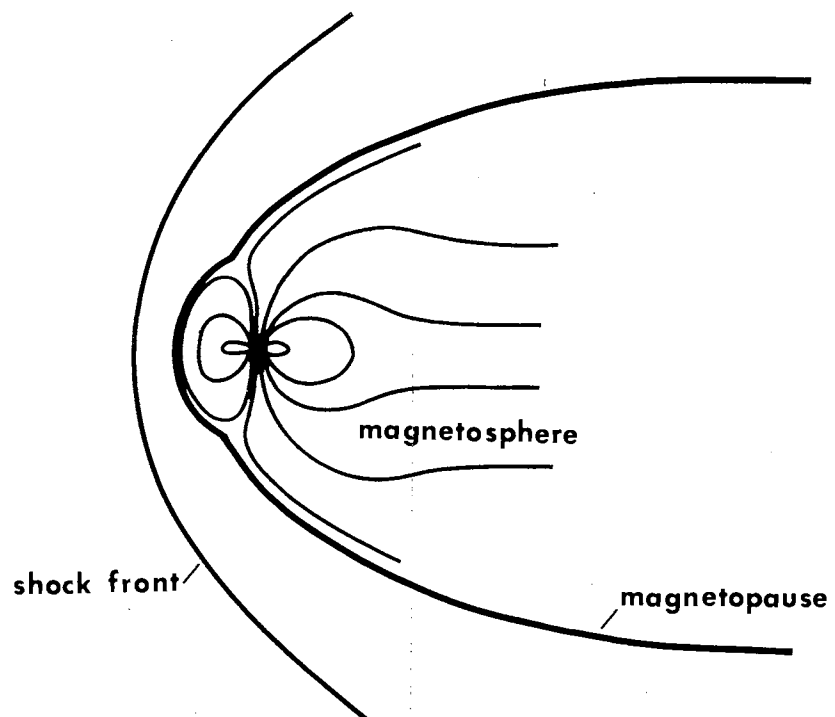
Figure 29. The Magnetosphere.

magnetospheric boundary may be significantly altered in a short time.

The magnetosphere itself is often divided into two regions. The inner region, sometimes called the trapping region, consists of the volume occupied by those field lines emerging from the earth at geomagnetic latitudes whose magnitudes are less than about 67°. The field lines in this region are only slightly distorted from a dipole-like configuration and are said to be 'simply closed,' or sometimes just 'closed.' Field lines emerging at latitudes greater than about 67° are pushed back into the tail of the magnetosphere where they may even connect with the interplanetary field. In the roughly cylindrical tail, the fields in the northern half and in the southern half are oppositely directed, the two regions being separated by a relatively thin neutral sheet (Ness, 1965). The intersection of the boundary between the simply closed field region and the field of the tail with the earth's ionosphere defines the so-called auroral oval. The locus of the midnight part of this oval corresponds to the earth's auroral zone, a band centered on $\approx 67°$, latitude where active aurorae are most frequently seen (Akasofu, 1966).

In addition to the major perturbations of the earth's magnetic field by large, sudden changes in the streaming velocity of the solar wind, small quasi-periodic variations are frequently observed. These so-called geomagnetic micropulsations are often associated with the larger non-periodic variations (magnetic storms), but are also commonly seen during relatively undisturbed periods. The micropulsations have been interpreted in terms of magnetospheric or ionospheric magnetohydro-namic waves (Hultquist, 1966) but the present theoretical understanding

of this phenomenon is very imperfect. Micropulsations are classified
according to their rate of damping as continuous (Pc), train (Pt), and
irregular (Pi) and further according to their fundamental frequency.
The continuous, only slightly damped, Pc pulsations are most commonly
seen around local noon with characteristic periods of $\approx$ 20 sec, $\approx$ 80 sec,
and $\approx$ 500 sec being most frequent (Kato and Saito, 1962). However, the
more highly damped Pt or Pi pulsations most frequently occur around local
midnight and exhibit broad frequency spectra (Yanagihara, 1960).

5.2 Charged particle trapping in the geomagnetic field.

The dipole-like configuration of the inner, closed region of the
earth's magnetic field presents the possibility of retaining (trapping)
a charged particle for a time which is long compared with the time
required for the particle to traverse the trapping region. In a time-
invarient dipole-like magnetic field the motion of a charged particle
can be described in terms of three independent motions (Alfvén and
Fälthammer, 1963):

(a) The particle, having mass m, velocity $v_\perp$ perpendicular to the
magnetic field B, and charge Ze, moves in a circle of radius a with
angular frequency ω_c where (in Gaussian units)

$$a = m v_\perp c / (Z e B)$$

$$\omega_c = Z e B / (m c)$$

and c is the velocity of light. The center of the circle is called the
particle's guiding center and the angular frequency is called its
cyclotron frequency.

(b) The quantity $\mu = \frac{1}{2} m v_\perp^2 / B$, the magnetic moment of the particle, is an invariant of the motion provided that the field strength is constant or changes linearly over the distance the particle moves in one cyclotron period. For a particle in a dipole-like field whose cyclotron radius is small compared with the scale size of the field, this implies that

$$\frac{\sin^2\alpha}{B} = \frac{1}{B_m} = const$$

where α is the pitch angle (the angle between the field direction and the particle's velocity vector) and B_m is the maximum field strength to which the particle can penetrate. That is, as the particle moves toward the polar regions the local field strength increases and, as B approaches B_m, so α approaches 90°. At this point the motion of the particle parallel to the field is reversed and the particle is said to have mirrored in the converging magnetic field. If the mirror point lies above the earth's atmosphere in both the north and south polar regions, then the particle may bounce back and forth between its mirror points with its guiding center always moving parallel to the field direction. A convenient approximate formula for the time required for one complete bounce is

$$T(sec) = 0.085 \frac{R_0}{\beta} \left(1.3 - 0.56 \sin\alpha_0\right)$$

where α_0 is the pitch angle at the geocentric equatorial distance R_0, and $\beta = \frac{v}{c}$ (Johnson, 1965).

(c) As a result of the non-linear variation in field strength along the path of a particle bouncing between its mirror points, the guiding center drifts slowly in longitude, westward for positively charged

particles and eastward for negatively charged particles, the time

required for one complete circuit of the earth being given approximately

by

$$T(min) = 172.4 \frac{1+\epsilon}{\epsilon(2+\epsilon)} \cdot \frac{1}{mR_0}$$

where

$$\epsilon = (1-\beta^2)^{-\frac{1}{2}} - 1$$

(Johnson, 1965).

A charged particle may long dwell in the closed region of the earth's

magnetic field before perturbing influences result in a basic change in

its trajectory. Such trapped radiation forms the well-known Van Allen

radiation belts around the earth which have been shown to consist of an

energetic proton component centered at approximately 10^4 km from the

earth's magnetic axis and an electron component centered at approximately

2.2×10^4 km from the earth's magnetic axis. The electron belt extends

through the region occupied by the proton belt and low energy radiation

having a penetrating power between $1gm/cm^2$ and $1mg/cm^2$ is observed

throughout the entire trapping region (Johnson, 1965).

5.3 <u>Energetic</u> <u>particle</u> <u>precipitation</u> <u>in</u> <u>the</u> <u>auroral</u> <u>zone</u>.

Particles whose trajectories lead to mirror points less than about

100 km above the earth's surface are likely to interact with the upper

atmosphere with their energy being dissipated through the production of

secondary particles, ionization, and photons. A particle so interacting

is said to 'precipitate' into the earth's upper atmosphere.

One of the most striking results of energetic particle precipitation

is the auroral phenomenon. The precipitating particles responsible for

auroral displays in the latitudes 65° to 70° have been shown to be electrons with mean energies of a few tens of keV (McIlwain, 1960). It was originally presumed that the precipitating electrons causing aurorae are electrons from the Van Allen belts which have been perturbed from their trapping orbits. Such an assumption has been conclusively shown to be false. McIlwain (1960) demonstrated that the energy distribution spectra of auroral electrons and trapped electrons are vastly different, and rocket measurements of the auroral electron flux have revealed that the entire amount of energy known to be stored in the Van Allen belts would supply a bright auroral display for only about 15 minutes. Bright displays have been observed continuously for many hours. In addition, O'Brien (1964) has discovered from studies with the Injun 3 satellite that electron fluxes in the radiation belts increase rather than decrease during auroral precipitation events. It thus seems more likely that the Van Allen electrons are the trapped remains of auroral electrons than the radiation belts being the source of the auroral radiation.

Important precipitation loss mechanisms are, however, known to exist in the trapping region (Hess, 1965):

(a) Elastic coulomb scattering is probably the most important way in which electrons are lost from the inner regions of the radiation belts. Scattering can result in large changes in the pitch angle of a particle, lowering its mirror point and causing precipitation.

(b) Inelastic nuclear collisions are important for high energy protons ($E > 300$ MeV).

(c) Protons with energies less than 100 keV may undergo charge-exchange interactions with slow moving neutral hydrogen atoms. The high energy proton acquires the electron of the neutral atom and, having

thus itself become electrically neutral, no longer mirrors and may intersect the earth's atmosphere.

(d) Ionization losses are important for protons in the energy range 100 keV to 100 MeV. Protons thus slowed are not necessarily removed from the radiation belt, but are degraded to energies where charge exchange interactions are likely.

(e) In the outer zone of the trapping region the above loss mechanisms are insufficient to explain the observed short lifetimes of both electrons and protons. The most often invoked process to explain the high loss rates is particle-hydromagnetic wave interaction.

Hydromagnetic waves, or Alfvén waves, may be regarded as transverse vibrations of plasma-imbedded magnetic field lines as if these lines were stretched strings with a tension $\frac{B^2}{4\pi}$ and having a line density ρ equal to the plasma density (Alfvén, 1963). The velocity of propagation of such waves is given by the so-called Alfvén velocity

$$V_A = B / (4\pi\rho)^{1/2}$$

Such waves are confined to move along the magnetic field lines and may be reflected by sudden spatial variations in the propagation characteristics along the line much as an electrical wave in a transmission line is reflected by discontinuities in the line's characteristic impedance. As a result, standing waves may be formed in the earth's magnetic field because of the reflection of hydromagnetic waves by the rapid changes in the plasma density along the field lines as the waves approach the points where the lines leave and re-enter the earth.

Hydromagnetic waves may be generated by changes in the pressure on the magnetopause when changes in the solar wind energy density occur,

such as during the passage of a solar flare generated shock wave in the interplanetary medium. Dessler and Walters (1964) have proposed that the presence of the interplanetary magnetic field may cause an asymmetry in the magnetosphere and, as the interplanetary field varies in strength and direction under the control of a turbulent solar wind, so may the asymmetry in the magnetosphere change, giving rise to hydromagnetic waves which, following field lines, arrive a few seconds later at the earth. Karplus, et al. (1962) have considered the attenuation of such waves as a function of the plasma parameters and find a cut-off frequency which varies from ≈ 0.5 cycles per second (cps) at sunspot maximum to ≈ 4 cps at sunspot minimum. Thus, although generation mechanisms may be more active during periods of high solar activity, the propagation characteristics are more favorable during quiet solar periods.

Numerous observations of geomagnetic pulsations which may be identified with hydromagnetic waves have been made, e.g., Benioff (1960) and Tepley (1961). Short period oscillations (0.3 to 2.5 sec) are most frequently noted around local midnight and exhibit a negative correlation with solar activity while longer period (3 to 8 sec) oscillations which seem to be correlated with local aurora are most frequent during periods of high solar activity. Similar oscillations with somewhat longer periods (7 to 30 sec) have been noted in daylight, but even longer period waves (40 to 120 sec) have been observed at night. Observations have been made of hydromagnetic emissions at nearly all geomagnetic latitudes, however these pulsations of the geomagnetic field are most frequent in the auroral zone.

The effect of hydromagnetic waves on the lifetime of energetic protons trapped in the earth's field has been investigated by Dragt (1961)

in an attempt to explain the relative lack of such particles in the
outer zone of the trapping region, as suggested by Welch and Whitaker
(1959). Strong, particle-magnetic wave interaction occurs whenever the
hydromagnetic wave frequency, as observed in the moving frame of
reference of the guiding center of the particle, equals the local
cyclotron frequency of the charged particle. For an assumed Fourier
spectrum of the hydromagnetic waves which is relatively constant
from zero to the cut-off frequency for non-dissipative propagation
(≈ 3 cps) and zero for higher frequencies, the lifetime of protons
exceeding a certain threshold energy related to the hydromagnetic wave
cut-off frequency is on the order of one-half day. The threshold energy
is a very steep function of geocentric radial distance, going as r^{-11} ,
with the result that a very rapid decrease in the energetic proton
population is predicted for geocentric distances greater than about
2.3 earth radii. This theoretical prediction agrees well with the
satellite observations of the Van Allen radiation. It should be noted
that the actual loss mechanism in this case is inelastic collisions in
the upper atmosphere of the earth made by trapped protons whose
trajectories have been altered by interaction with hydromagnetic waves.
Although the wave-particle interaction may be responsible for the loss
of protons over a wide range of energies as a result of the wide range
of frequencies possible for hydromagnetic waves, for any one given time
and magnetic region the process can be very energy dependent if only
single-frequency waves are present. It should also be noted that, since
both the perturbed particles and the perturbing hydromagnetic wave
are constrained to move along the field lines, both the precipitating
protons and the magnetic pulsations should be abservable at very nearly

the same time in the upper atmosphere even if the place of interaction were several earth radii removed from the earth.

5.4 An experiment to detect charged particle precipitation.

An experiment to detect charged particle precipitation in the upper atmosphere could possibly provide useful information on a number of different phenomena including:

(a) time variations of the low energy (0.1 - 1.0 GeV) portion of the galactic cosmic-ray flux. This is an energy region of considerable interest which is not viewed by the world net of cosmic-ray neutron monitors (Chapter I).

(b) charged particle acceleration mechanisms in the magnetosphere. Since the source of the auroral particles can not be scattered radiation from the Van Allen storage region (Section 5.3 of the present chapter) and since the auroral particle energies are orders of magnitude greater than the particle energies associated with the solar wind except during the relatively rare periods when high energy particles are generated in a solar flare, the existence of an acceleration mechanism for electrons and possibly protons in the magnetosphere is not an unreasonable possibility.

(c) charged particle loss mechanisms in the outer zone of the geomagnetic trapping region. The possibility that hydromagnetic wave scattering of trapped radiation, as outlined in the preceding section, can produce energy dependent, periodic proton precipitation which may correlate with magnetic micropulsations indicates that information concerning the interaction mechanism as well as information about the injection of energetic protons into the Van Allen region may be

obtained by studying the time variations of the proton flux in the range 0.1 GeV to 1.0 GeV in the upper atmosphere.

(d) backscatter of secondary particles from the upper atmosphere into the trapping region of the magnetic field. Precipitating particles may produce secondary particles whose direction of motion is away from the surface of the earth. This backscatter (sometimes referred to as the albedo flux), if injected into the closed geomagnetic field region, is constrained to follow the magnetic field lines and will return to the upper atmosphere in the hemisphere opposite from its origin.

Desirable characteristics of such an experiment could be listed as follows:

(a) The detector should be sensitive to charged particle radiation in the range 100 MeV to 1000 MeV for protons and be able to distinguish charged particle radiation from high energy photons.

(b) The detector should be placed high enough in the atmosphere to assure that 100 MeV protons entering the atmosphere can be detected and not so high that long-lifetime trapped radiation is observed.

(c) The detector should be large enough and the data sampling interval short enough that rapid variations (≈ 1 cps) can be discerned.

(d) The experiment should be conducted at a high geomagnetic latitude, preferably in the auroral zone, since the field lines entering or leaving the earth at these latitudes traverse the outermost edge of the trapping region.

(e) Magnetic field measurements capable of resolving the micro-pulsations associated with hydromagnetic waves in the magnetosphere should be made concurrent in time and place with the energetic particle measurements.

CHAPTER VI

A BALLOON-BORNE COSMIC RAY MONITOR

6.1 Detector.

The detector chosen for the balloon-borne monitor is a very simple

one (Figure 30) consisting of a stack of scintillators and absorbers.

The scintillators are a plastic phosphor (type NE102 produced by

Nuclear Enterprises Ltd., Canada) formed into highly polished sheets

two feet square and one-half inch thick; the absorbers are aluminum.

Each scintillator is viewed by two, ten-stage multiplier phototubes

(type 6199 produced by the Radio Corporation of America). By observing

coincident scintillations in two or more of the scintillators, charged

particle radiation is detected and, by determining just how far into the

stack any given particle penetrates, a rough measure of its initial

energy is obtained. Four levels of penetration are distinguished:

$$\text{Level } 1 = A \cdot \overline{B} \cdot \overline{C} \cdot \overline{D}$$
$$\text{Level } 2 = A \cdot B \cdot \overline{C} \cdot \overline{D}$$
$$\text{Level } 3 = A \cdot B \cdot C \cdot \overline{D}$$
$$\text{Level } 4 = A \cdot B \cdot C \cdot D$$

Here A, B, C, and D refer to responses from the four scintillators, as

labeled in Figure 30, and the indicated products are to be interpreted

as logical (Boolean) products. The bar over a symbol denotes negation.

Thus, for example, level 2 represents simultaneous scintillations (to

127

Figure 30. Detector for the Balloon-Borne Monitor.

within the resolving time of the associated instrumentation) from scintillators A and B and an absence, at the same time, of responses from scintillators C and D. For radiation incident from the top of the stack, levels 1 through 4 correspond to increasingly energetic radiation. Note that level 1 requires no coincidence of scintillations, merely an absence of response from all except the topmost scintillator. Thus, non-ionizing radiation (e.g., x-rays, gamma rays, or neutrons) which interact within the top scintillator producing ionizing radiation not reaching any of the remaining scintillators is not distinguishable from ionizing primary radiation. Also, level 4 represents penetration of the entire detector stack and therefore records all ionizing radiation with energy greater than the minimum required to penetrate to the bottom scintillator. Moreover, level 4 is unique in that no distinction is made between particles moving downwards and those moving upwards through the stack.

6.2 The response of the detector to energetic protons.

An analysis of the response of the detector to energetic protons as a function of zenith angle and energy requires a knowledge of the range-energy relationship for protons in the various substances composing the detector and any mass overlying the detector. For this the values given by Smith (1947) for protons in air and aluminum were used. The energies of interest for this balloon-borne detector lie in the range from about 60 MeV to a few hundred MeV. For such a small interval, the range-energy relationship may be represented to good accuracy (within 1%) by the simple empirical expression

$$R = CE^P$$

where R is the range (depth of penetration) measured in units of mass

per unit area and E the proton energy. The constants C and P must be

evaluated for each different kind of material. Table IV lists

appropriate values for these constants for the materials composing the

detector and the overlying air mass. The constants for plastic (mean

atomic number = 2.8) were interpolated from values for $(CH_2)_n$ (mean

atomic number = 1.8) and for air (mean atomic number = 7.2). For

these constants the appropriate units for proton energy and range are

MeV and mg/cm^2.

TABLE IV

RANGE-ENERGY CONSTANTS

Material	C	P
Air	2.17	1.81
Aluminum	3.03	1.76
Plastic	1.78	1.81

The basic problem in determining the total range of an energetic

charged particle in a layered medium may be simply stated: Given a

homogeneous layer of known thickness and the energy with which a normally

incident particle emerges from the layer, with what energy did the

particle enter the layer? If the range of the particle as a function

of energy is R(E) and the inverse relation, that is, energy as a

function of range is E(R), then

$$E_0 = E\left(R\left(E_1\right) + X\right)$$

where E_0 and E_1 are the entrance and exit energies respectively. For

the case at hand,

$$R(E) = CE^P$$

$$E(R) = \left(\frac{R}{C}\right)^{\frac{1}{P}}$$

so that,

$$E = \left(\frac{CE_1^P + X}{C}\right)^{\frac{1}{P}}$$

For particles whose paths are not normal to the layer, the expression

for X becomes

$$X = H/\cos\theta$$

where H is the thickness of the layer and θ is the angle between the

path of particle and the normal direction. Thus, starting at any point

within a layered medium the energy required to just reach that point, for

any given angle of incidence, may be computed by repeated use of the

above formula. Thicknesses for the balloon-borne monitor stack, includ-

ing the overlying air mass at an altitude of 115,000 feet and the

protective outer covering of the detector, are listed in Table V in

order from the top of the atmosphere to the bottom of the detector.

Critical depths in the detector lie at the interfaces between layers 2

and 3, layers 3 and 4, layers 5 and 6, and layers 7 and 8 since these

depths mark the limits of the energy intervals corresponding to the

logical levels previously defined. The energy required for a proton

incident upon the top of the atmosphere to reach these depths was computed

for zenith angles in the range $0° \leqslant \theta \leqslant 60°$ (Figure 31). The regions lying between the computed curves are labeled with the corresponding logical level and its Boolean expression. Note again that no upper limit in energy exists for level 4.

TABLE V

DETECTOR STRATIGRAPHY

Layer No.	Material	Thickness in mg/cm^2
1	Air	5920
2	Wood and plastic	510
3	Plastic phosphor	1310
4	Plastic phosphor	1310
5	Aluminum	1240
6	Plastic phosphor	1310
7	Aluminum	2480
8	Plastic phosphor	1310

If isotropic flux $J_o(E)$ is incident upon the top of the atmosphere then the rate observed for any logical level of the detector, due to particles having energies in the interval E to (E + dE) is given by

$$N(E)dE = J_o(E) \int_{\theta_1(E)}^{\theta_2(E)} A \cos\theta \sin\theta \frac{d\theta}{2} dE$$
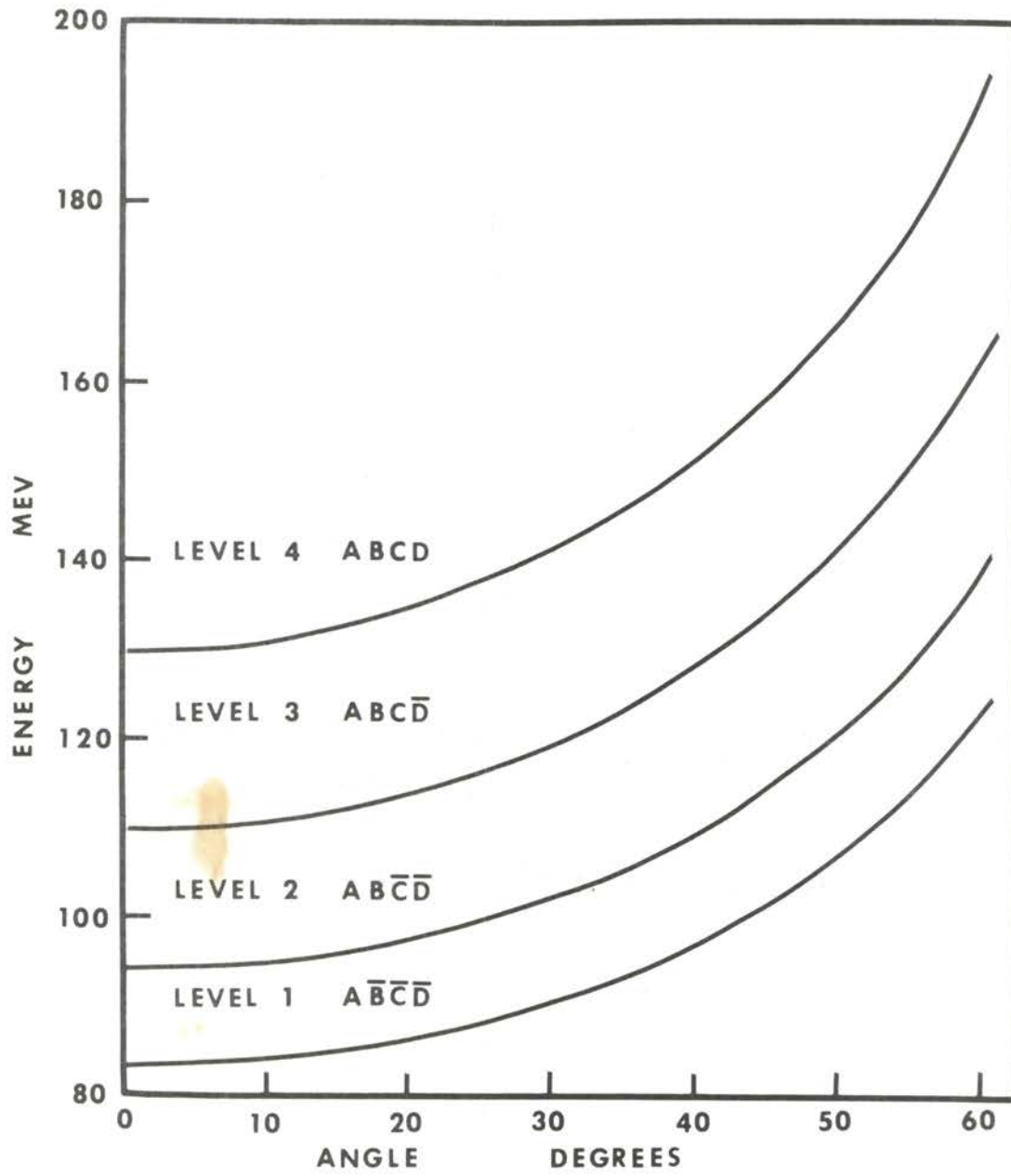
Figure 31. Energy Versus Angle for the Balloon Detector.

where $A\cos\theta$ is the projected area of the detector at zenith angle θ. The integral is taken over the interval $\theta_1 \leq \theta \leq \theta_2$ for which a particle of energy E will produce a response at the designated logical level. This interval may be determined (for protons) directly from Figure 31. The instrumental function W(E) defined by

$$W(E) = \frac{N(E)}{J_0(E)} = \frac{A}{2} \int_{\theta_1(E)}^{\theta_2(E)} \sin\theta \cos\theta\, d\theta = \frac{A}{4}\left[\sin^2\theta\right]_{\theta_1(E)}^{\theta_2(E)}$$

describes the detector's relative response, as a function of energy, to an isotropic flux. This sensitivity function is shown in Figure 32 for each of the four logical levels of the balloon-borne monitor. The relative response of each level for any energy-dependent isotropic flux is obtained by simply multiplying these sensitivity functions by the existing primary energy spectrum. It is important to note that the response of the detector is a strong function of the altitude of the balloon since, even at an altitude of 115,000 feet, the major contribution to the total mass through which a particle ending its range in the detector must pass is produced by the atmosphere remaining above the detector.

6.3 Electronic circuits associated with the detector.

The multiplier phototubes, two for each scintillator, view the plastic phosphor sheets edge-on from opposing corners--this arrangement having been found to produce optimum light collection from the entire area of the sheet. Each phototube is provided with its own high-voltage power supply affixed to the base of the tube. These high-voltage supplies are of the voltage-multiplier type (Figure 33) often used in this application because it provides directly all of the intermediate
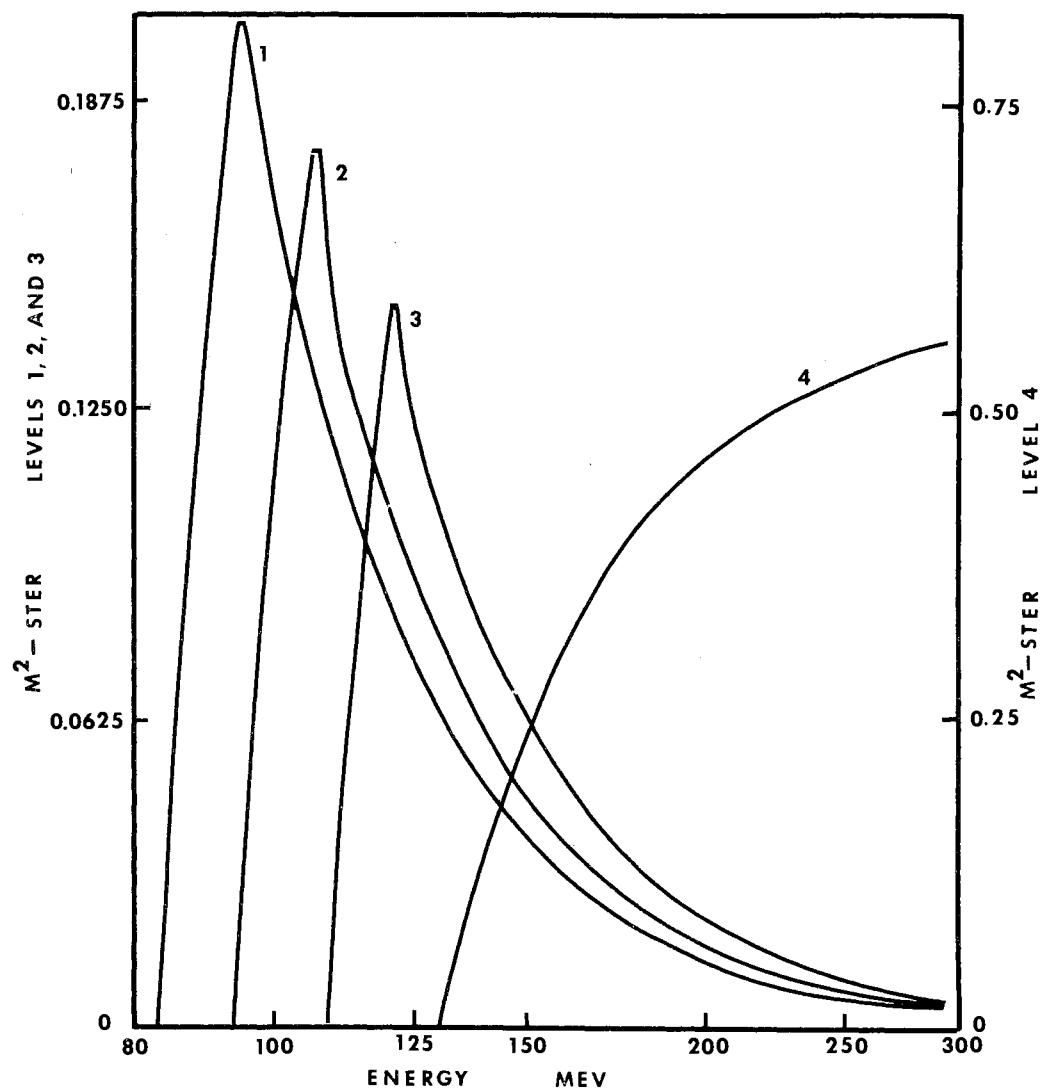
Figure 32. Balloon Detector Sensitivity Functions.
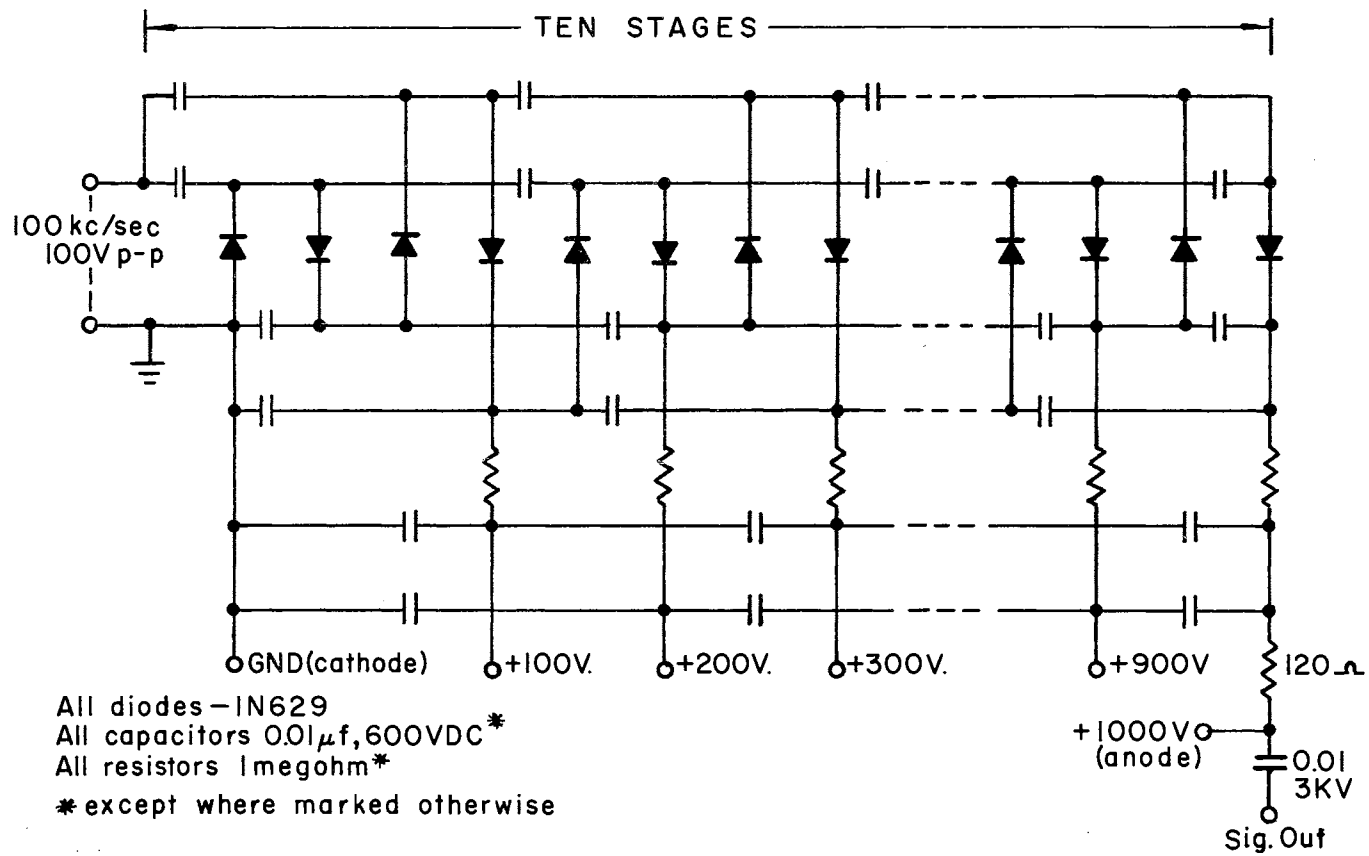
Figure 33. High-Voltage Supply.

All diodes—IN629
All capacitors 0.01μf, 600VDC*
All resistors 1megohm*

* except where marked otherwise

potentials required by the multiplier phototube dynodes as well as the anode potential. High frequency AC of approximately 100 volts peak-to-peak at 100 kc/sec is supplied to all eight voltage-multiplier assemblies by a single power oscillator circuit. The relatively high supply frequency allows electrically small filter capacitors to be used in the voltage-multipliers. The peak-to-peak AC voltage was chosen to provide an increase of about 100 volts for each full-wave multiplier stage, only ten stages being required to supply all dynode potentials and produce approximately a one kilovolt potential for the anode.

The 100 kc/sec power oscillator circuit is shown in Figure 34. An important feature of the AC supply is the incorporation of a peak-to-peak voltage sensing circuit and a negative feedback loop which regulates the amplitude of the output of the supply. This is necessary because the gain of the multiplier phototubes is an extremely strong function of the applied dynode and anode potentials.

It will be noticed that the anode is directly coupled to the signal cable (a coaxial transmission line) by a 0.01 μf capacitor and that the anode DC load impedance is only 120 ohms. Since the anode source impedance for signal currents is several megohms, a scintillation viewed by the phototube is transformed into a current pulse in the signal cable. Even though the total charge produced at the phototube anode by the smallest scintillation of interest may be quite small (on the order of 10^{-11} coulomb), the time scale of the scintillation is also very small (on the order of 4×10^{-9} seconds for NE102 plastic phosphor) with the result that the instantaneous signal current will be an appreciable fraction of a milliampere. Such a pulse is easily detected by a discriminator designed as a current triggered device. Advantages of this
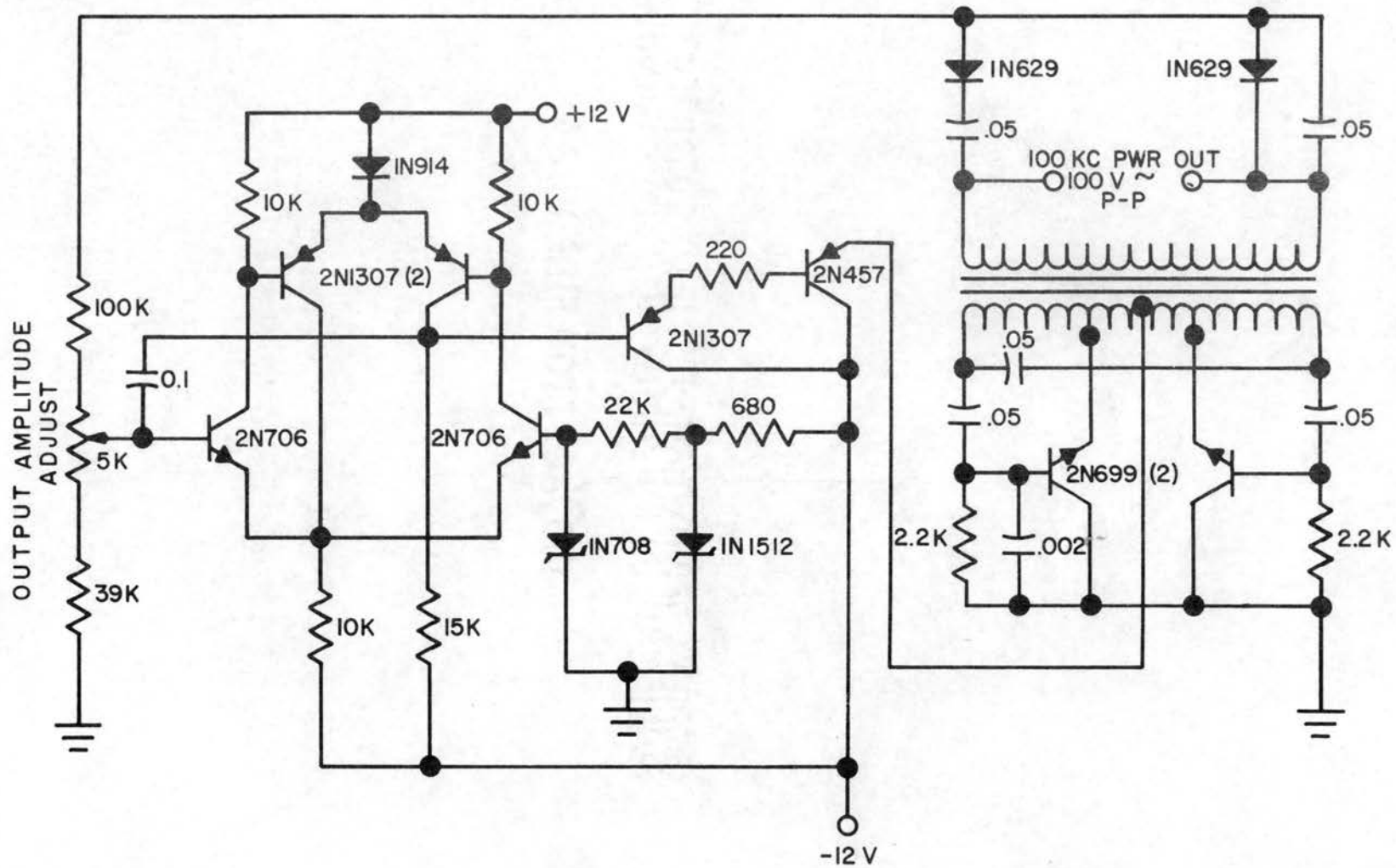
Figure 34. 100 kc/sec Power Oscillator.

system over the more common integrated-charge voltage-pulse producing

techniques, for the detector described here, are:

(a) The time scale of the signal pulse is short, being determined

mainly by the scintillation decay time-constant and, as a result, much

higher scintillation rates can be tolerated before serious pile-up of

signal pulses occurs.

(b) The signal pulse is well suited for transmission over relatively

long distances via shielded coaxial lines.

(c) The noise immunity of the system is good because of the low

impedances used and the excellent shielding provided by coaxial lines.

For these advantages to be fully realized, it is important that the

discriminators, one-shot multivibrators, and logic circuits used to

form the logical products corresponding to the four levels of the detec-

tor all operate at high speed and have short recovery times. The circuit

diagram for a high-speed current triggered discriminator and one-shot

multivibrator is shown in Figure 35. The current threshold device is

a 1 mA peak-current, germanium tunnel-diode biased from a constant current

source formed by transistor Q2. The signal current is added to this

constant bias current at the emitter of Q2, the dynamic collector impe-

dance of Q1 providing the necessary high source-impedance for the

signal current at the current summing point. At the same time, Q1

provides a good impedance match at its emitter for the signal transmis-

sion line. If the sum of the signal and bias currents exceed the peak

current of the tunnel diode, this diode switches to its high-voltage

state triggering a one-shot multivibrator formed by transistors Q3

and Q4 and having a period of about 100 nsec. The tunnel diode is

regeneratively reset to its low-voltage state by inductor L1 about 30 nsec

Figure 35. High-Speed Discriminator.

after the instant of triggering. A current-switching differential

amplifier formed by Q5 and Q6 provides complementary outputs for the

discriminator suitable for operating the logic circuitry. At these

outputs logical true is represented by about -5.0 volts and logical

false by about +1.0 volt. The recovery time of the discriminator,

measured from the instant of triggering is about 300 nsec.

The logic circuit used is also of the current-switching type

(Figure 36). Four inputs are provided so that the four-factor logical

products required to define the logical levels of the detector may be

generated. The logical function performed by the circuit is the AND

function with the result that an output pulse is produced only when all

four inputs are simultaneously logically true. In all, four such logic

circuits are used--one for each of the detector levels. The resolving

time of this circuit, when operating with the discriminators just

described, has been measured and found to be approximately 80 nsec.

6.4 Telemetry.

Pulses from the logic circuits are counted in four, ten-stage,

binary counters of conventional design. Periodically the numerical

contents of each counter are transferred to a ten-stage, binary shift-

register where the bit-configuration of the counter is converted into

a ten-bit, serial, binary, data word which is used to frequency modulate

a subcarrier oscillator, one of several, in a standard IRIG FM/FM

telemetry system. Each counter is reset to zero at the time of the

transfer. Data from levels 2, 3, and 4 share a single subcarrier

channel with two other ten-stage counters which record the time by

continuously counting pulses spaced 4 sec apart. The time-counters are

not reset at the time of transfer. The time pulses are derived from a
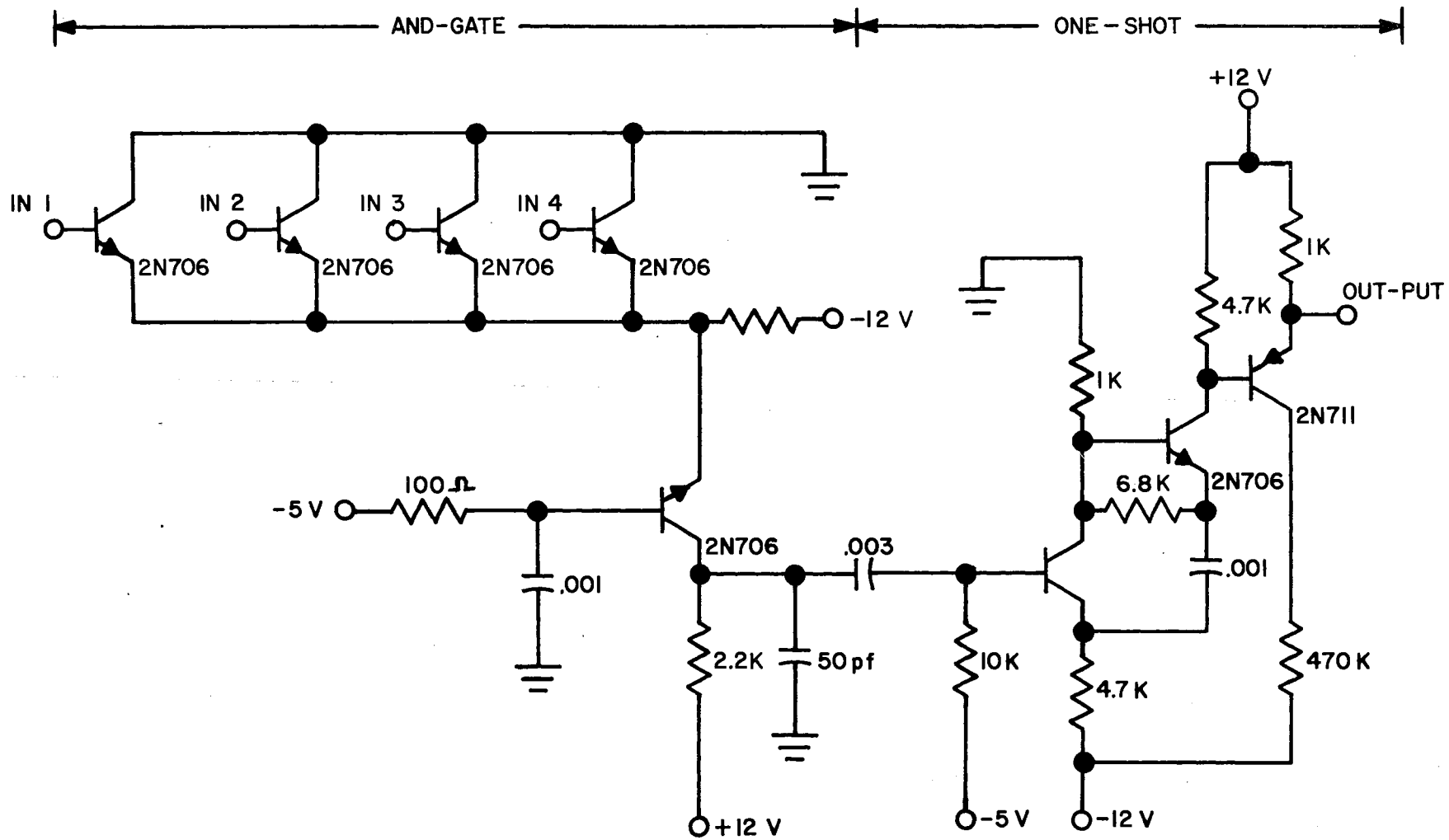
Figure 36. High-Speed Logic.

quartz-crystal controlled oscillator, as are all of the various timing

signals required to operate the various digital circuits such as the

shift-registers. A separate subcarrier channel is reserved for the

data from level 1 and, since the bit transmission rate is the same

(20 bits per second) for both subcarrier channels, the counter for this

level is examined and reset five times as often (every 0.4 sec) as the

counters for levels 2, 3, 4, and the time counters (every 2 sec). The

sum of the signals from the subcarrier oscillators is used to frequency

modulate a 0.5 watt, 72 mc/sec radio transmitter.

At the ground-based receiving station, the received radio-

telemetry signal is processed to recover the binary data transmitted

from the balloon-borne monitor. The binary data words are printed on a

digital printer for immediate examination and recorded on magnetic tape

for further data processing. This telemetry system (shown in functional

block-diagram form in Figure 37) has been described in detail by Bickel

(1965).

6.5 The balloon gondola and the system power supplies.

The requirements for the mechanical support and the electrical

power needs of the balloon-borne monitor may be summarized as follows:

(a) So that the monitor can reach desirable altitudes of greater

than 110,000 feet with the commonly available stratospheric balloons

having capacities ranging from about 1.6×10^6 to 3×10^6 cubic feet, it

is necessary that the total weight of the instrument be held to a

minimum and in any case should not exceed about 200 pounds.

(b) Since it is desirable to recover the instrument package

after each flight and be able to prepare it for another flight with a

radio-link

100 kc/s pwr. osc. → 100 kc/s AC → Detector Stack

Detector Stack → PMT Signals → Discriminators

Discriminators → One-shot pulses → Logic

Logic → Data / Pulse Rates → Scalers

Scalers → Count totals → Shift Registers

Shift Registers → Bit Streams → FM/FM Telemetry

Primary Power (to all units)

Timing and control (to all units)

Balloon-Borne Instrument

Telemetry Receiver → Subcarriers → Subcarrier Demodulators

Subcarrier Demodulators → Bit streams → Digital Decoder

Digital Decoder → Data Control Signals → Printer

Tape Recorder → Digitally coded time signals → Digital Clock

Digital Clock → WWV Time Signals → WWV Receiver

Ground Station

Figure 37. Functional Block Diagram.

144

minimum of repair work, the framework of the balloon gondola should be strong, flexible, and easily repairable.

(c) In order to insulate the instrument package from the intense cold at stratospheric altitudes (typically less than -50°C) the gondola should be covered with a thermal insulator. This insulator may be made to perform double duty by using it as a disposable, shock-absorbing material to help prevent damage to the instrument when landing by parachute after the termination of a flight.

(d) The typical duration of a stratospheric balloon flight is between 10 and 20 hours. Obviously the electrical supplies should be capable of operating the instruments for the full duration of the flight.

(e) If, as it is often desirable, no provision is made for maintaining normal atmospheric pressure in the instrument package, precautions must be taken so that the high voltages present in the instrument (anything above about 100 volts) do not produce arcing or glow discharge in the rarified atmosphere at the operating altitude.

A gondola which has been found to be strong, yet light, consists of a framework of light aluminum tubes (1 inch diameter, 0.032 inch wall thickness) joined by small blocks of aluminum bored with three mutually perpendicular holes of the same diameter as the tubing. The tubes are prevented from coming out of these corner-blocks by flexible steel pins which are inserted through both the block and the tubes. For joining one tube to a second, not at the end, a block with only two holes is used. Particular advantages of this system are a high strength-to-weight ratio, freedom of design, and good repairability by simply replacing damaged members.

Both rigid polyureathane foam plastic and expanded polystyrene foam plastic were found to serve adequately as a combination thermal insulating shield and as a shock-absorbing material. Two to four inches thickness provides adequate insulation for instruments rated for operation to -20°C. Additional shock absorbing material was often added to the bottom of the package.

Mercury-cell batteries were chosen as the primary electrical supply because of their high energy-to-weight ratio (in excess of 40 w-hr/lb). Disadvantages of these cells include high cost and poor performance at temperatures below 15°C. Because of the temperature problem, the mercury cells were placed in a box insulated with two inches of polyureathane foam. The internal dissipation of the cells when supplying power proved to be sufficient to prevent their temperature from falling below 20°C, when insulated in this manner.

All high-voltage terminals were encapsulated in silicone rubber compounds and laboratory tested at reduced pressures to insure that no arcing or glow discharge could take place. It was found to be unnecessary to protect the 100 kc/sec AC used to supply the voltage multipliers.

A view of the completed instrument, stripped of its insulating shield, is shown in Figure 38.
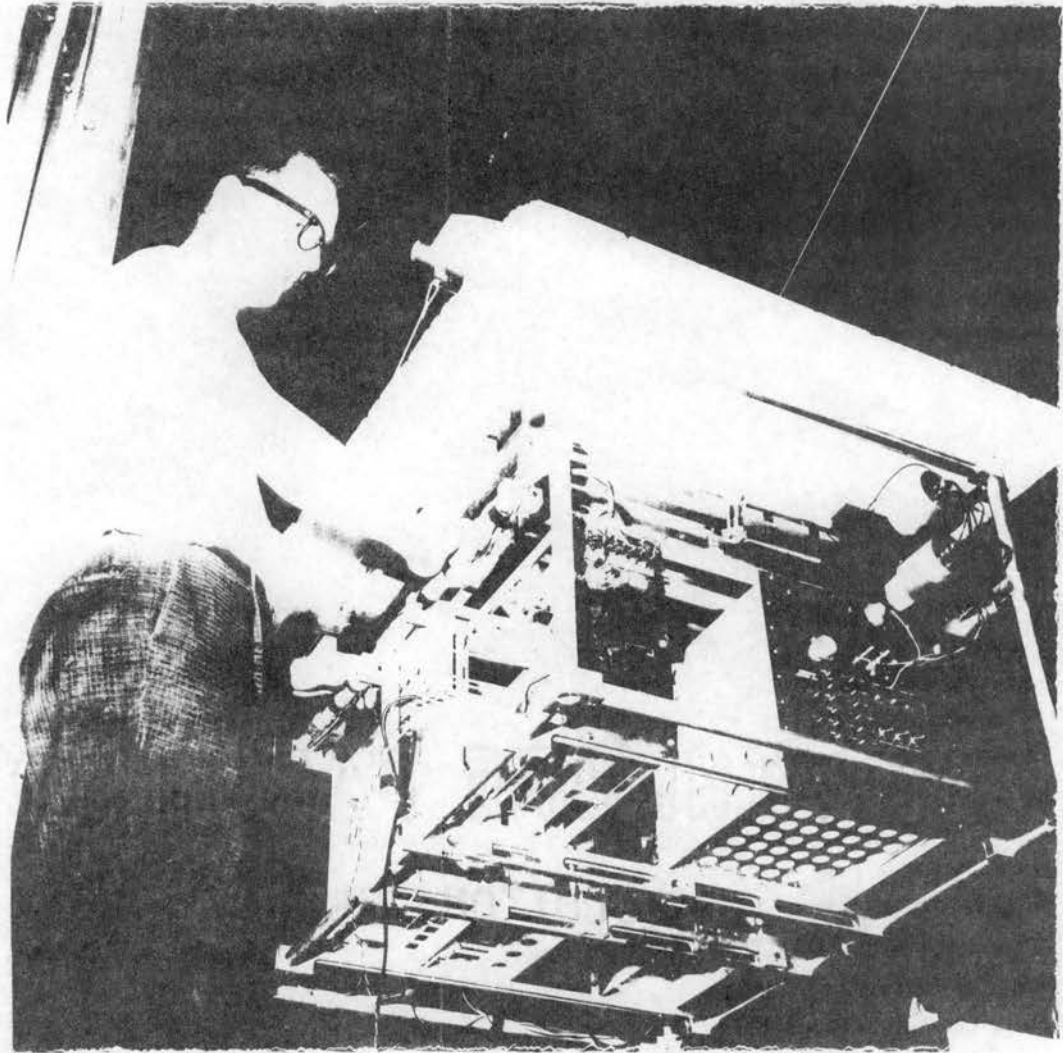
Figure 38. The Balloon-Borne Monitor.

CHAPTER VII

A HIGH-LATITUDE FLIGHT OF THE BALLOON-BORNE COSMIC RAY MONITOR

7.1 Description of the flight.

The cosmic-ray monitor described in the preceding chapter was

successfully carried by a balloon to an altitude greater than 115,000

feet on August 6, 1965, at Ft. Churchill, Manitoba, Canada. The flight

was conducted by Winzen Research Inc. of Minneapolis in co-operation

with the Southwest Center for Advanced Studies as part of the 1965

Project Skyhook sponsored by the Office of Naval Research. The balloon

vehicle was an ambient pressure, 0.5 mil, 1.6×10^{6} cu ft, polyethylene

film balloon manufactured by Winzen Research Inc. Launch was at 0600 UT

and the ultimate ceiling altitude of slightly greater than 115,000 feet

was reached two hours later. Termination of the flight was made by

radio-command at 2207 UT on the same day. Recovery of the instrument

package was made near Reindeer Lake, Manitoba (geographic co-ordinates

of the impact point were 101°01' W-57°34' N) about 300 miles west-southwest

from the launch point (94°6' W-58°45' N). An altitude versus time profile

for the flight is shown in Figure 39. The instrument package suffered

no damage which allowed a post-flight check to be made of the detector

circuitry. All circuits were found to operate normally and the discrimi-

nator thresholds were found to be unchanged from their preflight values.

The radio-telemetry signal was relatively strong and noise-free

for the first six hours of the flight; after this time the signal became

148
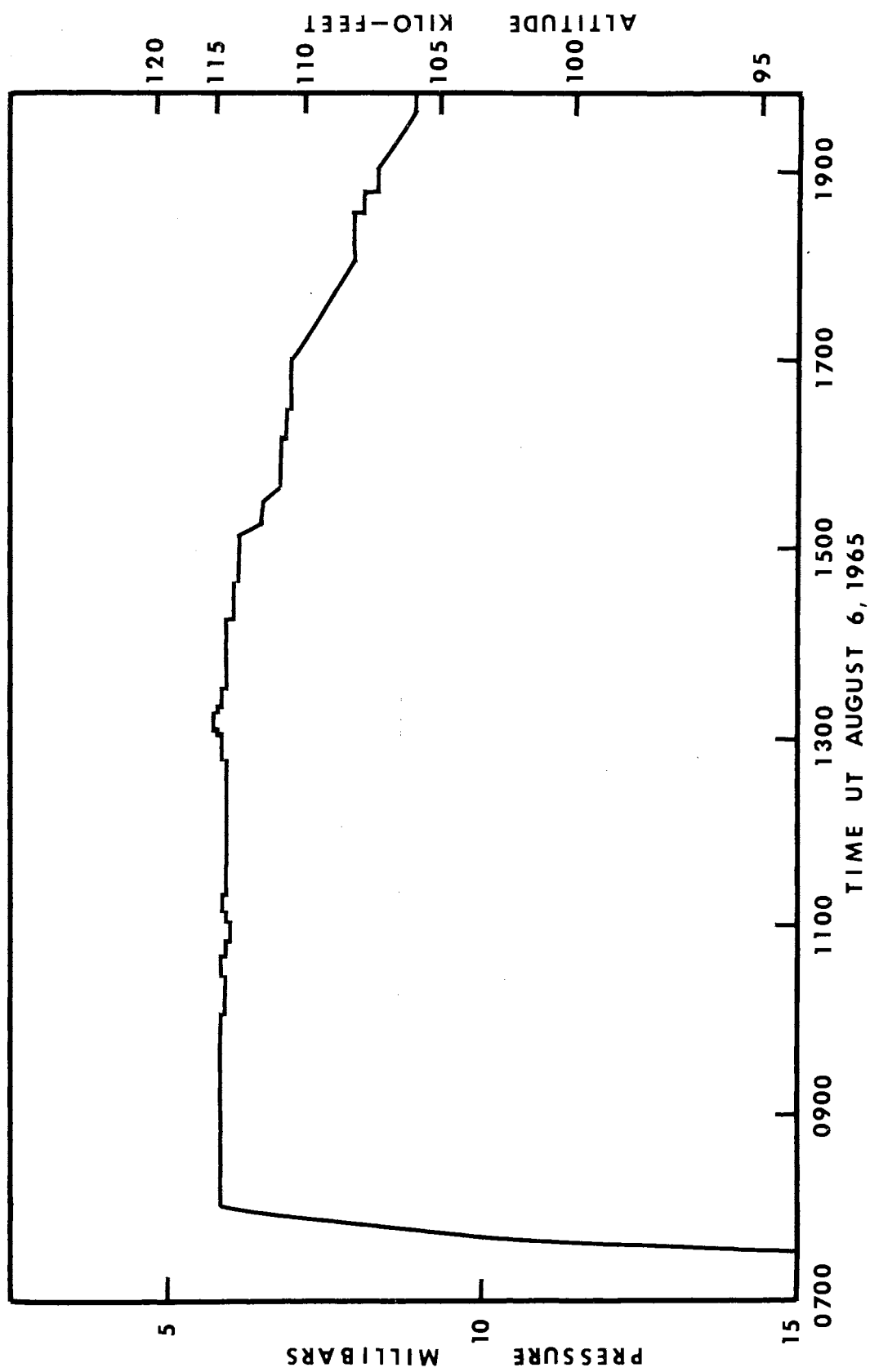
Figure 39. Flight Profile (Altitude Versus Time).

noticeably weaker and interference from vehicles and machinery near the

receiving station more severe. Monitoring of the digital data during

the flight revealed no indication of equipment failure up to the time

that the worsening radio signal caused decoding of the data to become

unreliable. The telemetry signal was recorded throughout the flight

on a multi-track, magnetic tape recorder, along with a time signal,

for use in further data processing.

7.2 Preliminary data reduction.

Since the total binary information rate of the balloon-borne monitor

is 40 bits/sec and the duration of this flight was greater than 17 hours,

the total amount of information recorded for the entire flight is in

excess of 2.4×10^6 bits. To decode and process such a large amount of

information without the aid of a high-speed, electronic data processor

would require an excessive amount of labor. For this reason, the first

step taken in the analysis of these data was to convert the magnetic

recording of the telemetry signal into an electronic computer compatible

form.

To accomplish this conversion, an intermediate magnetic tape record

was generated having, on one track, a requantized version of the

demodulated telemetry signal. That is, for each unit of time coinciding

with the transmission of one data-bit, an integral was taken, electroni-

cally, of the demodulator output. At the end of this time interval the

value of the integral was examined and the integrator reset to zero to

begin the integration for the following data-bit. If the output of

integrator, when examined, exceeded a preset level equal to the mid-

point between the levels representing logical one and logical zero, then

a logical one was recorded until, one bit-time later, the integrator was

re-examined; otherwise, a logical zero was recorded. Synchronization with the recorded telemetry signal was maintained throughout this process by a system utilizing a manual vernier adjustment of timing circuitry locked to one of the timing signals recorded on the original tape. Since the balloon-borne monitor produces two, simultaneous, 20 bit/sec bit-streams, two such re-quantized bit-streams were simultaneously formed and independently recorded on two of the tracks of the intermediate tape. On two more tracks of this tape, timing signals produced by the synchronized timing circuit were recorded to indicate the bit-timing and frame-timing (a frame in this case consisting of 100 bits). The advantages of the intermediate tape so produced are:

(a) The data exists as a definite string of logical ones and zeros--no intermediate, undefined states are allowed.

(b) Timing signals which are noise-free and directly related to the bit-stream are available on the same tape as the bit-streams themselves. This eliminates entirely the need for manual adjustment of the timing circuits for all subsequent processing.

(c) The recording of the intermediate tape was made in such a way that the playback could be made at increased tape speeds, reducing the time required for playback. This advantage was not available in the original recordings of the telemetry signals because of the restrictions imposed by the demodulation of the sub-carriers.

Finally an IBM computer tape was generated from the intermediate tape by using an incremental, digital tape-recorder. The only problem encountered in this conversion was caused by the necessity of producing, on the IBM-format tape, records of relatively short length. The time required to generate an inter-record gap on the incremental recorder is

almost as long as that required to write a data-frame, which could mean
a loss of about one-half of the original data. The difficulty was
resolved by making two conversion passes, the first to record the odd-
numbered data-frames using the times of the even-numbered frames to
produce inter-record gaps, the second to record, in like manner, the
even-numbered frames. Having reduced the data to a form compatible
with IBM electronic computers, all subsequent processing was accomplished
on these machines, first on an IBM 1401 and later on an IBM 360/50.

7.3 Mean counting rates.

During the time of the ascent from ground level to about 2000 feet
a decrease was noted in the counting rate of level 1. Since level 1,
as has been noted, has no coincidence requirement and is therefore
sensitive to gamma-rays, this decrease is believed to be indicative
of the presence, at ground level, of gamma-rays from the natural radio-
activity of the earth. In the early history of cosmic-ray research a
similar effect was used as evidence to support a theory of an earthly
origin for the cosmic radiation. Levels 2, 3, and 4, which are
sensitive mainly to energetic charged-particle radiation, showed no
such decrease. After the first 2000 feet all levels increased smoothly
in counting rate, reaching a maximum at about 70,000 feet. Above this
altitude the rates decreased--indicating that secondary radiation
effects were lessening--until, at the maximum altitude reached
($\approx$115,000 feet) the rates were about 20% less than the values at
70,000 feet.

Above 90,000 feet considerable fluctuation of the counting rates
was observed, but mean values taken over 10 minutes time resulted

in the following rates:

<div align="center">

Level 1   400 counts/sec

Level 2   440 counts/sec

Level 3   230 counts/sec

Level 4   150 counts/sec

</div>

Freier and Waddington (1965) have measured the flux of primary protons in the energy range 80-150 MeV over Ft. Churchill on August 26, 1960, and report a value of 53 ± 6 protons m^{-2} sec^{-1} $ster^{-1}$. This value, which was derived from nuclear emulsion data, is probably more accurate than an earlier value of 121 ± 6 protons m^{-2} sec^{-1} $ster^{-1}$ reported by Vogt (1962) for the same energy range; however, Vogt's instrument was similar in many respects to the instrument described here and therefore his raw, uncorrected rates are of interest. The rates Vogt reported, uncorrected for secondary production in the overlying air mass, were:

22 August 1960--165 ± 5 protons/m^2 sec-ster (70 MeV $\leqslant E \leqslant$ 187 MeV)

79 ± 4 protons/m^2 sec-ster (187 MeV $\leqslant E \leqslant$ 350 MeV)

8 September 1960--594 ± 9 protons/m^2 sec-ster (70 MeV $\leqslant E \leqslant$ 187 MeV)

158 ± 4 protons/m^2 sec-ster (187 MeV $\leqslant E \leqslant$ 350 MeV)

15 September 1960--191 ± 5 protons/m^2 sec-ster (70 MeV $\leqslant E \leqslant$ 187 MeV)

87 ± 3 protons/m^2 sec-ster (187 MeV $\leqslant E \leqslant$ 350 MeV)

Since the area of the balloon-borne monitor is about one-third of a square meter, the rates observed at 115,000 feet are several times the values which would be expected from Vogt's data. There are

several reasons, other than equipment failure, why this could be true:

(a) The Vogt instrument was a narrow-angle device looking only in the zenith direction. The balloon-borne monitor has little directional selectivity, and since at angles far removed from the zenith the amount of overlying atmosphere which must be traversed by a primary particle is much greater than at the zenith direction, the relative contribution of secondary particles to the total counting rate may be very much larger than in the Vogt instrument.

(b) The Vogt instrument was capable of separating protons, alpha particles, mesons, electrons and heavier particle components of the primary and secondary cosmic radiation. Since the balloon-borne monitor made no distinction between charged particles, its counting rates are due in part to charged particles other than protons.

(c) The portion of the cosmic-ray spectrum considered is particularly sensitive to changes in the interplanetary conditions over the solar cycle. Since the Vogt measurements were made near the peak of the solar sun-spot cycle and those of the balloon-borne monitor near the time of the sun-spot minimum, the primary fluxes may have differed very significantly.

The balloon-borne monitor was not designed to make good measurements of the absolute proton flux, but rather to give relative measurements on a short time scale with good statistical accuracy. Thus, the above discussion should be interpreted only as indicating that the counting rates observed were not completely inconsistent with previous measurements.

7.4 <u>Rapid</u> <u>variations</u> <u>of</u> <u>the</u> <u>charged</u> <u>particle</u> <u>flux</u>.

As the balloon-borne detector approached its ceiling altitude and for a period of about six hours afterward the count-rate data was conspicuously marked with rapid variations having time scales of a few seconds to a few minutes and amplitudes which were, at times, as large as 50% of the average counting rate. All of the data acquired during the time interval 0900 UT to 1200 UT, representing a period of large variations which also coincided with a period of excellent altitude stability of the balloon and good telemetry reception, was subjected to autocorrelation and power-spectrum analysis. The analysis of the time-history function from level 1 showed little more than the expected random variance due to the finite counting rate. Level 2 also produced featureless power spectra except for a general rise in the variance at frequencies with periods longer than about 30 sec. Power spectra for levels 3 and 4, which displayed considerably greater variance than levels 1 and 2, are shown in Figures 40 and 41. Features common to both of these spectra are:

(a) a strong peak at a period of about 280 sec. This periodicity is very evident in the data from level 3 where it can be traced through at least 30 consecutive, unbroken cycles. It is weaker in the data from level 4, being only occasionally visible in the raw data plots. Visual inspection of these times indicates, and cross-correlation analysis confirms, that the 280 sec variation in level 4 is in anti-phase with the 280 sec variation in level 3.

(b) two, closely-spaced, periodic variations with periods of 9.28 sec and 9.00 sec. These variations are about equally strong in the data from both level 3 and level 4 and are in phase in both levels.
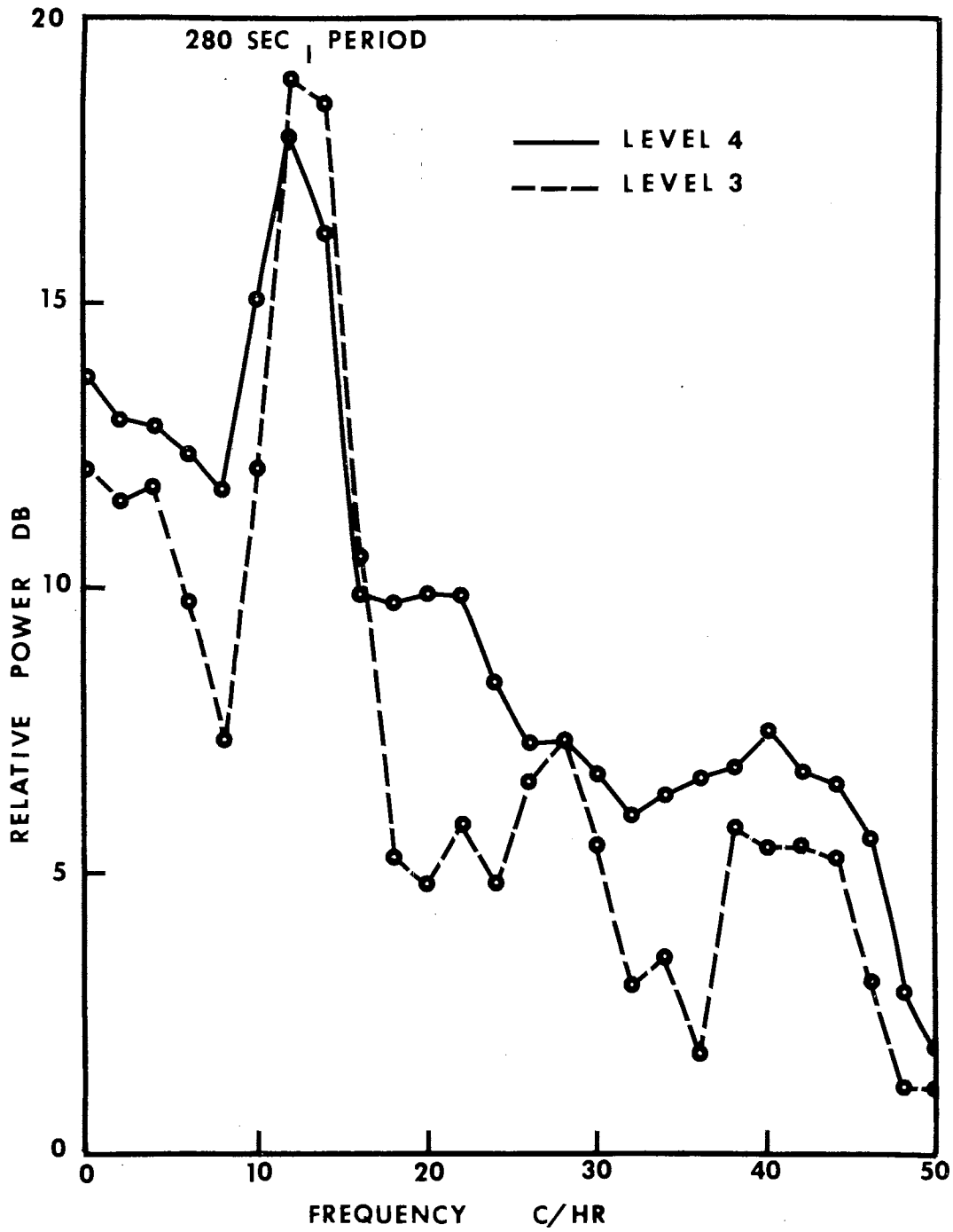
Figure 40. Power Spectrum (0—50 c/hr).
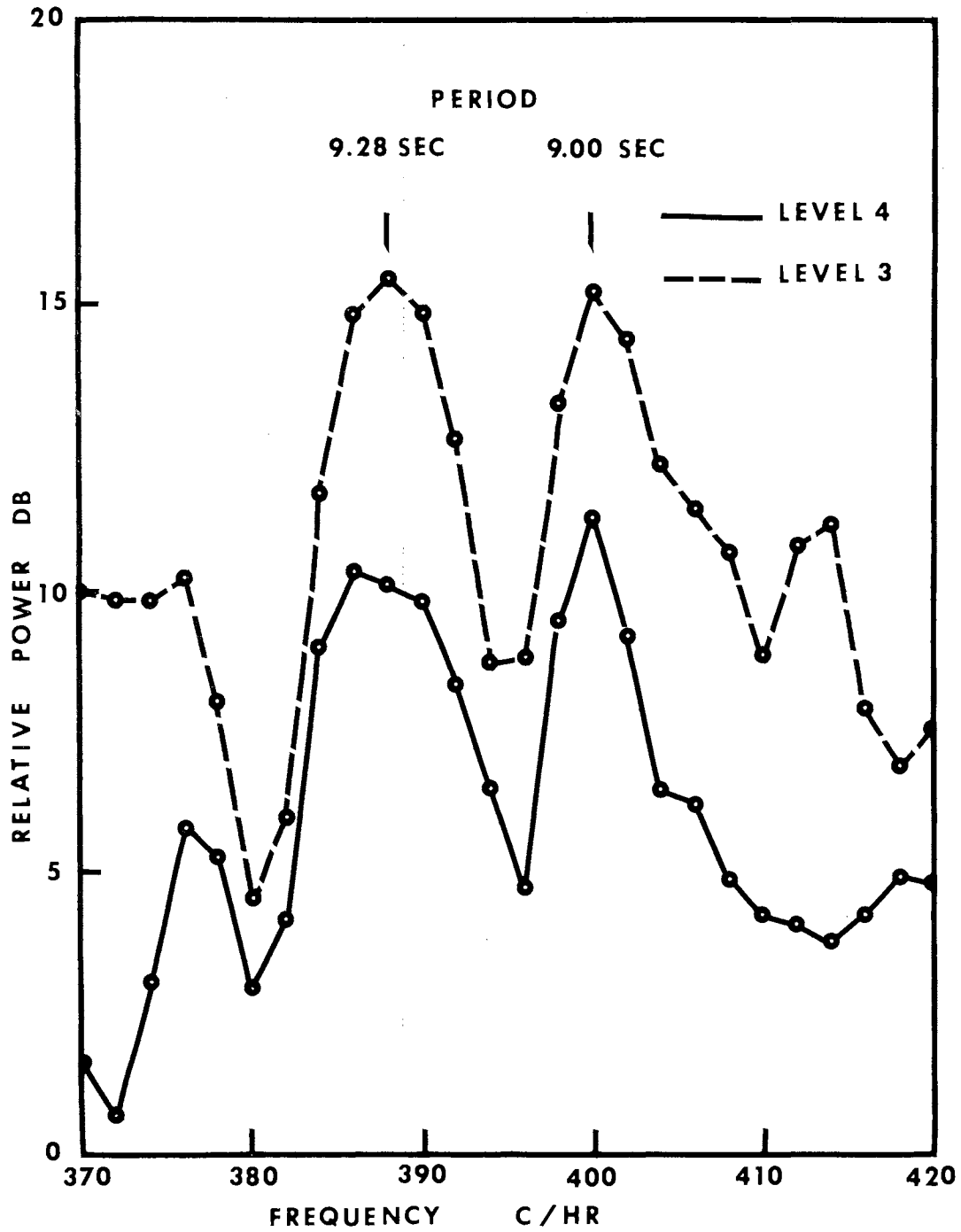
Figure 41. Power Spectrum (370—420 c/hr).

7.5   The 5-min periodicity.

The strong periodicity with a period of 280 sec (referred to here-
after as simply the 5-min periodicity) appears to belong to a rather
large class of periodic, geophysical phenomena with periods of about
5 min:

(a) Singh (1964) has reported periodic particle precipitation
phenomena (e.g., riometer absorption, 5577 Å photometer records, and
visual observation of pulsating aurora) often exhibit periods of about
5 min and suggests that a common cause may lie in longitudinal magneto-
acoustic standing waves in the magnetosphere which he computes to have
a fundamental period of 5 min for the equatorial belt through which the
magnetic field lines from the auroral zone pass.

(b) Parthasarathy and Hessler (1964) have observed periodic
covariation of the earth's magnetic field, earth currents, and 5577 Å
emission from the zenith with the most probable period being 5 min.

(c) Judge and Coleman (1962) have reported the observation of
covariant magnetic field and energetic particle fluxes detected by the
instruments carried by the Explorer 6 satellite in the distant (several
earth radii) magnetic field of the earth.   Periods ranged from 100 sec
to 500 sec.

(d) Vaisala oscillations (gravity-controlled, periodic oscillations
of air masses) have been identified in noctilucent clouds (Witt, 1962)
with periods of about 5 min (Parthasarathy and Hessler, 1964).

One possible extraterrestrial source of 5-min periodic modulations
of geophysical phenomena and, perhaps indirectly, energetic ($>$ 85 MeV)
proton fluxes at high geomagnetic latitudes lies in the solar photospheric
oscillations which were found to have a unique 5-min period by Leighton,
et al. (1962).

To this diverse list of phenomena and effects, whose common attribute is simply that all share a similar periodicity, the present experiment now adds the fluctuations of the energetic ($>$ 85 MeV) charged particle flux at high geomagnetic latitudes. Certainly not all of these observations are, in truth, related, but the nature of the interdependencies which may well link a number of them is, at the present time, very unclear.

7.6 The 10-sec periodicity.

This periodicity lies in a rather broad band of frequencies commonly observed in geomagnetic records from stations at all latitudes, although the effects are stronger and more frequent in the auroral zone (see Chapter V). It is interesting to note that the difference frequency between the two components of this variation (9.28 sec period 9.00 sec period) has a period of 5 min.

7.7 Critique of the experiment.

This experiment, while providing some evidence of a phenomena not reported previously, is deficient in several aspects:

(a) No effort was made to measure simultaneously the earth's magnetic field to an accuracy and time resolution required to test hypotheses concerning possible particle-magnetic field interactions. If at all possible, such measurements should be made by instruments carried with the energetic particle detector.

(b) The inability of the detector to distinguish between various charged particles also severely limited the usefulness of the data. The minimum requirement should be the ability to separate protons, alphas, and heavier particles from electrons and mesons.

(c) When only a single measurement of a phenomenon exists there is always some question of the possibility of an undetected equipment failure. The best way to eliminate this possibility is through an independent experiment or, if that is not possible, through an internal checking and calibrating feature of the experiment itself. No such checks were available for the present experiment which were completely satisfactory and so equipment failure can not be ruled out with certainty.

SUMMARY

Although the cosmic radiation is notable for its relative lack of
temporal and spatial variance, careful measurements have revealed small
but significant periodic time-variations, aperiodic time-variations,
persistent anisotropies, and transient anisotropies. Early hopes of
discovering the origin of cosmic rays through measurements of the persis-
tent anisotropies have not been fulfilled. However, the very effects
which have frustrated the search for cosmic-ray origins, that is, the
strong diffusive mixing of the cosmic rays in the turbulent inter-
planetary magnetic field and the generation of anisotropies and transient
variations which are related to the large-scale bulk motions of the inter-
planetary medium, have provided powerful tools for the investigation of
the interplanetary medium itself and a number of related solar-surface
phenomena. While early investigators were hindered by a lack of good
data, the recent resurgence of interest in cosmic-ray propagation
phenomena brought about by the International Geophysical Year and the
more recent International Year of the Quiet Sun programs have almost
inundated the researcher with data. The output of a single deep-space
probe over a few months time can exceed, both in volume and in scientific
content, the result of a lifetime's work with the older instruments. The
central problems now often lie in the formulation of analytical methods
for attacking the data, in the interpretation of the data in the context
of existing theoretical models, and, where existing models are shown

to be inadequate, in the creation of new theories to explain the observations.

For earth-based monitors and non-stationary space-probes the problems of data analysis are often related to the need to separate temporal and spatial effects--a requirement which is almost always complicated by random variation in the data, or even the presence of strong, but irrelevant, real variations, and instrumental characteristics, which may be quite basic to the measurement, that severely distort the observed variations.

In the present work, the methods of the statistical theory of communication, particularly those concerning frequency-domain analysis, linear convolution filtering, heterodyning, and demodulation have been adapted for use with cosmic-ray data. The results stemming from this effort include:

(a) The time-honored techniques of harmonic analysis and super-position analysis have been reformulated in the language of modern numerical filter theory with the result that new insight is gained into the workings of these very useful methods, and ways to improve their performance are suggested.

(b) Direct evidence, in the form of modulation sidebands, has been given for a random modulation of the diurnal anisotropy and also for a periodic modulation with a period of 27 days.

(c) A world-wide survey of the semi-diurnal variation observed by neutron monitors has revealed that a persistent semi-diurnal anisotropy exists having a peak-to-peak amplitude of about 0.14% and maxima which lie along a line perpendicular to the mean interplanetary

magnetic field. This anisotropy has existed with this amplitude and orientation over the entire solar cycle 1953-1965.

(d) The absence of a 3-cpd component of the diurnal anisotropy has been verified to an accuracy of ± 1 dB relative to the random-variation power in the immediate neighborhood of 3 cpd. This observation lends some support to the thought that the semi-diurnal variation is a phenomenon independent from the diurnal variation and not merely part of a continuing harmonic structure of the diurnal variation.

(e) The well-known 27-day variation of the cosmic radiation has been detected in a power-spectrum analysis of neutron-monitor data. The strong harmonic structure which is revealed is attributed to the impulsive nature of the 27-day variation. The autocorrelation function for the same data indicates a most probable lifetime of about two solar rotations for the active solar regions producing these impulses.

(f) The 11-year and $\frac{1}{2}$-year periodicities of the variation of the international magnetic character figure C_i have been observed in the power-spectrum analysis of the C_i data for the period 1884-1964. The absence of any variation with a period of 1 year is interpreted as indicating that the magnetic disturbances characterized by C_i are a global phenomenon related to the magnitude of the angle made between the earth's magnetic moment and the earth-sun line. This contrasts with the reported strong annual modulation of the daily magnetic variations which are thus indicated to be probably related to the annual variation of the sun-zenith angle for each station.

(g) The problem of detecting a sidereal variation of the cosmic-ray intensity as observed by neutron monitors has been considered with the conclusion that, due to the interfering effects of the diurnal

variation and its annual modulation sidebands as well as the presence
of considerable random-variation power in the frequency interval of
interest, a span of data on the order of 100 years would be required for
a meaningful study.

(h) The effect of the directional variation in the transmission
of the asymptotic cone of acceptance of a cosmic-ray neutron monitor
has been expressed as a linear convolution filter, allowing a band-
limited inverse filter to be formulated. Application of the inverse
filter to the data of a neutron monitor results in smoothed data which
accurately portrays the directional variations of the cosmic-ray flux
allowing direct inter-comparisons between stations.

(i) Computational algorithms have been constructed which produce time-
direction cosmic-ray intensity-contour maps utilizing deconvolved
(inverse filtered) data. The method uses two-dimensional, non-uniformly-
weighted, convolution filters which do not require uniformly spaced data.

(j) An analysis has been made of the 20 January 1966 Forbush
decrease by means of an intensity-contour map. The data from the world-
wide net of neutron monitors is found to be in excellent quantitative
and qualitative agreement with the Parker 'blast wave' model for such
decreases.

(k) A study of the intensity-contour maps for the times of
occurrence of the recurring Forbush decreases reported by McCracken,
et al. (1966) reveals that, at least on one occasion, the form of the
decrease was consistent with that expected from a standing shock in the
interplanetary medium.

A large aperture (≈ 0.3 m^2-ster) balloon-borne cosmic-ray monitor has been designed and constructed. A flight of this instrument at high geomagnetic latitudes (launch point was Ft. Churchill, Manitoba, Canada) to an altitude greater than 115,000 feet on August 6, 1965, has resulted in data which indicate the presence of rapid periodic temporal fluctuations in the cosmic radiation ($>$ 85 MeV) having periods of 280 sec and 9 sec.

BIBLIOGRAPHY

Ahluwalia, H. S. "Semidiurnal Variation of Cosmic Rays on Geomagneti-
    cally Disturbed Days." Proc. Phys. Soc., 80 (1962), 472-478.

Ahluwalia, H. S., and A. J. Dessler. "Diurnal Variation of Cosmic
    Radiation Intensity Produced by a Solar Wind." Planet Space Sci.,
    9 (1962), 195-210.

Akasofu, S. T. "Electrodynamics of Magnetosphere: Geomagnetic Storms."
    Space Sci. Rev., 6 (1966), 21-143.

Alfven, H., and C. Fälthammer. Cosmical Electrodynamics. 2nd ed.
    London: Oxford University Press, 1963.

Axford, W. I. "The Modulation of Galactic Cosmic Rays in the Inter-
    planetary Medium." Planet Space Sci., 13 (1965), 115-130.

Babcock, H. W. "The Solar Magnetograph." Astrophys. J., 118 (1953), 387.

Beard, D. B. "The Solar Wind Geomagnetic Field Boundary." Rev.
    Geophys., 2 (1964), 335-365.

Benioff, H. "Observations of Geomagnetic Fluctuations in the Period
    Range 0.3 to 120 Seconds." J. Geophys. Res., 65 (1960), 1413-1422.

Bennett, W. R. "Methods of Solving Noise Problems." Proc. IRE, 44
    (1956), 609-611.

Bickel, R. L. Economical Cosmic-Ray Data Reduction and Transmission
    Systems for Balloon Experiments. Unpublished Southern Methodist
    University Master's Thesis, 1965.

Biermann, L. "Kometenschweife und Solare Korpuscular Strahlung."
    Z Astrophys., 29 (1951), 274.

Biswas, S., and C. E. Fichtel. "Nuclear Composition and Rigidity
    Spectra of Solar Cosmic Rays." Astrophys. J., 193 (1964), 941-950.

Blackman, R. B., and J. W. Tukey. "The Measurement of Power Spectra
    from the Point of View of Communications Engineering--Part I."
    Bell System Tech. J., 37 (1958), 185-282.

Blackman, R. B., and J. W. Tukey. "The Measurement of Power Spectra
    from the Point of View of Communications Engineering--Part II."
    Bell System Tech. J., 37 (1958), 485-569.

Bogert, B. P., M. J. R. Healey, and J. W. Tukey. "The Quefrency Alanysis of Time Series for Echoes: Cepstrum, Psuedo-Autocovariance, Cross-Cepstrum and Saphe Cracking." Proc. of the Symposium on Time Series Analysis. Ed. Murray Rosenblatt. New York: John Wiley and Sons, 1963.

Bryant, D. A., T. L. Cline, U. D. Desai, and F. B. McDonald. "Explorer 12 Observations of Solar Cosmic Rays and Energetic Storm Particles After the Solar Flare of September 28, 1961." J. Geophys. Res., 67 (1962), 4983-5000.

Burch, J. J., A. W. Green, Jr., and H. H. Grote. "Restoration and Correction of Time Functions by Synthesis of Inverse Filters on Analog Computers." IEEE Transactions on Geoscience Electronics, GE-2, No. 1 (1964), 19-24.

Chapman, S., and J. Bartels. Geomagnetism. London: Oxford University Press, 1951.

Compton, A. H., and I. A. Getting. "An Apparent Effect of Galactic Rotation on the Intensity of Cosmic Rays." Phys. Rev., 47 (1935), 817-821.

Conforto, A. M., and J. A. Simpson. "The 24 Hour Intensity Variations of the Primary Cosmic Rays." Nuovo Cimento, 6 (1957), 1052-1063.

Davenport, W. B., and W. L. Root. Random Signals and Noise. New York: McGraw-Hill Book Co., Inc., 1958.

Dessler, A. J. "Length of Magnetosphere Trail." J. Geophys. Res., 69 (1964), 3913-3918.

Dessler, A. J., and B. J. O'Brien. "Penetrating Particle Radiation." Satellite Environment Handbook. Ed. Francis S. Johnson. Stanford: Stanford University Press, 1965.

Dessler, A. J., and G. K. Walters. "Hydromagnetic Coupling Between Solar Wind and Magnetosphere." Planet Space Sci., 12 (1965), 227-234.

Dragt, A. J. "Effect of Hydromagnetic Waves on the Lifetime of Van Allen Radiation Protons." J. Geophys. Res., 66 (1961), 1641-1649.

Farley, F. J. M., and J. R. Storey. "Sidereal Correlation of High-Energy Cosmic Rays." Nature, 173 (1964), 445.

Fenten, A. G., K. G. McCracken, D. C. Rose, and B. G. Wilson. "The Onset Times of Forbush Type Cosmic Ray Intensity Decreases." Can. J. Phys., 37 (1959), 970-982.

Forbush, S. E. "On Cosmic Ray Effects Associated with Magnetic Storms." Terrestrial Magnetism and Atmospheric Electricity, 43 (1938), 203-218.

Freier, P. S., and C. J. Waddington. "Intensity of 80- to 200-MeV Protons Over Fort Churchill on August 26, 1960." J. Geophys. Res., 70 (1965), 2111.

George, C. F., H. W. Smith, and F. X. Bostick. "The Application of Inverse Convolution Techniques to Improve Signal Response of Recorded Geophysical Data." Proc. IRE, 50 (1962), 2313-2319.

Gold, T. "Plasma and Magnetic Fields in the Solar System." J. Geophys. Res., 64 (1959), 1665-1674.

Gold, T. "Magnetic Storms." Space Sci. Rev., 1 (1962), 100-114.

Handbook of Geophysics, Rev. ed., Prepared by the Geophysics Research Directorate of the Air Force Cambridge Research Center. New York: Macmillan, 1960.

Hatton, C., and H. Carmichael. "Experimental Investigation of NM-64 Neutron Monitor." Can. J. Phys., 42 (1964), 2443-2472.

Heppner, J. P., N. F. Ness, C. S. Scearce, and T. L. Skillman. "Explorer 10 Magnetic Field Measurements." J. Geophys. Res., 68 (1963), 1-46.

Hess, W. N. Introduction to Space Science. New York: Gordon-Breach Science Publishers, 1965.

Hultquist, B. "Plasma Waves in the Frequency Range 0.001-10 cps in the Earth's Magnetosphere and Ionosphere." Space Sci. Rev., 5 (1966), 599-695.

Jacklyn, R. M. "The Apparent Sidereal and Anti-Sidereal Daily Variations of Cosmic Ray Intensity." Nuovo Cimento, 24 (1962), 1034-1065.

Johnson, F. S. "The Gross Character of the Geomagnetic Field in the Solar Wind." J. Geophys. Res., 65 (1960), 3049-3051.

Johnson, F. S. Satellite Environment Handbook. 2nd ed. Stanford: Stanford University Press, 1965.

Judge, D. L., and P. J. Coleman. "Observations of Low-Frequency Hydromagnetic Waves in the Distant Geomagnetic Field: Explorer 6." J. Geophys. Res., 67 (1962), 5071.

Karplus, R., W. E. Frances, and A. J. Dragt. "The Attenuation of Hydromagnetic Waves in the Ionosphere." Planet Space Sci., 9 (1962), 771-775.

Kato, Y., and T. Saito. "Morphological Study of Geomagnetic Pulsations." J. Phys. Soc. Japan, 17, Supplement A-II (1962), 34-39.

Katzman, J., and D. Venkatesan. "A World-Wide Study of the Daily Variation of the Nucleonic Component of Cosmic Rays." Can. J. Phys., 38 (1960), 1011-1026.

Kolmogoroff, A. "Interpolation und Extrapolation von stationaren zufalligen Folger." Bulletin de l'academic des sciences de U.R.S.S., 5 (1941), 3-14.

Lee, Y. W. Statistical Theory of Communication. New York: John Wiley and Sons, Inc., 1960.

Leighton, R. B., R. W. Noyes, and G. W. Simon. "Velocity Fields in the Solar Atmosphere." Astrophys. J., 135 (1962), 474.

McCracken, K. G. A Study of the Properties of Transient Changes in the Cosmic Ray Intensity. Unpublished University of Tasmania Doctoral Thesis, 1958.

McCracken, K. G. "The Cosmic Ray Flare Effect." J. Geophys. Res., 67 (1962), 423-434.

McCracken, K. G., and N. F. Ness. "The Collimation of Cosmic Rays by the Interplanetary Magnetic Field." J. Geophys. Res., 71 (1955) 3315-3318.

McCracken, K. G., and U. R. Rao. "A Survey of the Diurnal Anisotropy." Proceedings of the Ninth International Conference on Cosmic Rays, I. London: The Institute of Physics and Physical Society, 1965.

McCracken, K. G., U. R. Rao, and R. P. Bukata. "Recurrent Forbush Decreases Associated with M-region Magnetic Storms." Phys. Rev. Let., 17 (1966), 928-932.

McCracken, K. G., U. R. Rao, and B. C. Fowler. Cosmic Ray Tables (Asymtotic Directions, Variational Coefficients and Cut-off Rigidities). IQSY Instruction Manual, No. 10. London: IQSY Committee, 1965.

McCracken, K. G., U. R. Rao, and M. A. Shea. The Trajectories of Cosmic Rays in a High Degree Simulation of the Geomagnetic Field. Massachusetts Institute of Technology, Laboratory for Nuclear Science, Technical Report No. 77, 1962.

McIlwain, C. E. "Direct Measurement of Particles Producing Visible Auroras." J. Geophys. Res., 65 (1960), 2727-2747.

Meyer, P., and R. Vogt. "Electrons in the Primary Cosmic Radiation." Phys. Rev. Letters, 6 (1961), 193-196.

Nagashima, K., S. P. Duggal, and M. A. Pomerantz. "Long Term Modulation of Primary Cosmic Ray Intensity." Planet Space Sci., 14 (1966), 177-206.

Ness, N. F. "The Earth's Magnetic Trail." J. Geophys. Res., 70 (1965), 2989-3005.

Ness, N. F., C. A. Scearce, and J. B. Seek. "Initial Results of the Imp I Magnetic Field Experiment." J. Geophys. Res., 69 (1964), 3531-3569.

Ness, N. F., and J. M. Wilcox. "Solar Origin of the Interplanetary Magnetic Field." Phys. Rev. Letters, 13 (1964), 461-464.

Neugebauer, M., and C. W. Snyder. "The Mission of Mariner II: Preliminary Observation-Solar Plasma Experiment." Science, 138 (1962), 1095-1097.

O'Brien, B. J. "High-Latitude Geophysical Studies With Satellite Injun 3." J. Geophys. Res., 69 (1964), 13-14.

Palmeira, R. A., and G. F. Pieper. "Cosmic Rays." Introduction to Space Science. Ed. W. N. Hess. New York: Gordon and Breach

Parker, E. N. "Dynamics of the Interplanetary Gas and Magnetic Fields." Astrophys. J., 132 (1958), 132.

Parker, E. N. "Sudden Expansion of the Corona Following a Large Solar Flare and the Attendant Magnetic Field and Cosmic-Ray Effects." Astrophys. J., 133 (1961), 1014.

Parker, E. N. Interplanetary Dynamical Processes. New York: Interscience Publishers-John Wiley and Sons, 1963.

Parker, E. N. "Theory of Streaming of Cosmic Rays and the Diurnal Variation." Planet Space Sci., 12 (1964), 735-747.

Parker, E. N. "The Effect of Adiabatic Deceleration on the Cosmic Ray Spectrum in the Solar System." Planet Space Sci., 14 (1966), 371-380.

Parthasarathy, R., and V. P. Hessler. "Periodic Covariation of Radio-wave Absorption, Earth Currents, and Other Associated Phenomena in the Auroral Zone." J. Geophys. Res., 69 (1964), 2867.

Rao, U. R., K. G. McCracken, and D. Venkatesan. "Asymptotic Cones of Acceptance and Their Use in the Study of the Daily Variation of Cosmic Radiation." J. Geophys. Res., 68 (1963), 345-369.

Rao, U. R., and V. Sarabhai. "Cosmic Ray Intensity at Low Latitudes I." Proc. Roy. Soc., 263 (1961), 101-117.

Simpson, J. A., and W. C. Fagot. "Properties of the Low Energy Nucleonic Component at Large Atmosphere Depths." Phys. Rev., 90 (1953), 1068-1072.

Simpson, J. A., W. Fonger, and S. B. Treiman. "Cosmic Radiation Intensity-Time Variations and Their Origin. I. Neutron Intensity Variation Method and Meteorological Factors." Phys. Rev., 90 (1953), 934-950.

Singh, R. N. "Periodic Precipitation of the Particle Flux in the Auroral Zone." Nature, 203 (1964), 69.

Smith, J. H. "Theoretical Range-Energy Values for Protons in Air and Aluminum." Phys. Rev., 71 (1947), 32-33.

Snyder, C. W., M. Neugebauer, and U. R. Rao. "The Solar Wind Velocity and Its Correlation With Cosmic-Ray Variations and With Solar and Geomagnetic Activity." J. Geophys. Res., 68 (1963), 6361-6370.

Stokes, A. R. "A Numerical Fourier-Analysis Method for the Correction of Widths and Shapes of Lines on X-ray Powder Photographs." Proc. Phys. Soc. London, 61 (1948), 382-391.

Stormer, C. The Polar Aurora. London: Oxford University Press, 1955.

Swinnerton-Dyer, H. P. F. "The Calculation of Power Spectra." Computer J., 5 (1963), 16-23.

Tepley, L. R. "Observations of Hydromagnetic Emissions." J. Geophys. Res., 66 (1961), 1651-1665.

Thomas, R. N., and R. G. Athay. Physics of the Solar Chromosphere. New York: Interscience Publishers, Inc., 1961.

Treitel, S., and E. A. Robinson. "The Stability of Digital Filters." IEEE Trans. Geoscience Electronics, GE-2, No. 1 (1964), 6-18.

van de Hulst, H. C. "The Chromosphere and the Corona." The Sun. Ed. G. P. Kniper. Chicago: University of Chicago Press, 1953.

Vogt, R. "Primary Cosmic-Ray and Solar Protons." Phys. Rev., 125 (1962), 366.

Welch, J. A., and W. A. Whitaker. "Theory of Geomagnetically Trapped Electrons from an Artificial Source." J. Geophys. Res., 64 (1959), 909-922.

Wiener, N. Extrapolation, Interpolation, and Smoothing of Stationary Time Series. New York: John Wiley and Sons, 1959.

Wilcox, J. M., and N. F. Ness. "Quasi-Stationary Corotating Structure in the Interplanetary Medium." J. Geophys. Res., 70 (1965), 5793-5805.

Witt, G. "Height, Structure, and Displacements of Noctilucent Clouds." Tellus, 14 (1962), 1.

Yanagihara, K. Memoirs of the Kakioka Magnetic Observatory, 9(2) (1960), 15.

APPENDIX A

VARIATIONAL COEFFICIENTS

The concept of the variational coefficients of a detector has been defined by Rao, et al. (1962) as

$$\nu(\Omega_i, \beta) = \int_{R_{CUT-OFF}}^{\infty} W(R) \cdot R^{\beta} \frac{Y(\Omega_i, R)}{Y(4\pi, R)} dR$$

where $\nu(\Omega_i, \beta)$ is the variational coefficient appropriate to the incremental solid angle Ω_i for a primary anisotropy rigidity spectrum of the form AR^{β}. The coupling function $W(R)$ is the fractional differential change of the detector counting rate due to a change in the intensity of radiation of rigidity R. The function $Y(\Omega_i, R)$ is related to the atmospheric attenuation function $T(R, \phi, \theta)$, a separable function of rigidity and direction such that $T(R, \phi, \theta) = S(R)Z(\phi, \theta)$, and

$$Y(\Omega_i, R) = \int Z(\phi, \theta) d\Omega$$

The integral is taken over only those directions which are accessible to the detector from solid angle Ω_i.

The numerical evaluation of variational coefficients requires a knowledge of the asymptotic directions of primary particle trajectories for all directions of entry at the top of the atmosphere which contribute significantly to the detector counting rate. This information is usually supplied by detailed trajectory computations for a large number of directions and rigidities for each position on the earth's surface for

which the variational coefficient function is desired. The following
table of variational coefficients is excerpted from McCracken, et al.
(1965), by permission. The trajectory computations were made using a
high degree simulation of the geomagnetic field (McCracken, et al.,
1962).

VARIATIONAL COEFFICIENTS

$$\beta = 0$$

ASYMPTOTIC LONGITUDE		CALGARY	CHURCHILL	DALLAS	DEEP RIVER	GOOSE BAY	INUVIK	KERGUELEN	MT. WELLINGTON	SULPHUR MT.
0	5	0.20	0.0	0.0	6.49	11.85	1.21	0.12	0.0	0.0
5	10	0.08	0.0	0.43	7.11	15.89	3.12	0.11	0.0	0.0
10	15	0.04	0.0	0.25	5.16	2.16	9.21	0.0	0.0	0.0
15	20	0.0	0.0	0.28	2.49	1.80	20.23	0.0	0.0	0.0
20	25	0.0	0.0	0.32	3.63	2.66	15.79	0.0	0.0	0.0
25	30	0.0	0.0	0.15	1.01	0.97	11.66	0.0	0.0	0.0
30	35	0.0	0.0	0.13	1.63	1.07	3.97	0.0	0.0	0.0
35	40	0.0	0.0	0.0	0.54	0.64	1.51	0.0	0.0	0.0
40	45	0.0	0.0	1.18	0.21	0.71	0.0	0.0	0.0	0.14
45	50	0.0	0.0	1.15	0.0	0.20	0.0	0.0	0.0	0.68
50	55	0.0	0.0	1.80	0.0	1.06	0.0	0.0	0.0	0.14
55	60	0.0	0.0	0.61	0.0	0.31	0.0	0.0	0.0	0.14
60	65	0.0	0.0	0.03	0.0	0.0	0.0	0.22	0.0	0.0
65	70	0.0	0.0	0.0	0.0	0.0	0.0	0.55	0.0	0.0
70	75	0.0	0.0	1.28	0.0	0.0	0.0	0.27	0.0	0.0
75	80	0.0	0.0	1.29	0.04	0.0	0.0	0.21	0.0	0.0
80	85	0.0	0.0	0.64	0.16	0.01	0.0	0.14	0.0	0.0
85	90	0.0	0.0	0.0	0.16	0.04	0.0	0.39	0.0	0.0
90	95	0.0	0.0	0.61	0.0	0.03	0.0	0.78	0.0	0.0
95	100	0.0	0.0	0.60	0.0	0.0	0.0	0.29	0.0	0.0
100	105	0.0	0.0	0.0	0.0	0.0	0.0	4.88	0.0	0.0
105	110	0.0	0.0	0.0	0.0	0.0	0.0	2.83	0.0	0.0
110	115	0.0	0.0	0.0	0.0	0.0	0.0	3.45	0.0	0.0
115	120	0.0	0.0	0.0	0.0	0.0	0.0	6.40	0.0	0.0
120	125	0.0	0.0	0.0	0.0	0.0	0.0	18.77	0.0	0.0
125	130	0.0	0.0	0.0	0.0	0.0	0.0	13.84	0.0	0.0
130	135	0.0	0.0	0.0	0.0	0.0	0.0	9.81	0.0	0.0
135	140	0.0	0.0	0.60	0.0	0.0	0.0	14.95	0.0	0.0
140	145	0.0	0.0	0.0	0.0	0.0	0.0	2.81	0.0	0.0
145	150	0.0	0.0	0.0	0.0	0.0	0.0	4.40	0.0	0.0
150	155	0.0	0.0	0.0	0.0	0.0	0.0	0.78	0.96	0.0
155	160	0.0	0.0	0.0	0.0	0.0	0.0	1.56	0.32	0.0
160	165	0.0	0.0	0.0	0.0	0.0	0.0	1.18	0.25	0.0
165	170	0.0	0.0	1.36	0.0	0.0	0.0	0.80	0.27	0.0
170	175	0.0	0.0	0.0	0.0	0.0	0.0	0.20	0.98	0.0
175	180	0.0	0.0	0.0	0.0	0.0	0.52	0.19	0.0	0.0
180	185	0.0	0.0	0.0	0.0	0.0	0.16	0.20	0.85	0.0
185	190	0.0	0.0	0.0	0.0	0.0	0.0	0.0	0.39	0.0
190	195	0.0	0.0	0.64	0.0	0.0	0.0	0.0	2.70	0.0
195	200	0.40	0.0	0.0	0.0	0.0	0.0	0.0	4.25	0.0
200	205	0.30	0.0	0.0	0.0	0.0	0.0	0.0	1.55	0.0
205	210	0.23	0.0	0.0	0.0	0.0	0.0	0.0	2.77	0.0
210	215	0.08	0.0	0.67	0.0	0.0	0.0	0.0	1.58	0.0
215	220	0.09	0.0	0.0	0.0	0.0	0.0	0.0	3.06	0.0
220	225	0.31	0.0	0.0	0.0	0.0	0.10	0.0	3.98	0.0
225	230	0.33	0.0	0.0	0.0	0.0	0.09	0.04	7.15	0.0
230	235	0.31	0.0	0.0	0.0	0.0	0.14	0.04	21.37	0.0
235	240	2.74	0.0	0.0	0.0	0.0	0.95	0.04	9.46	0.34
240	245	2.24	0.0	0.0	0.0	0.0	2.32	0.08	5.66	0.26
245	250	2.45	0.04	0.0	0.0	0.0	0.04	0.08	5.06	0.20
250	255	2.41	0.26	0.0	0.0	0.0	1.72	0.0	5.14	0.15
255	260	2.16	0.16	0.0	0.0	0.0	1.07	0.0	3.41	0.10
260	265	12.45	0.10	0.0	0.0	0.0	3.06	0.08	2.14	0.33
265	270	20.18	0.0	0.30	0.0	0.0	7.74	0.0	1.08	0.39
270	275	17.55	0.0	0.29	0.0	0.0	25.61	0.0	0.54	0.0
275	280	9.94	0.43	0.48	0.0	0.0	8.67	0.0	0.0	3.41
280	285	6.99	0.25	0.51	0.84	0.0	4.51	0.0	2.04	2.05
285	290	1.90	0.26	0.46	0.28	0.0	3.40	0.0	0.82	2.02
290	295	0.90	2.05	0.57	0.21	0.0	1.63	0.0	0.83	1.96
295	300	0.96	1.77	0.26	0.14	1.15	1.23	0.0	0.0	3.74
300	305	1.47	2.71	2.16	0.61	0.22	1.86	0.0	0.0	15.98
305	310	1.34	1.37	3.38	0.35	0.14	0.22	0.0	0.0	15.24
310	315	0.0	1.20	2.66	0.50	0.0	0.75	0.0	0.0	20.17
315	320	0.0	5.65	3.00	0.22	0.57	0.93	0.0	0.0	6.70
320	325	0.0	19.74	2.49	3.57	0.31	0.0	0.0	0.23	7.03
325	330	0.0	20.08	3.14	2.55	0.43	0.27	0.0	0.69	2.58
330	335	0.0	9.40	3.75	2.67	0.12	0.18	0.0	0.23	0.0
335	340	0.0	2.91	3.53	2.05	0.37	0.13	0.0	0.45	1.33
340	345	0.0	3.02	5.24	2.26	4.59	0.10	0.0	0.0	2.63
345	350	0.0	1.83	6.62	2.59	2.43	0.29	0.0	0.22	1.47
350	355	0.0	0.0	5.66	9.85	1.65	0.0	0.0	0.22	0.0
355	360	0.04	0.68	4.67	22.83	1.08	0.22	0.0	0.0	0.0

APPENDIX B

COMPUTER PROGRAMS

The following computer programs, written in the machine-independent
language FORTRAN, represent only a small part of the total number of
programs used in the data reduction and analyses reported in this thesis.
However, these programs are considered to have some lasting value to
other researchers and therefore were selected for reproduction here.
The programs have been internally documented through the use of comment
statements so that they are self-explanatory. Should more information
concerning the methods used be sought, the references cited in these
comments should be consulted. The first two programs, dealing with the
computation of power spectra and cross-power spectra may be recommended
without hesitation. The third program, consisting of a main program
and several subroutines and dealing with the computation of time-direction
cosmic-ray intensity contour map, is, however, included more as a
guide for persons wishing to formulate similar algorithms than as a
practical working routine. This stems necessarily from the somewhat
specialized form of the input-output routines which were made to conform
to the format of an existing data library and computer system.

```
C
C      SUBROUTINE PSA
C
C      PURPOSE
C         COMPUTE THE POWER SPECTRUM AND AUTOCORRELATION FUNCTION OF
C         A GIVEN SERIES.
C
C      USAGE
C         CALL PSA(D,A,S,P,C,AV,VAR,SD,N,M,NDF)
C
C      DESCRIPTION OF PARAMETERS
C         D    -INPUT VECTOR OF LENGTH N CONTAINING THE SERIES WHOSE
C               POWER SPECTRUM AND AUTOCORRELATION ARE TO BE COMPUTED.
C         A    -OUTPUT VECTOR OF LENGTH M+1 CONTAINING THE AUTOCORRE-
C               LATIONS FOR LAGS OF 0,1,2,....,M.
C         S    -OUTPUT VECTOR OF LENGTH M+1 CONTAINING THE UNSMOOTHED
C               POWER SPECTRUM.
C         P    -OUTPUT VECTOR OF LENGTH M+1 CONTAINING THE SMOOTHED
C               (HANNED) SPECTRUM.
C         C    -OUTPUT VECTOR OF LENGTH 2M CONTAINING COS(C*PI/M)
C               C=0,1,2,....,(2M-1).
C         AV   -THE AVERAGE OF THE INPUT SERIES (OUTPUT).
C         VAR  -THE VARIANCE OF THE INPUT SERIES (OUTPUT).
C         SD   -THE STANDARD DEVIATION OF THE INPUT SERIES (OUTPUT).
C         N    -THE LENGTH OF THE INPUT SERIES (INPUT).
C         M    -MAX LAG.  AUTOCORRELATIONS ARE COMPUTED FOR LAGS OF
C               0,1,2,....,M    (INPUT).
C         NDF -THE NUMBER OF DEGREES OF FREEDOM (OUTPUT).
C
C      REMARKS
C         N MUST BE GREATER THAN M. THE SERIES CONTAINED IN THE D
C         VECTOR IS NORMALIZED TO ZERO MEAN AND UNIT VARIANCE.
C         THE FIRST VALUE OF THE S AND P VECTORS CORRESPOND TO
C         ZERO FREQUENCY. THE SPACING BETWEEN SPECTRAL ESTIMATES
C         IS 1/2*T*M WHERE T IS THE TIME BETWEEN ELEMENTS IN THE
C         INPUT SERIES.
C
C      SUBROUTINES AND FUNCTION SUBPROGRAMS REQUIRED
C         SQRT
C         COS
C
C      METHOD
C         THE METHOD IS ESSENTIALLY STATED BY H. P. F. SWINNERTON-
C         DYER IN 'THE COMPUTER JOURNAL',16,P16-23,1963.
C
C      PROGRAMMER
C         J. G. ABLES, SOUTHWEST CENTER FOR ADVANCED STUDIES.
C
       SUBROUTINE PSA(D,A,S,P,C,AV,VAR,SD,N,M,NDF)
       DIMENSION D(1),A(1),S(1),P(1),C(1)
C
C      REDUCE THE INPUT SERIES TO ZERO MEAN.
C
       FN=N
       DO 2 J=1,2
       R=0.0
       DO 1 I=1,N
     1 R=D(I)+R
       R=R/FN
       A(J)=R
       DO 2 I=1,N
     2 D(I)=D(I)-R
       AV=A(1)
```

```
C
C        COMPUTE THE AUTOCORRELATIONS, VARIANCE, AND STANDARD DEVIATION.
C
         MAX=N-M
         FMAX=MAX
         LMAX=M+1
         DO 4 K=1,LMAX
         J=K
         R=0.0
         DO 3 I=1,MAX
         R=C(I)*C(J)+R
       3 J=J+1
       4 A(K)=R
         VT=A(1)
         VAR=VT/FMAX
         SD=SQRT(VAR)
         DO 5 I=1,LMAX
       5 A(I)=A(I)/VT
C
C        REDUCE THE INPUT SERIES TO UNIT VARIANCE.
C
         DO 6 I=1,N
       6 C(I)=C(I)/SD
C
C        COMPUTE THE COSINE TABLE
C
         KMOD=2*M
         FM=M
         R=3.14159/FM
         DO 7 I=1,KMOD
         FIMC=I-1
       7 C(I)=COS(FIMC*R)
C
C        COMPUTE THE FINITE COSINE TRANSFORM OF THE AUTOCORRELATIONS.
C
         AEND=A(LMAX)
         FLIP=1.0
         DO 10 J=1,LMAX
         IP=J-1
         K=1
         R=0.0
         DO 9 I=1,LMAX
         R=A(I)*C(K)+R
         K=K+IP
         KM=K-KMOD
         IF(KM)9,9,8
       8 K=KM
       9 CONTINUE
         S(J)=2.0*R-1.0-AEND*FLIP
      10 FLIP=-FLIP
C
C        SMOOTH THE SPECTRAL ESTIMATES.
C
         DO 11 I=2,M
      11 P(I)=0.23*S(I-1)+0.54*S(I)+0.23*S(I+1)
         P(1)=0.54*S(1)+0.46*S(2)
         P(LMAX)=0.54*S(LMAX)+0.46*S(LMAX-1)
C
C        COMPUTE THE NUMBER OF DEGREES OF FREEDOM.
C
         NDF=(FN/FM)-0.5
         RETURN
         END
```

```
C      SUBROUTINE XPSA
C
C
C      PURPOSE
C         COMPUTE THE CROSS-POWER SPECTRUM AND CROSS-CORRELATION FUNCTION
C         OF TWO GIVEN SERIES.
C
C
C      USAGE
C         CALL XPSA(D,E,X,XE,XO,SR,SI,PR,PI,PMAG,PARG,S,C,AVD,AVE,VARD,
C         VARE,SDD,SDE,N,M,NDF)
C
C
C      DESCRIPTION OF PARAMETERS
C         D      -INPUT VECTOR OF LENGTH N CONTAINING THE FIRST OF THE TWO
C                 SERIES TO BE CROSS-CORRELATED.
C         E      -INPUT VECTOR OF LENGTH N CONTAINING THE SECOND OF THE
C                 TWO SERIES TO BE CROSS-CORRELATED
C         X      -OUTPUT VECTOR OF LENGTH 2M+1 CONTAINING THE CROSS-CORRE-
C                 LATIONS FOR LAGS OF -M,....,-2,-1,0,1,2,...,M.
C         XE     -OUTPUT VECTOR OF LENGTH M+1 CONTAINING THE EVEN PART OF
C                 THE CROSS-CORRELATION FUNCTION (FOR LAGS OF 0,1,...,M).
C         XO     -OUTPUT VECTOR OF LENGTH M+1 CONTAINING THE ODD PART OF
C                 THE CROSS-CORRELATION FUNCTION (FOR LAGS OF 0,1,...,M).
C         SR     -OUTPUT VECTOR OF LENGTH M+1 CONTAINING THE REAL PART OF
C                 THE UNSMOOTHED CROSS-POWER SPECTRUM.
C         SI     -OUTPUT VECTOR OF LENGTH M+1 CONTAINING THE IMAGINARY PART
C                 OF THE UNSMOOTHED CROSS-POWER SPECTRUM.
C         PR     -OUTPUT VECTOR OF LENGTH M+1 CONTAINING THE REAL PART OF
C                 THE SMOOTHED CROSS-POWER SPECTRUM.
C         PI     -OUTPUT VECTOR OF LENGTH M+1 CONTAINING THE IMAGINARY PART
C                 OF THE SMOOTHED CROSS-POWER SPECTRUM.
C         PMAG   -OUTPUT VECTOR OF LENGTH M+1 CONTAINING THE MAGNITUDE OF
C                 THE SMOOTHED CROSS-POWER SPECTRUM.
C         PARG   -OUTPUT VECTOR OF LENGTH M+1 CONTAINING THE PHASE (IN
C                 DEGREES) OF THE SMOOTHED POWER SPECTRUM.
C         S      -OUTPUT VECTOR OF LENGTH 2M CONTAINING SIN(Q*PI/M)
C                 Q=0,1,2,...,(2M-1).
C         C      -OUTPUT VECTOR OF LENGTH 2M CONTAINING COS(Q*PI/M)
C                 Q=0,1,2,...,(2M-1).
C         AVD    -AVERAGE OF FIRST INPUT SERIES (OUTPUT).
C         AVE    -AVERAGE OF SECOND INPUT SERIES (OUTPUT).
C         VARD   -VARIANCE OF FIRST INPUT SERIES (OUTPUT).
C         VARE   -VARIANCE OF SECOND INPUT SERIES (OUTPUT).
C         SDD    -STANDARD DEVIATION OF FIRST INPUT SERIES (OUTPUT).
C         SDE    -STANDARD DEVIATION OF SECOND INPUT SERIES (OUTPUT).
C         N      -LENGTH OF INPUT SERIES (INPUT).
C         M      -MAX LAG (CROSS-CORRELATIONS ARE COMPUTED FOR LAGS OF
C                 -M,....,-2,-1,0,1,2,...M) (INPUT).
C         NDF    -NUMBER OF DEGREES OF FREEDOM (OUTPUT).
C
C
C      REMARKS
C         N MUST BE GREATER THAN M. THE INPUT SERIES ARE NORMALIZED TO
C         ZERO MEAN AND UNIT VARIANCE. THE FIRST ELEMENT IN THE SPECTRUM
C         VECTORS CORRESPONDS TO ZERO FREQUENCY. THE SPACING BETWEEN
C         SPECTRAL ESTIMATES IS 1/(2*T*M) WHERE T IS THE TIME BETWEEN
C         ELEMENTS IN THE INPUT SERIES. THE FIRST SERIES IS LAGGED WITH
C         RESPECT TO THE SECOND SERIES.
C
C
C      SUBROUTINES AND FUNCTION SUBPROGRAMS REQUIRED
C         SQRT
C         SIN
C         COS
C         ATAN
C
C
C      METHOD
C         THE OUTPUT CROSS-POWER SPECTRUM IS COMPUTED BY FORMING THE
C         SMOOTHED (HAMMED) FINITE SINE AND COSINE TRANSFORMS,
C         RESPECTIVELY, OF THE ODD AND EVEN PARTS OF THE TWO-SIDED CROSS-
C         CORRELATION FUNCTION OF THE GIVEN INPUT SERIES. THE FIRST
C         SERIES IS LAGGED WITH RESPECT TO THE SECOND SERIES.
C
C
C      PROGRAMMER
C         J. G. ABLES, SOUTHWEST CENTER FOR ADVANCED STUDIES.
C
```

```
C
      SUBROUTINE XPSA(D,E,X,XE,XC,SR,SI,PR,PI,PMAG,PARG,S,C,AVD,AVE,
     1VARD,VARE,SDD,SDE,N,M,NDF)
      DIMENSION D(1),E(1),X(1),XE(1),XC(1),SR(1),SI(1),PR(1),PI(1),
     1PMAG(1),PARG(1),S(1),C(1)
C
C     REDUCE BOTH INPUT SERIES TO ZERO MEAN
C
      FN=N
      DO 2 J=1,2
      R=0.0
      T=0.0
      DO 1 I=1,N
      R=D(I)+R
    1 T=E(I)+T
      R=R/FN
      T=T/FN
      XE(J)=R
      XC(J)=T
      DO 2 I=1,N
      D(I)=D(I)-R
    2 E(I)=E(I)-T
      AVD=XE(1)
      AVE=XC(1)
C
C     COMPUTE THE VARIANCE AND STANDARD DEVIATION OF BOTH INPUT SERIES
C
      R=0.0
      T=0.0
      DO 3 I=1,N
      R=D(I)*D(I)+R
    3 T=E(I)*E(I)+T
      VARD=R/FN
      VARE=T/FN
      SDD=SQRT(VARD)
      SDE=SQRT(VARE)
C
C     REDUCE BOTH INPUT SERIES TO UNIT VARIANCE
C
      DO 4 I=1,N
      D(I)=D(I)/SDD
    4 E(I)=E(I)/SDE
C
C     COMPUTE THE CROSS-CORRELATION FUNCTION OF THE INPUT SERIES
C
      MAX=2*M+1
      LAG=-M
      DO 8 K=1,MAX
      R=0.0
      LD=N
      ID=1-LAG
      IF(ID)5,5,6
    5 ID=1
      LD=N-LAG
    6 J=ID+LAG
      XN=LD-ID+1
      DO 7 I=ID,LD
      R=D(I)*E(J)+R
    7 J=J+1
      X(K)=R/XN
    8 LAG=LAG+1
C
C     RESOLVE THE CROSS-CORRELATION FUNCTION INTO EVEN AND ODD FUNCTIONS
C
      MID=M+1
      K=M
      DO 9 I=1,MID
      K=K+1
      J=MAX-K+1
      XE(I)=0.5*(X(K)+X(J))
    9 XC(I)=0.5*(X(K)-X(J))
```

```
C
C       FILL THE SINE AND COSINE TABLES
C
        KMOD=2*M
        FN=N
        R=3.14159/FN
        DO 10 I=1,KMOD
        FIMO=I-1
        ARG=FIMO*R
        S(I)=SIN(ARG)
   10   C(I)=COS(ARG)
C
C       COMPUTE THE FINITE SINE AND COSINE TRANSFORM OF THE EVEN AND ODD
C       PARTS OF THE CROSS-CORRELATION FUNCTION
C
        XEND=XE(MID)
        XONE=XE(1)
        FLIP=1.0
        DO 13 J=1,MID
        IP=J-1
        K=J
        R=C.0
        T=C.0
        DO 12 I=2,M
        R=XE(I)*C(K)+R
        T=XO(I)*S(K)+T
        K=K+IP
        KM=K-KMOD
        IF(KM)12,12,11
   11   K=KM
   12   CONTINUE
        SR(J)=2.0*R+XONE+XEND*FLIP
        SI(J)=2.0*T
   13   FLIP=-FLIP
C
C       SMOOTH THE REAL AND IMAGINARY SPECTRA
C
        DO 14 I=2,M
        PR(I)=0.23*(SR(I-1)+SR(I+1))+0.54*SR(I)
   14   PI(I)=0.23*(SI(I-1)+SI(I+1))+0.54*SI(I)
        PR(1)=0.54*SR(1)+0.46*SR(2)
        PI(1)=0.54*SI(1)+0.46*SI(2)
        PR(MID)=0.54*SR(MID)+0.46*SR(M)
        PI(MID)=0.54*SI(MID)+0.46*SI(M)
C
C       COMPUTE THE MAGNITUDE AND PHASE SPECTRA
C
        DO 16 I=1,MID
        PMAG(I)=SQRT(PR(I)**2+PI(I)**2)
        PARG(I)=ATAN(PI(I)/PR(I))*57.2958
        IF(PR(I))15,16,16
   15   PARG(I)=PARG(I)+180.0
   16   CONTINUE
C
C       COMPUTE THE NUMBER OF DEGREES OF FREEDOM
C
        NDF=(FN/FM)-0.5
        RETURN
        END
```

```
C
C          PROGRAM COSMOGRAM
C
C      PURPOSE
C          COMPUTE COSMIC-RAY INTENSITY VALUES FROM NEUTRON MONITOR DATA
C          FOR THE CONSTRUCTION OF TIME-DIRECTION INTENSITY CONTOUR MAPS.
C
C      USAGE
C          THIS IS THE MAIN PROGRAM
C
C      DESCRIPTION OF PARAMETERS
C          CODE -JOB IDENTIFICATION
C          ICORR-CORRECTION CONTROL PARAMETER
C          IDAY -INITIAL DAY NUMBER
C          ND   -NUMBER OF DAYS
C          N    -NUMBER OF STATIONS
C          TAU  -TIME CONSTANT FOR TIME FILTER
C          ALPHA-ANGLE CONSTANT FOR ANGLE FILTER
C          IDS  -STATION IDENTIFICATION NUMBER
C          P    -STATION ASYMPTOTIC LONGITUDE
C          R    -STATION BASE COUNT RATE
C          LAMDA-STATION ASYMPTOTIC LATITUDE
C          IVC  -DECONVOLUTION WEIGHTS
C
C      REMARKS
C          DATA INTERVAL WILL BE SHORTENED BY AN AMOUNT EQUAL TO THE
C          SUM OF THE DURATIONS OF THE DECONVOLUTION AND TIME FILTERS.
C
C      SUBROUTINES AND FUNCTIONS USED
C          ABS
C          SIN
C          COS
C          SQRT
C          NORM
C          NMDATA
C          PATCH
C          XOFF
C          SMO
C          TILT
C          RXFER
C          RALLY
C          SAMDEN
C          GENWTS
C          GFUN
C          HFUN
C          MAPLIN
C          METHOD
C          SEE TEXT
C
C      PROGRAMMER
C          J. G. ABLES, SOUTHWEST CENTER FOR ADVANCED STUDIES.
C
       DIMENSION A(750),D(7200),G(960),H(75),XN(24),XL(24),P(20),M(20),
      1S(20),G(20),IVC(73),BD(20),B(750),TOTAL(20),AVER(20),SD(20),R(20),
      2VMIN(20),VMAX(20) ,SNAME(20,5),IDS(20),DELTA(20)
       REAL IVC
       EXTERNAL GFUN,HFUN
C
C      READ GENERAL INFORMATION
C
  3030 READ(1,1) CODE,IDAY,ND,N,TAU,ALPHA,IG,ICORR
     1 FORMAT(A4,1X,I5,1X,I2,1X,I2,1X,F4.0,1X,F4.0,1X,I1,1X,I1)
       WRITE(3,2)CODE,IDAY,ND,N,TAU,ALPHA
     2 FORMAT('1JCACG JOB ',A4,3X,'STARTS ',I5,3X,'NO. DAYS ',I2,3X,'NO.
      21STA. ',I2,3X,'TAU=',F5.1,3X,'ALPHA=',F5.1///)
       IF(IG)101,102,101
   101 WRITE(8,2) CODE,IDAY,ND,N,TAU,ALPHA
   102 CONTINUE
       NP=ND*24
       XNP=NP
       DO 8 L=1,N
```

```
C
C       READ STATICN PARAMETER CARD
C
        READ(1,3) IDS(L),(SNAME(L,JK),JK=1,5),P(L),R(L),DELTA(L)
      3 FCRMAT(I3,1X,5A4,1X,F5.2,1X,F5.C,1X,F5.4)
C
C       READ DECCNVCLUTICN WEIGHTS
C
        RFAD(1,4) IVC
      4 FCRMAT(3X,F8.4/(3X,8F8.4))
        IF(ICCRR-2)201,202,201
    201 IF(ICCRR-4)2C3,2C2,2C3
    202 CELTA(L)=CCS(DELTA(L)/57.296)
C
C       NCRMALIZE DECCNVCLUTICN WEIGHTS
C
        CALL NCRM(IVC,73,C.C)
        CALL NCRM(IVC,73,DELTA(L))
        GC TC 2C4
    203 CALL NCRM(IVC,73,C.C)
    204 CCNTINUE
C
C       READ DATA FCR CNE STATICN
C
        CALL NMCATA(NC,A,IER,NC)
        IF(IFR)5,7,5
      5 WRITE(3,6) L,NC
      6 FCRMAT(' BAD DATA   STA. ',I2,' CARD ',I2,'    NC GC')
        STCP
C
C       FILL IN MISSING VALUES IN DATA
C
      7 CALL PATCH(A,NP,NZ)
        BD(L)=FLCAT(NZ)*1CC.C/XNP
C       NCRMALIZE NEUTRCN MCNITCR DATA
C
C
        CALL NCRM(A,NP,R(L))
        CALL XCFF(A,1.C,1CCC.C,NP)
C
C       DECCNVCLVE DATA
C
        CALL SMC(A,NP,IVC,73,1,B)
        LE=NP-36
C
C       TRANSFER DATA TC PERMANENT STCRACE
C
      8 CALL RXFER(B,N,L,37,LE,C)
        NP=NP-72
C
C       CCMPUTE STATISTICS
C
        CALL RALLY(C,TCTAL,AVER,SD,VMAX,VMIN,NP,N)
C
C       CCMPUTE RECIPRCCAL STATICN CENSITIES
C
        ITIE=C
        CALL SAMCEN(P,C,M,S,N,ITIE)
        IF(ITIE)9,12,9
      9 WRITE(3,1C)(P(I),I=1,N)
     1C FCRMAT(' ANGLE CUPLICATICN ',20F5.2)
        WRITE(3,11)
     11 FCRMAT(' NC GO ')
        STCP
```

```
C
C       WRITE HEADING
C
   12 WRITE(3,13)
   13 FORMAT('C NAME              NO.  SEG  RANK  ANGLE  1/DEN   RATE
  131  TOTAL    AVER     SD    MAX    MIN PCT.BAD  DELTA')
      DO 14 L=1,N
   14 WRITE(3,15)(SNAME(L,JK),JK=1,5),IDS(L),L,M(L),P(L),Q(L),R(L),
  141TOTAL(L),AVER(L),SD(L),VMAX(L),VMIN(L),PC(L),DELTA(L)
   15 FORMAT('C',5A4,I4,I6,I6,F7.2,F7.2,F7.0,F7.2,F7.3,F7.3,F7.2,F7.2,
  151F8.2,F7.4)
      IF(ICORR-1)205,206,205
  205 IF(ICORR-5)220,206,220
  206 CALL TILT(D,P,DELTA,Q,IDAY,N,NP)
  220 CONTINUE
      IF(ICORR-3)207,209,207
  207 IF(ICORR-4)208,209,208
  208 IF(ICORR-5)212,209,212
  209 SDA=0.0
      DO 210 I=1,N
  210 SDA=SDA+SD(I)
      SDA=SDA/FLOAT(N)
      DO 211 I=1,N
      SDR=SDA/SD(I)
      DO 211 J=1,NP
      IJ=N*(J-1)+I
  211 D(IJ)=D(IJ)*SDR
  212 CONTINUE
C
C       GENERATE FILTER WEIGHTS
C
      CALL GENWTS(GFUN,HFUN,P,Q,N,TAU,ALPHA,G,H,XN)
      WRITE(3,16)
   16 FORMAT('1    DATE    1     2     3     4     5     6     7     8     9    10
  161   11    12    13    14    15    16    17    18    19    20    21    22    23
  162   24'//)
C
C       INITIALIZE HOUR AND DAY COUNTERS
C
      ICT=IDAY+1
      MTAU=TAU+0.001
      IHR=13+(MTAU-1)/2
   17 IF(IHR-24)19,19,18
   18 IHR=IHR-24
      ICT=ICT+1
      GO TO 17
   19 KEND=NP-MTAU+37
      DO 22 IT=37,KEND
C
C       COMPUTE INTENSITY VALUES (24)
C
      CALL MAPLIN(D,G,H,XN,N,MTAU,IT,XL)
C
C       PRINT INTENSITY VALUES (24)
C
      WRITE(3,20)ICT,IHR,(XL(I),I=1,24)
   20 FORMAT(1X,I5,I2,24F5.1)
      IF(IO)103,104,103
  103 WRITE(8,20) ICT,IHR,(XL(I),I=1,24)
  104 CONTINUE
C
C       INCREMENT HOUR AND DAY COUNTERS
C
      IHR=IHR+1
      IF(IHR-24)22,22,21
   21 IHR=IHR-24
      ICT=ICT+1
   22 CONTINUE
```

```
C
C       DUMP ALL IMPORTANT ARRAYS
C
        WRITE(3,23)
   23 FORMAT('1 DATA MATRIX')
        KB=1
        KE=N
        DO 25 I=1,NP
        WRITE(3,24)(D(J),J=KB,KE)
   24 FORMAT('C',20F6.1)
        KB=KB+N
   25 KE=KE+N
        WRITE(3,26)
   26 FORMAT('1 C MATRIX')
        KB=1
        KE=N
        DO 28 I=1,24
        WRITE(3,27)(G(J),J=KB,KE)
   27 FORMAT('C',20F6.1)
        KB=KB+N
   28 KE=KE+N
        WRITE(3,29) XN
   29 FORMAT('C XN ',12F10.3)
        WRITE(3,30)(G(I),I=1,N)
   30 FORMAT('C   G ',20F6.2)
        WRITE(3,31)(H(I),I=1,NTAL)
   31 FORMAT('C   H ',20F6.2)
        IF(IG)105,106,105
  105 END FILE 8
  106 IF(IG-1)108,107,108
  107 REWIND 8
  108 CONTINUE
        GO TO 3030
        END
```

185

```
C
C
C      ............................................................
C
C      SUBROUTINE SMO
C
C      PURPOSE
C         TO SMOOTH OR FILTER SERIES A BY WEIGHTS W.
C
C      USAGE
C         CALL SMO %A,N,W,M,L,R<
C
C      DESCRIPTION CF PARAMETERS
C         A - INPUT VECTOR OF LENGTH N CONTAINING TIME SERIES DATA.
C         N - LENGTH OF SERIES A.
C         W - INPUT VECTOR CF LENGTH M CCNTAINING WEIGHTS.
C         M - NUMBER OF ITEMS IN WEIGHT VECTOR. M MUST BE AN OCD
C             INTEGER. %IF M IS AN EVEN INTEGER, ANY FRACTION
C             RESULTING FROM THE CALCULATICN OF %L*%M-1<</2 IN %1<
C             AND %2< BELOW WILL BE TRUNCATED.<
C         L - SELECTION INTEGER. FCR EXAMPLE, L#12 MEANS THAT WEIGHTS
C             ARE APPLIED TO EVERY 12-TH ITEM CF A. L#1 APPLIES
C             WEIGHTS TO SUCCESSIVE ITEMS CF A. FCR MONTHLY DATA,
C             L#12 GIVES YEAR-TO-YEAR AVERAGES AND L#1 GIVES MONTH-TO-
C             MCNTH AVERAGES.
C         R - CUTPLT VECTOR CF LENGTH N. FRCM IL TO IH ELEMENTS CF
C             THE VECTOR R ARE FILLED WITH THE SMOOTHED SERIES AND
C             CTHER ELEMENTS WITH ZERO, WHERE
C                    IL#%L*%M-1<</2&1   ................ %1<
C                    IH#N-%L*%M-1<</2   ................ %2<
C
C      REMARKS
C         N MUST BE GREATER THAN CR EGUAL TC THE PRODUCT OF L*M.
C
C      SUBROUTINES AND FUNCTION SUBPROGRAMS REQUIRED
C         NCNE
C
C      METHCD
C         REFER TO THE ARTICLE aFCRTRAN SUBROUTINES FCR TIME SERIES
C         ANALYSISa, BY J. R. HEALY AND B. P. BOGERT, COMMUNICATIONS
C         CF ACM, V.6, NC.6, JUNE, 1963.
C
C      ............................................................
C
       SUBROUTINE SMO %A,N,W,M,L,R<
       DIMENSION A%1<,W%1<,R%1<
C
C      INITIALIZATION
C
       DC 110 I#1,N
  110  R%I<#C.C
       IL#%L*%M-1<</2&1
       IH#N-%L*%M-1<</2
C
C      SMCCTH SERIES A BY WEIGHTS W
C
       DC 120 I#IL,IH
       K#I-IL&1
       DC 120 J#1,M
       IP#%J*L<-L&K
  120  R%I<#R%I<&A%IP<*W%J<
       RETURN
       END
```

```
      SUBROUTINE NMDATA(ND,A,IER,NC)
      DIMENSION A(1)
    1 FORMAT(10X,I1,1X,8(F4.C,2X))
      M=C
      J=-7
      K=C
      NC=NC*3
      DO 4 I=1,NC
      M=M+1
      IF(M-4)3,2,3
    2 M=1
    3 J=J+8
      K=K+8
      READ(1,1) NC,(A(L),L=J,K)
      IF(M-NC)5,4,5
    4 CONTINUE
      IER=C
      GO TO 6
    5 IER=1
      NC=I
    6 RETURN
      END
```

```
      SUBROUTINE PATCH(A,N,NZ)
      DIMENSION A(1)
      IZ=C
      NZ=C
      DO 3 I=1,N
      IF(A(I))1,2,1
    1 IF(IZ)7,3,7
    2 IZ=IZ+1
    3 CONTINUE
      IF(IZ)4,6,4
    4 J=N-IZ+1
      DO 5 L=J,N
    5 A(L)=A(L-1)
      NZ=NZ+IZ
    6 RETURN
    7 K=I-IZ-1
      L=A(I)
      IF(K)8,8,1C
    8 DO 9 L=1,IZ
    9 A(L)=U
      GO TO 12
   1C V=A(K)
      X=(L-V)/FLCAT(IZ+1)
      DO 11 J=1,IZ
      L=K+J
   11 A(L)=V+FLCAT(J)*X
   12 NZ=NZ+IZ
      IZ=C
      GO TO 3
      END
```

```
      SUBROUTINE NORM(A,N,R)
      DIMENSION A(1)
      IF(R)3,3,1
    1 DO 2 I=1,N
    2 A(I)=A(I)/R
      RETURN
    3 S=0.0
      DO 4 I=1,N
    4 S=S+A(I)
      IF(R)5,6,6
    5 S=S/FLOAT(N)
    6 R=S
      GO TO 1
      END
```

```
      SUBROUTINE XOFF(A,B,C,NP)
      DIMENSION A(1)
      DO 1 I=1,NP
    1 A(I)=(A(I)-B)*C
      RETURN
      END
```

```
      SUBROUTINE RXFER(A,N,NR,LB,LE,C)
      DIMENSION A(1),C(1)
      I=NR-N
      DO 1 L=LB,LE
      I=I+N
    1 C(I)=A(L)
      RETURN
      END
```

```
      SUBROUTINE RALLY(A,TOTAL,AVER,SD,VMAX,VMIN,NP,N)
      DIMENSION A(1),TOTAL(1),AVER(1),SD(1),VMAX(1),VMIN(1)
      XNP=FLOAT(NP)
      DO 5 L=1,N
      TT=0.0
      XS=0.0
      XMAX=1.0E-50
      XMIN=1.0E+50
      J=L-N
      DO 4 I=1,NP
      J=J+N
      X=A(J)
      TT=TT+X
      IF(X-XMIN)1,2,2
1     XMIN=X
2     IF(X-XMAX)4,4,3
3     XMAX=X
4     XS=XS+X*X
      TOTAL(L)=TT
      SD(L)=XS
      VMAX(L)=XMAX
5     VMIN(L)=XMIN
      DO 6 I=1,N
      AVER(I)=TOTAL(I)/XNP
6     SD(I)=SQRT(ABS((SD(I)-TOTAL(I)*TOTAL(I)/XNP)/(XNP-1.0)))
      RETURN
      END
```

```
      SUBROUTINE TILT(D,P,DELTA,G,IDAY,N,NP)
      DIMENSION D(1),P(1),DELTA(1),G(1),A(20)
      SWT=0.0
      DO 1 I=1,N
      DELTA(I)=DELTA(I)/57.29578
1     SWT=SWT+G(I)
      XHR=(IDAY-(IDAY/1000)*1000)*24+12
      XHR=XHR-0.5
      DO 2 I=1,N
2     A(I)=P(I)*0.2617994+1.744093+0.2625162*XHR
      DO 6 K=1,NP
      J=(K-1)*N
      SUM=0.0
      DO 3 I=1,N
      IJ=I+J
3     SUM=SUM+D(IJ)*G(I)
      SUM=SUM/SWT
      DO 6 I=1,N
      IJ=I+J
      A(I)=A(I)+0.2625162
4     R=A(I)-6.283185
      IF(R)6,5,5
5     A(I)=R
      GO TO 4
6     D(IJ)=(D(IJ)-SUM)/SQRT(1.0-((0.917*SIN(DELTA(I))-0.399*COS(DELTA(I)
     61)*SIN(A(I)))**2)+SUM
      RETURN
      END
```

```
      SUBROUTINE GENWTS(GFUN,FFUN,P,C,N,TAU,ALPHA,G,F,XN)
      DIMENSION P(1),C(1),G(1),F(1),XN(1)
      M=N*24
      MTAU=TAU+C.CC1
      DO 1 I=1,24
      J=I-1
      TADIF=FLOAT(J)
      DO 1 K=1,N
      L=K+(J*N)
      THETA=TADIF+P(K)
 10   IF(THETA-12.C)30,30,20
 20   THETA=THETA-24.0
      GO TO 10
 30   CVAL=GFUN(THETA,ALPHA)*C(K)
      G(L)=CVAL
      LL=L+M
 1    G(LL)=CVAL
      DO 2 I=1,MTAU
      T=FLOAT(I)
 2    F(I)=FFUN(T,TAU)
      DO 5 K=1,24
      IB=((K-1)*N)+1
      IE=IB+N-1
      TOT=0.C
      DO 4 J=1,MTAU
      SUM=C.C
      DO 3 I=IB,IE
 3    SUM=SUM+G(I)
      TOT=SUM*F(J)+TOT
      IB=IB+N
 4    IE=IE+N
 5    XN(K)=1.C/TOT
      RETURN
      END



      FUNCTION FFUN(T,TAU)
      TC=(TAU+1.C)/2.0
      FFUN=TC-ABS(T-TC)
      IF(FFUN)1,2,2
 1    FFUN=C.C
 2    RETURN
      END



      FUNCTION GFUN(THETA,ALPHA)
      GFUN=(ALPHA/2.C)-ABS(THETA)
      IF(GFUN)1,2,2
 1    GFUN=C.C
 2    RETURN
      END
```

```
      SUBROUTINE SANDEN(P,C,M,S,N,ITIE)
      DIMENSION P(1),C(1),M(1),S(1)
      DO 6 I=1,N
      NE=-1
      NR=1
      X=P(I)
      DO 3 J=1,N
      IF(X-P(J))3,2,1
    1 NR=NR+1
      GO TO 3
    2 NE=NE+1
    3 CONTINUE
      IF(NE)5,5,4
    4 ITIE=1
      RETURN
    5 M(I)=NR
    6 S(NR)=X
      XN=FLOAT(N)/48.0
      DO 12 I=1,N
      L=M(I)
      J=L-1
      IF(J)7,7,8
    7 J=N
    8 K=L+1
      IF(N-K)9,10,10
    9 K=1
   10 X=S(K)-S(J)
      IF(X)11,4,12
   11 X=X+24.0
   12 G(I)=X*XN
      RETURN
      END




      SUBROUTINE MABLIN(D,C,F,XN,N,MTAU,IT,XL)
      DIMENSION D(1),C(1),F(1),XN(1),XL(1)
      LP=(IT-37)*N
      DO 3 K=1,24
      ID=IT-K
      ID=ID-(ID/24)*24
      IB=(ID*N)+1
      IE=IB+N-1
      KS=ID+1
      B=0.0
      L=LP
      DO 2 J=1,MTAU
      A=0.0
      DO 1 I=IB,IE
      L=L+1
    1 A=D(L)*C(I)+A
      B=A*F(J)+B
      IB=IB+N
    2 IE=IE+N
    3 XL(K)=B*XN(KS)
      RETURN
      END
```

VITA

Jon Gordon Ables

Candidate for the Degree of

Doctor of Philosophy

Thesis: PERSISTENT AND TRANSIENT ANISOTROPIES OF THE COSMIC RADIATION

Major Field: Physics

Biographical:

Personal Data: Born at Durant, Oklahoma, October 11, 1937, the
    son of Joe W. and Hildred Ables.

Education: Graduated from Miami High School, Miami, Oklahoma, in
    May, 1955. Awarded the George F. Baker Scholarship for four
    years of undergraduate study. Attended Knox College, Galesburg,
    Illinois, elected to Phi Beta Kappa in the junior year,
    graduated magna cum laude, with the Bachelor of Arts degree
    with majors in Physics and Mathematics, May, 1959. Made
    Honorary Woodrow Wilson Fellow, 1959. Awarded a National
    Science Foundation grant for one year of graduate study at
    the California Institute of Technology, Pasadena, California,
    completing the year of study in May, 1960. Received the
    Master of Science degree from Oklahoma State University,
    with a major in Physics, in May, 1963; completed requirements
    for the Doctor of Philosophy degree in August, 1967.

Professional experience: Graduate assistant in School of Physics,
    Oklahoma State University, 1960-62; research assistant, Oklahoma
    State Research Foundation, 1962-63; instructor, Oklahoma State
    Technical Institute, 1963; graduate research assistant, South-
    west Center for Advanced Studies, 1963-66; research scientist,
    Southwest Center for Advanced Studies, 1966-67. Member of
    Sigma Pi Sigma. Publications: With K. G. McCracken and
    U. R. Rao, "The Semi-Diurnal Anisotropy of the Cosmic Radia-
    tion," The Proceedings of the Ninth International Conference
    on Cosmic Rays, London, 1965; with E. Barouch and K. G.
    McCracken, "The Cosmic Radiation Anisotropy as a Separable
    Function of Time and Radiation," Planet. Space Sci., Vol. 15
    (1967); with G. H. Riley, "A Filament Current Regulator for
    Solid Source Mass Spectrometers," submitted to Review of
    Scientific Instruments, June, 1967.